

**Ni/Mg/Al catalysts derived from hydrotalcite-type  
precursors for the partial oxidation of propane.  
Synthesis and characterisation of physicochemical  
and catalytic properties**

Vom Fachbereich 6 (Chemie-Geographie)

der

Gerhard-Mercator-Universität – Gesamthochschule Duisburg

zur Erlangung des akademischen Grades eines

Doktors der Naturwissenschaften (Dr. rer. nat.)

genehmigte Dissertation

von

**Kai Schulze**

aus

Duisburg

Referent: Prof. Dr. Roman Dziembaj

Korreferent: Prof. Dr. Günter Geismar

Tag der mündlichen Prüfung: 11. Juli 2001

Die vorliegende Arbeit entstand in der Zeit vom 4. März bis 14. August 1997 im Fachbereich 6 an der Gerhard-Mercator-Universität – Gesamthochschule Duisburg (Deutschland) unter Betreuung von Prof. Dr. Günter Geismar und vom 15. August 1997 bis 8. Juni 2001 an der Chemischen Fakultät der Jagiellonischen Universität in Krakau (Polen) unter Betreuung von Prof. Dr. Roman Dziembaj.

## **Acknowledgements**

I would like to thank Prof. Dr. Roman Dziembaj for allowing me to work on this very interesting project, his invaluable assistance and all his support.

I would also like to thank Prof. Dr. Günter Geismar for all his cooperation and his kind support.

I would also like to express my sincere gratitude to Dr. Wacław Makowski for his willingness to share his ideas on various issues and his constant support.

Above all, I would like to recognise all the people that were involved in this work at the Jagiellonian University and the Gerhard-Mercator-University Duisburg. Without their support this work would have not been possible.

**For my mother**

## **Ni/Mg/Al catalysts derived from hydrotalcite-type precursors for the partial oxidation of propane. Synthesis and characterisation of physicochemical and catalytic properties**

Ph.D. thesis by Kai Schulze from Duisburg (Germany) submitted to the Gerhard-Mercator-University, Duisburg, Germany in June 2001

The work was performed from 4<sup>th</sup> March 1997 to 14<sup>th</sup> August 1997 at the Department of Inorganic Chemistry, Gerhard-Mercator-University, Duisburg, Germany, supervisor Prof. Dr. Günter Geismar and from 15<sup>th</sup> August 1997 to 8<sup>th</sup> June 2001 at the Faculty of Chemistry, Jagiellonian University, Krakow, Poland, supervisor Prof. Dr. Roman Dziembaj.

### **Abstract**

Anionic clays of hydrotalcite-type structure of the approximate formula  $[\text{Ni}_x\text{Mg}_{72-x}\text{Al}_{28}(\text{OH})_{200}][(\text{NO}_3)_y(\text{CO}_3)_{(28-y)/2}] \cdot 50\text{H}_2\text{O}$  ( $x = 0, 5, 10, 15, 30, 50, 72$  and  $11 \leq y \leq 16$ ) were synthesised by coprecipitation at low supersaturation at  $\text{pH } 8 \pm 0.2$ . Their composition and structure was determined by elemental analysis, XRD, TG-MS and DSC. Their calcination at temperature  $\geq 900^\circ\text{C}$  in a flow of air resulted in the transformation into the corresponding solids of well crystallised divalent metal oxide phases with periclase structure and spinel phases. At lower temperatures poorly crystallised divalent metal oxides and amorphous  $\text{Al}_2\text{O}_3$  phases with poorly crystallised spinel at their interfaces were formed. The degree of crystallinity increased with increasing calcination temperature. Catalysts with a lower nickel content exhibited remarkably high surface areas. This suggests that the fast removal of the gases formed during the calcination process combined with a slow heating rate had a beneficial influence on the catalysts' preparation.

Temperature programmed reduction/oxidation of  $\text{Ni}^{2+}/\text{Ni}^0$  and high temperature XRD studies of the catalysts calcined at  $900^\circ\text{C}$  showed that their reduction takes place in two distinct steps. First the  $\text{Ni}^{2+}$  ions in the divalent metal oxide phase are reduced followed at higher temperatures by the  $\text{Ni}^{2+}$  ions in the spinel phase. The catalysts with a lower nickel content were more difficult to reduce but exhibited higher nickel dispersion. These results are attributed to the substitution of  $\text{Mg}^{2+}$  by  $\text{Ni}^{2+}$  leading to the formation of a NiO-MgO solid solution upon calcination, which stabilises the  $\text{Ni}^{2+}$  ions against reduction and sintering. The formed metallic nickel particles are not stabilised by the MgO matrix against the consecutive oxidation. The reduction temperature increases slightly with increasing crystallinity of the catalysts.

The partial oxidation of  $\text{C}_3\text{H}_8$  to syngas ( $\text{CO} + \text{H}_2$ ) could be successfully performed at temperatures between  $600^\circ\text{C}$  and  $900^\circ\text{C}$  over reduced Ni containing catalysts. CO and  $\text{H}_2$  were the main products,  $\text{H}_2\text{O}$ ,  $\text{CO}_2$  and  $\text{CH}_4$  the only considerable side products. The conversion of  $\text{C}_3\text{H}_8$  and the yield of syngas increased with increasing reaction temperature. Unreduced Ni exhibited no specific catalytic activity. The catalysts with a low to medium Ni content exhibited better catalytic performance than those with a higher Ni content or the reference catalyst (conventional steam reforming catalyst, 20 wt% NiO/ $\text{Al}_2\text{O}_3$  + 2 wt%  $\text{K}_2\text{O}$ ). Coking was found to decrease with increasing reaction temperature and to increase with increasing Ni content. No clear relation was observed between coking and catalyst deactivation. So it was concluded that different types of coke could be formed over the catalysts of which not all were deactivating. Since several factors characterising the catalysts (BET surface area, Mg content and available Ni surface) follow the same or the opposite trend with the Ni content, so it was impossible to differentiate between these properties and their effect on the catalyst performance or coking.

The catalyst with an approximate metal composition  $\text{Ni}_{10}\text{Mg}_{62}\text{Al}_{28}$  calcined at  $900^\circ\text{C}$  exhibited the best catalytic performance, a good stability with time-on-stream and a high resistance against coking (the highest at  $800^\circ\text{C}$ ). The partial oxidation of propane performed over this catalyst compared with the results of the non-catalytic reaction showed at least two-fold increase in the yield of CO and eight-fold increase of the  $\text{H}_2$  yield.

Studies of  $\text{O}_2/\text{C}_3\text{H}_8$  feed ratio and the space velocity revealed that the total  $\text{C}_3\text{H}_8$  conversion was only achieved in excess of  $\text{O}_2$  because even under  $\text{O}_2$  deficient conditions part of the  $\text{O}_2$  leads to the total oxidation products  $\text{CO}_2$  and especially  $\text{H}_2\text{O}$ . Coking showed no dependence on the  $\text{O}_2/\text{C}_3\text{H}_8$  feed ratio. Under  $\text{O}_2$  deficient conditions only small amounts of unsaturated hydrocarbons were formed. It was also found that the catalytic partial oxidation of  $\text{C}_3\text{H}_8$  could be performed at gas hourly space velocities as high as  $1200 \text{ dm}^3 \cdot \text{h}^{-1} \cdot \text{g}(\text{catalyst})^{-1}$ .

### **Most important publications related to this work**

Kai Schulze, Waław Makowski, Rafał Chyży, Roman Dziembaj and Günter Geismar 'Nickel doped hydrotalcites as catalyst precursors for the partial oxidation of light paraffins', Proceedings of the International Conference 'Euroclay 1999', 5-9 September 1999, Cracow, Poland, p.131

Kai Schulze, Waław Makowski, Rafał Chyży, Roman Dziembaj and Günter Geismar, 'Verhalten von Ni/Mg/Al-Katalysatoren in der Partiellen Oxidation von Propan', Proceedings of the National Conference on Catalysis (XXXIII. Jahrestreffen Deutscher Katalytiker), 22-24 March 2000, Weimar Germany, p. 250

Kai Schulze, Waław Makowski, Rafał Chyży, Roman Dziembaj and Günter Geismar, 'Synthesis and characterisation of hydrotalcite derived Ni-Mg-Al catalysts for the partial oxidation of propane', Proceedings of the International Symposium 'Catalysis in the XXI century. From quantum chemistry to industry', 4-7 May 2000, Cracow, Poland, p. 104

Kai Schulze, Waław Makowski, Rafał Chyży, Roman Dziembaj and Günter Geismar, 'Syngas production by partial oxidation of light paraffins using mixed metal oxide nickel catalysts', Proceedings of the National Congress on Chemical Technology (III Kongres Technologii Chemicznej), 5-8 September 2000, Gliwice, Poland, published in 'Technologia Chemiczna na Przełomie Wieków' pp. 103-106

Kai Schulze, Waław Makowski, Roman Dziembaj and Günter Geismar, 'Basicity and metal dispersion as factors influencing catalytic performance of Ni catalysts prepared from anionic clay materials', Proceedings of the 'XIV<sup>th</sup> International Symposium on the Reactivity of Solids', 27-31 August 2000, Budapest, Hungary, p. 51

Kai Schulze, Waław Makowski, Rafał Chyży, Roman Dziembaj and Günter Geismar, 'Nickel doped hydrotalcites for the partial oxidation of light paraffins', Appl. Clay Sci. **18** (2001) 59-69

Waław Makowski, Kai Schulze, Iwona Gądek and Roman Dziembaj, 'Basicity of Ni/Mg/Al oxide catalysts studied by temperature programmed desorption of  $\text{CO}_2$  and catalytic test reactions', International Conference on Catalysis 'EuropaCat-5', September 2001, Limerick, Ireland, accepted

---

**Contents**

<b>1.</b>	<b>Introduction.....</b>	<b>1</b>
1.1.	Motivation.....	1
1.2.	Hydrotalcite-type compounds.....	5
1.2.1.	Preparation of hydrotalcite-type compounds (HTs).....	7
1.2.1.1.	Coprecipitation by titration.....	10
1.2.1.2.	Coprecipitation at high supersaturation.....	10
1.2.1.3.	Coprecipitation at low supersaturation.....	10
1.2.1.4.	Hydrothermal treatment at low temperature.....	11
1.2.1.5.	Hydrothermal treatment at high temperature.....	11
1.2.1.6.	Synthesis of HTs containing anions other than carbonate.....	12
1.2.2.	Thermal decomposition.....	15
1.2.3.	Application of HTs and HT derived materials.....	19
1.2.3.1.	HTs as catalyst precursors in heterogeneous catalysis.....	19
1.3.	Production of hydrogen and syngas using hydrocarbon feedstock.....	22
1.3.1.	Steam reforming.....	23
1.3.2.	Other processes for syngas production.....	26
1.4.	Catalyst deactivation.....	27
1.4.1.	Coking.....	28

---

1.4.1.1.	Coking in gas phase reactions.....	30
1.4.1.2.	Coking in gas-solid catalytic reactions.....	31
1.5.	Catalytic partial oxidation.....	33
1.5.1.	Catalytic partial oxidation of methane over Ni catalysts.....	34
1.5.1.1.	Direct syngas formation.....	35
1.5.1.2.	Total oxidation followed by reforming.....	36
1.5.1.3.	Pyrolysis mechanism.....	37
1.5.1.4.	Parallel pathways.....	38
1.5.1.5.	Activation of the catalyst.....	39
1.5.1.6.	State of the active catalyst.....	40
1.5.1.7.	Influence of the reaction conditions.....	42
1.5.1.8.	Stability of the catalysts.....	43
1.5.2.	Catalytic partial oxidation of higher hydrocarbons.....	44
1.6.	The scope of this work.....	45
1.6.1.	Methodology.....	46
<b>2.</b>	<b>Experimental.....</b>	<b>51</b>
2.1.	Synthesis of the hydrotalcite-type solids.....	51
2.2.	Preparation of the catalysts.....	54



---

2.3.	Elemental and structural analysis.....	55
2.4.	Temperature programmed reduction and oxidation.....	56
2.5.	In-situ reduction combined with high temperature XRD.....	58
2.6.	Temperature programmed desorption of CO <sub>2</sub> .....	59
2.7.	Test reactions for determination of basicity.....	60
2.8.	Catalytic partial oxidation of propane.....	61
2.8.1.	Catalytic reactor set up.....	61
2.8.2.	Procedure.....	64
2.8.3.	Modification of the furnace.....	68
<b>3.</b>	<b>Results and discussion - catalyst preparation and characterisation....</b>	<b>73</b>
3.1.	Catalyst precursors.....	73
3.1.1.	Elemental analysis.....	73
3.1.2.	Structural analysis.....	74
3.1.3.	Analysis of the thermal degradation.....	76
3.2.	Catalysts.....	79
3.2.1.	Preparation.....	79
3.2.2.	Structure and morphology.....	79
3.2.3.	BET surface measurements.....	85

---

3.2.4.	Reducibility.....	86
3.2.4.1.	Temperature programmed reduction.....	86
3.2.4.2.	Verifications of the existing reduction model.....	89
3.2.5.	Ni dispersion.....	93
3.2.6.	Temperature programmed oxidation.....	96
3.2.7.	Influence of the calcination temperature on reducibility and Ni dispersion...	98
3.2.8.	Basicity measurements.....	101
3.2.8.1.	Temperature programmed desorption of CO <sub>2</sub> .....	101
3.2.8.2.	Determination of basicity by catalytic test reactions.....	105
<b>4.</b>	<b>Results and discussion - catalytic partial oxidation of propane.....</b>	<b>109</b>
4.1.	Catalytic screening.....	109
4.2.	Catalytic tests of different configurations.....	116
4.2.1.	Blank experiments.....	116
4.2.2.	Active catalyst (reduced Ni10C900).....	118
4.3.	Influence of the O <sub>2</sub> /C <sub>3</sub> H <sub>8</sub> ratio.....	124
4.4.	Influence of the space velocity.....	129
4.5.	Influence of the calcination temperature.....	133

---

<b>5.</b>	<b>Conclusions.....</b>	<b>141</b>
<b>6.</b>	<b>Literature.....</b>	<b>145</b>

## 1. Introduction

### 1.1. Motivation

Hydrotalcite-type anionic clays, which were chosen as catalyst precursors, consist of positively charged metal hydroxide sheets with metals in the oxidation state +2 and +3. The positive charge is compensated by anions intercalated between the sheets, the space between the metal hydroxide layers is further filled with water. These anionic clays exhibit remarkable properties as catalytic precursors [1, 2, 3]. They retain the same structure despite changes in their composition. Another advantage is the uniform distribution of the metal ions in the layers. This allows investigating changes in the catalysts related to the composition, being able to neglect structural differences. Furthermore, as a result of an appropriate activation, metal containing catalysts may be obtained with a good dispersion of metallic particles that are stable at high temperatures even in the presence of steam [1, 4, 5, 6, 7, 8]. Because of that nickel catalysts derived from hydrotalcite-type precursors are regarded as promising catalysts for the study of high temperature reactions such as the catalytic partial oxidation of hydrocarbons to syngas, a mixture of CO and H<sub>2</sub>. Such catalysts have recently been proven successful in the partial oxidation of methane by Basile et al. [9]. The catalytic partial oxidation is attracting much attention as new more economic way to produce hydrogen.

Hydrogen is a widely used feedstock in the chemical, the food and the refining industry. Especially in refineries the production of hydrogen has achieved increased importance in recent years. This is due to the increasing necessity to treat heavier and more contaminated crude oil supplies, the need to produce less heavy fuel oils and the risen demand for higher quantities of transport fuels. Additionally transport fuels of better

---

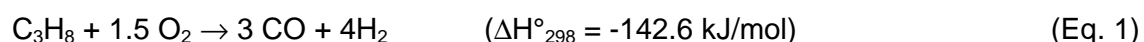
quality are demanded, which must contain less aromatics, less sulphur and nitrogen due to new environmental laws [10, 11, 12, 13]. To fulfill these needs hydrocracking and hydrotreatment are applied, consuming large quantities of hydrogen. Furthermore, the drop in the allowed amount of aromatics in the car fuels led to a reduction of the amount of hydrogen produced as side product in other refinery processes. All this led to a sharp increase in the need of refineries for hydrogen. It was projected in 1994 that between 1994 and 2000 the hydrogen growth rate would be approximately 10% per year in the USA and in 21% in Western Europe [10], making the installation of new units for the production of hydrogen necessary. This trend is believed to continue further in the next years [10, 11, 14].

On an industrial scale hydrogen is mainly produced by the transformation of fossil fuels to syngas ( $\text{CO} + \text{H}_2$ ). The environmentally attractive water splitting to yield  $\text{H}_2$  and  $\text{O}_2$  is very endothermic ( $\Delta H_f^\circ (\text{H}_2\text{O}) = -285.85 \text{ kJ/mol}$  [15]). Therefore it is currently far from being economically viable on a large scale and is projected to be suitable only in the long run, at the end of the 21<sup>st</sup> century or even later [11]. One process widely applied in refineries is the non-catalytic partial oxidation of hydrocarbons in which hydrocarbons are transformed into syngas by the exothermic partial oxidation with oxygen. As it is a non-catalysed process it requires high reaction temperatures, making it only economically viable when so called bottom-of-the-barrel feedstock is used, which is of low quality and difficult to process [10, 11, 16]. The main process currently applied for the production of hydrogen is catalytic steam reforming. Here hydrocarbons are transformed into syngas by the endothermic reaction with steam. This process has been well established and optimised over the decades. Most often nickel catalysts, which combine low costs and high activity are used [17, 18]. Methane as well as other alkanes and naphtha can be used as feedstock. The most important problem of this technology is catalyst deactivation, mainly due to coking. Coking can be minimised by

the choice of the reaction conditions, especially by the use of excess steam and higher reaction temperatures as well as by the choice of the catalyst. Catalysts with high nickel dispersion and basic additives are known to minimise coke formation. Despite all this, the steam reforming process faces several drawbacks, the most significant one being the large energy input needed for the reaction. Consequently the exothermic catalytic partial oxidation has received considerable attention over the last few years. It is thought to be the most economic way to produce hydrogen, cutting the costs by 25% compared to steam reforming [10].

Research concerning the catalytic partial oxidation has been focused on methane, as it is a major feedstock for the production of hydrogen. As in the related steam reforming process the main reason for the catalyst deactivation is coking. Currently the main interest is in coke resistant nickel catalysts. In contrast to methane, only introductory studies concerning the partial oxidation of higher hydrocarbons have been reported in open literature. These studies have been limited to noble metal catalysts [19, 20, 21, 22, 23]. Like in the steam reforming process noble metal catalysts do not seem to be acceptable for this process due to their high cost.

The aim of this work is the development of inexpensive, active and stable Ni catalysts for the catalytic partial oxidation of light paraffins using propane as a model substance (Eq. 1).



Such a process may lead to the broadening of the feedstock used in catalytic partial oxidation, being more suitable for refineries where the whole range of inexpensive C<sub>1</sub>-C<sub>4</sub> alkanes could be used [12, 24]. Furthermore, natural gas, the main source for

---

methane, contains considerable amounts of light paraffins, mainly ethane and propane [11], which are more prone to coking than methane. In the steam reforming of methane these fractions are prereformed, before entering the steam reformer. For the partial oxidation of natural gas this might not be necessary, instead converting all natural gas fraction simultaneously to syngas. This would simplify the process and the reactor design. A basic necessity for this would be the development of a catalyst also suitable for the partial oxidation of light paraffins.

As propane is much more prone to coking than methane factors concerning the resistance against coking of the nickel catalysts may be much better studied than using methane. Here, in analogy to the related steam reforming process, especially the influence of the reaction conditions, the nickel dispersion and the basicity of the catalysts are of interest. The influence of the reaction conditions can be practically studied on any catalyst, but for the determination of the influence of the Ni dispersion and the basicity of the catalysts it is necessary to be able to exclude structural differences between the catalysts.

In order to fulfill all these requirements and demands Ni/Mg/Al catalysts derived from hydrotalcite-type precursors have been chosen for this project. They are inexpensive basic nickel catalysts and are expected to be active and stable in the partial oxidation of propane, having already proven their activity and stability in the partial oxidation of methane. Another reason is that  $\text{Ni}^{2+}$  can substitute  $\text{Mg}^{2+}$  in hydrotalcite-type anionic clays, and hence the Ni dispersion and the basicity of the catalysts can be varied, without significant structural changes in the hydrotalcite-type precursor or the calcined catalyst. This allows studying the influence of the basicity and the Ni dispersion on the coke resistance of the catalysts.

## 1.2. Hydrotalcite-type compounds

Hydrotalcite,  $\text{Mg}_6\text{Al}_2(\text{OH})_{16}\text{CO}_3 \cdot 4\text{H}_2\text{O}$ , is a natural occurring anionic clay. It was first discovered in Sweden around 1842 and its name derives from the fact that it can be easily crushed into a white powder similar to talc [1, 25]. The structure of hydrotalcite can be derived from brucite,  $\text{Mg}(\text{OH})_2$ , which exhibits layers of edge-sharing hydroxide octahedra centred by magnesium according to  $\text{Mg}(\text{OH})_{6/3}$  (Fig. 1). The sheets are stacked one on top of the other and are held together by weak interactions through hydrogen bonds. Isomorphous replacement of  $\text{Mg}^{2+}$  ions by  $\text{Al}^{3+}$  results in an overall positive charge of the layers. The positive charge is compensated by the intercalation of  $\text{CO}_3^{2-}$  in the interlayer space. Also the equilibrium products of aqueous  $\text{CO}_3^{2-}$  solutions ( $\text{OH}^-$ ,  $\text{HCO}_3^-$ ) are present in the interlayer space as water molecules are also intercalated. The water molecules participate in hydrogen bonding to the hydroxide layers [1, 2, 25, 26].

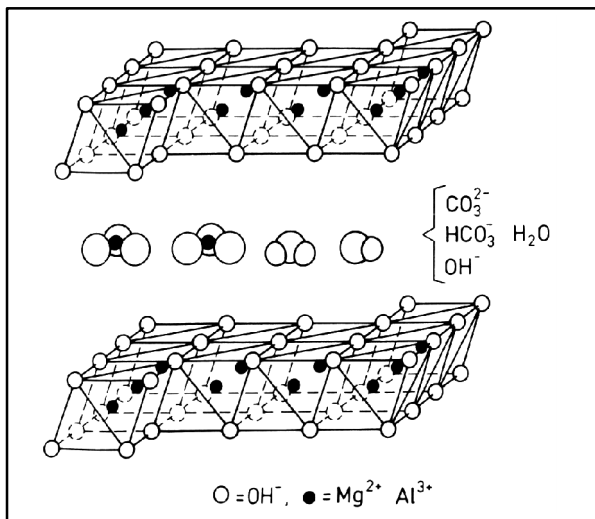


Fig. 1  
Structure of hydrotalcite [27]



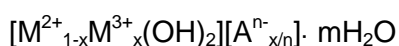
At the same time as hydrotalcite, a compound of the composition  $\text{Mg}_6\text{Fe}_2(\text{OH})_{16}\text{CO}_3 \cdot 4.5\text{H}_2\text{O}$  was found, called pyroaurite due to its likeness to gold when heated. Later pyroaurite was recognised to be isostructural with hydrotalcite. In nature many compounds have been found, which have the approximate composition  $\text{M}(\text{II})_6\text{M}(\text{III})_2(\text{OH})_{16}\text{CO}_3 \cdot 4\text{H}_2\text{O}$  and which are isomorphous to hydrotalcite. Also minerals like sjögrenite,  $\text{Mg}_6\text{Fe}_2(\text{OH})_{16}\text{CO}_3 \cdot 4.5\text{H}_2\text{O}$ , have been found that have also the approximate formula  $\text{M}(\text{II})_6\text{M}(\text{III})_2(\text{OH})_{16}\text{CO}_3 \cdot 4\text{H}_2\text{O}$  and the same layered structure but a different stacking sequence, corresponding to a hexagonal instead a rhombohedral symmetry. Some naturally occurring minerals of these two polytype structures are presented in Table 1.

Tab. 1: Composition and symmetry of some natural anionic clays [1, 2]

Name	Chemical composition	Symmetry
Barbertonite	$\text{Mg}_6\text{Cr}_2(\text{OH})_{16}\text{CO}_3 \cdot 4\text{H}_2\text{O}$	hexagonal
Desautelsite	$\text{Mg}_6\text{Mn}_2(\text{OH})_{16}\text{CO}_3 \cdot 4\text{H}_2\text{O}$	rhombohedral
Hydrotalcite	$\text{Mg}_6\text{Al}_2(\text{OH})_{16}\text{CO}_3 \cdot 4\text{H}_2\text{O}$	rhombohedral
Manasseite	$\text{Mg}_6\text{Al}_2(\text{OH})_{16}\text{CO}_3 \cdot 4\text{H}_2\text{O}$	hexagonal
Pyroaurite	$\text{Mg}_6\text{Fe}_2(\text{OH})_{16}\text{CO}_3 \cdot 4.5\text{H}_2\text{O}$	rhombohedral
Reevesite	$\text{Ni}_6\text{Fe}_2(\text{OH})_{16}\text{CO}_3 \cdot 4\text{H}_2\text{O}$	rhombohedral
Sjögrenite	$\text{Mg}_6\text{Fe}_2(\text{OH})_{16}\text{CO}_3 \cdot 4.5\text{H}_2\text{O}$	hexagonal
Stichtite	$\text{Mg}_6\text{Cr}_2(\text{OH})_{16}\text{CO}_3 \cdot 4\text{H}_2\text{O}$	rhombohedral
Takovite	$\text{Ni}_6\text{Al}_2(\text{OH})_{16}\text{CO}_3 \cdot 4\text{H}_2\text{O}$	rhombohedral

### 1.2.1. Preparation of hydrotalcite-type compounds (HTs)

Many compounds with the same structural elements as the above mentioned compounds have been synthesised and also found in nature. They will be referred to in the following as hydrotalcite-type compounds (HTs) as in most publications, though they are frequently also referred to as Feitknecht's compounds, mixed hydroxides or layered double hydroxides. Since not only the metals can be exchanged in a wide range, but also the anion present, their formula is best described as:



where M are metal cations and A are anions

Though a great variety of HT compounds with even more than three different metals and several anions have been synthesised, three fundamental rules need to be fulfilled to obtain pure HT phases [1, 25]:

The first one concerns the radii of the metals ions. Though a wide range of metal cations in the oxidation state +2 and +3 can be used for the preparation of HTs, their radius should not be too different from that of  $Mg^{2+}$ . For example  $Be^{2+}$  is too small to form HTs,  $Ca^{2+}$  and  $Cd^{2+}$  are too large (Tab. 2). They give rise to other types of compounds [1, 25]. Nevertheless natural and synthetic HTs containing small amounts of 'large cations' like  $Ca^{2+}$  and  $Cd^{2+}$  have been described in the literature [1, 25, 44]. The synthesis of HTs containing ions that have a suitable ion radius but favour a distorted octahedral structure due to the Jahn-Teller effect, like  $Cu^{2+}$ ,  $Ni^{3+}$ ,  $Mn^{3+}$ , is more difficult because these ions are prone to form separate phases [1, 25, 28]. Studies on Cu containing hydrotalcites by extended X-ray adsorption fine structure

(EXAFS), X-ray adsorption near edge structure (XANES), electron spin resonance (ESR) and X-ray photoemission spectroscopy (XPS) revealed that the hydroxide ions surrounding the  $\text{Cu}^{2+}$  ions are situated at the vertices of a distorted octahedra [29, 30, 31].

Tab. 2: Ionic radius of some divalent and trivalent cations (pm) [1, 25]

<b>M<sup>2+</sup></b>	Be	Mg	Cu	Ni	Co	Zn	Fe	Mn	Cd	Ca
	30	65	69	72	74	74	76	80	97	98
<b>M<sup>3+</sup></b>	Al	Ga	Ni	Co	Fe	Mn	Cr	V	Ti	In
	50	62	62	63	64	80	69	74	76	81

The second rule for the preparation of HTs concerns the ratio of the cations  $\text{M(II)}_{1-x}\text{M(III)}_x$ . The synthesis of pure HTs has been claimed in the range  $x = 0.1$  to  $0.5$ , but the formation of amorphous side phases not detectable by powder X-ray diffraction (XRD) may have occurred. These amorphous side-phases may be detected by thermogravimetry (TG), electron microscopy and solid state  $^{27}\text{Al}$  MAS-NMR (magic angle spin-nuclear magnetic resonance) [1, 2, 25, 32]. The range  $0.2 \leq x \leq 0.33$  is generally acknowledged to be suitable for the synthesis of HT compounds. According to Brindley and Kikkawa [1, 2, 25], at  $x > 0.33$  the increased number of neighbouring Al-containing octahedra leads to the formation of  $\text{Al(OH)}_3$  and, analogously, values of  $x < 0.2$  lead to a high density of Mg-containing octahedra in the brucite-like sheets resulting in the precipitation of  $\text{Mg(OH)}_2$ . However, these limits of the value of  $x$  must be regarded as the maximum interval, which can be narrower depending on the composition of the HT. For instance the successful synthesis of HTs of the metal composition  $\text{Ni}_{1-x}\text{Al}_x$  was reported only in the range of  $0.25 \leq x \leq 0.33$  [4, 6, 33].

The third rule is that the positive charge of the brucite-type layers due to the trivalent metal ions must be neutralised by the intercalation of anions according to:

$$\frac{[A^{n-}]}{[M^{3+}]} = \frac{1}{n} \leq 1$$

$[A^{n-}]$  = amount of anions,  $n$  = charge of anion,  $[M^{3+}]$  = amount of trivalent metal ions

Though numerous anions have been intercalated there are some general limitations [1, 2, 25, 34, 35, 36]. Most important is that the anions are stable at the same pH as the HT and stable with respect to hydrolysis. Another problem is the purity and crystallinity of the materials. For example, when preparing HTs with anions different than carbonate great care has to be taken to avoid contamination of CO<sub>2</sub> because of the high stability of carbonate containing HTs, due to the formation of strong hydrogen bonds. Furthermore, line broadening in the XRD patterns and the possible presence of amorphous phases or adsorbed species at the HT surface may prevent definite answers.

HTs are commonly prepared by coprecipitation. In order to coprecipitate two or more cations it is necessary to carry out the precipitation under the condition of supersaturation [1]. Usually supersaturation is achieved by physical (evaporation) or chemical (variation of pH etc.) methods. For the preparation of HTs the method of pH variation is most frequently used. The pH value must be chosen carefully because if it is too low not all the different metal ions will precipitate together and if it is too high the dissolution of one or more metal ions may occur. The pH value needed for the precipitation of HTs is not necessarily equal to the pH value of the precipitation of the most soluble metal hydroxide. For instance pure Al(OH)<sub>3</sub> precipitates at pH 4.5 and

$\text{Ni}(\text{OH})_2$  around pH 7 and  $\text{Mg}(\text{OH})_2$  at pH 9.5 [1, 37], whereas Ni/Al-HT precipitates already at pH 4.0-4.5 and Mg/Al-HT at 7.7-8.5 as determined by potentiometric titration [1]. Generally HTs are synthesised at pH 7-10. Three variations of the method of pH variation have been reported in the literature [1, 2, 25].

#### **1.2.1.1. Coprecipitation by titration**

In the titration method the metal salt solution is titrated by a basic solution. By this method often not only solids of HT structure, but also other solid phases are formed, due to the precipitation of less soluble metal hydroxides prior to the precipitation of the HT.

#### **1.2.1.2. Coprecipitation at high supersaturation**

During the precipitation at high supersaturation the metal ions containing solution is simply quickly added to the basic solution or the solutions are mixed together rapidly. The concentrations of the solutions are rather high ( $> 2 \text{ mol/l}$ ). The precipitants are generally not very crystalline and sometimes even amorphous, owing to the high number of crystallisation nuclei created by the rapid mixing and the high concentrations of the solutions.

#### **1.2.1.3. Coprecipitation at low supersaturation**

Coprecipitation at low supersaturation at constant pH is the method most frequently used in the preparation of HTs. It usually yields the most crystalline precipitate. Normally, both the solution containing the metal salts containing solution and the base solution are low in concentration ( $0.5 - 2 \text{ mol/l}$ ). They are mixed together slowly in a

---

separate vessel at constant pH and at temperatures between 60-80°C. This method ensures the best condition to obtain crystalline material of pure HT structure. This is mainly due to the fact that at constant pH the rate of crystal growth is generally lower than the rate of nucleation. This method is most often used, as it is the most effective one. For example in the preparation of Cu/Co/Al hydrotalcites catalysts, Marchi et al. obtained an amorphous precipitate by coprecipitation at high supersaturation while under the conditions of low supersaturation a crystalline HT was precipitated [1].

In all three methods of coprecipitation the precipitants are washed with distilled water in order to eliminate adsorbed ions and are dried at temperatures up to 120°C [1, 25]. To improve the degree of crystallinity of the freshly precipitated HTs and to turn amorphous phases into crystalline ones, the precipitates can be hydrothermally treated. Two different forms of hydrothermal treatment are frequently applied [1, 25].

#### **1.2.1.4. Hydrothermal treatment at low temperature**

Hydrothermal treatment at low temperature is also often referred as 'ageing'. In its most simple form, it does not need special equipment. The freshly precipitated HT is kept in a heated aqueous suspension at temperatures below 100°C. Stirring can be applied [1, 25]. It generally increases the crystallinity of the precipitates. However, it has been reported for Cu containing HTs that this treatment led to the partial destruction of the HT structure with the formation of a malachite-like side phase [2, 25].

#### **1.2.1.5. Hydrothermal treatment at high temperature**

Autoclaves must be used, because this treatment requires temperatures above 100°C and high pressure. The efficiency of the hydrothermal treatment at high temperature is

generally far larger than that at low temperatures. Under the conditions of hydrothermal treatment at high temperatures even the preparation of HTs from mechanical mixtures of the metal oxides in aqueous solution in the presence of CO<sub>2</sub> has been reported in the literature [1, 25].

#### 1.2.1.6. Synthesis of HTs containing anions other than carbonate

The synthesis of HTs with a wide range of different anions has been reported in the literature [1, 2, 4, 25, 27, 31, 33, 34, 35, 36, 38, 39, 40, 41, 42, 43, 45, 46, 47, 48, 49, 50, 51, 52]. These can be divided into five classes:

- Simple halides and oxyanions [Cl<sup>-</sup>, ClO<sub>4</sub><sup>-</sup>, CO<sub>3</sub><sup>2-</sup>, NO<sub>3</sub><sup>-</sup>, SO<sub>4</sub><sup>2-</sup>, OH<sup>-</sup>, CrO<sub>4</sub><sup>2-</sup>, WO<sub>4</sub><sup>2-</sup>, S<sub>2</sub>O<sub>3</sub><sup>2-</sup>, etc.]
- Iso- and heteropolyanions [V<sub>10</sub>O<sub>28</sub><sup>6-</sup>, Mo<sub>7</sub>O<sub>24</sub><sup>6-</sup>, PMo<sub>12</sub>O<sub>40</sub><sup>3-</sup>, PW<sub>12</sub>O<sub>40</sub><sup>3-</sup>, NaP<sub>5</sub>W<sub>30</sub>O<sub>110</sub><sup>16-</sup> etc.]
- Complex anions [Fe(CN)<sub>6</sub><sup>3-</sup>, Fe(CN)<sub>6</sub><sup>4-</sup> etc.]
- Organic anions [carboxylates and dicarboxylates, benzenecarboxylates, alkylsulphates, chlorocinnamate etc.]
- Layer compounds like the mineral chlorite [(Mg, Fe, Al)<sub>6</sub>[(Si, Al)<sub>4</sub>O<sub>10</sub>](OH)<sub>8</sub>]

Of special interest is the synthesis of HTs with large and highly charged anions, because they increase the spacing between the brucite-like layers (gallery height) and decrease the anion population in the interlayer (Tab. 3). This can have several purposes like the enlargement of the gallery height in order to obtain larger porous volume and a larger surface area in the HT as well as providing space in the interlayer region for other guest species [1, 2, 25].

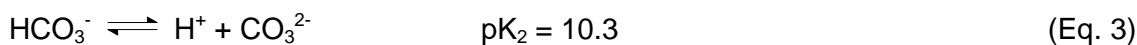
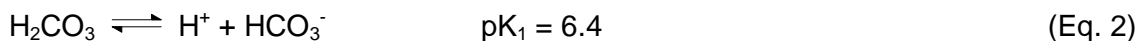
Tab. 3: Gallery heights for HTs with different anions [25,35]

Anion	Gallery height [ $\mu\text{m}$ ]
$\text{CO}_3^{2-}$	290
$\text{SO}_4^{2-}$	390
$\text{CrO}_4^{2-}$	390
$\text{HVO}_4^{2-}$	460
$\text{V}_{10}\text{O}_{28}^{6-}$	690
$\text{HV}_4\text{W}_8\text{PO}_{40}^{6-}$	970
$\text{NaP}_5\text{W}_{30}\text{O}_{110}^{16-}$	1590

Most important for their synthesis is that the anions are stable at the same pH value as the HT and that they are stable with respect to hydrolysis. Only anionic complexes can be incorporated into the interlayer structure. Cationic complexes are only adsorbed on the outer surface of the HT crystallites [25]. Three methods are generally used for the preparation of HTs with unusual anions.

Coprecipitation of the HTs in the presence of the desired anion is the most straightforward method. Without special care taken for the exclusion of carbon dioxide sources (degassed water, inert gas atmosphere, etc.) it is impossible to prepare carbonate free HTs, due to the high affinity of  $\text{CO}_2$  to the positively charged brucite-like layers. The only exception is when the preparation of the HT is possible at pH-value  $\leq 5$ , because at this pH-value virtually no carbonate is present in solution which can be explained by Equation 2 and 3 [4, 33]. Despite all precautions coprecipitation is not always suitable due to the possible formation of side phases during the synthesis.





Another method is to exchange the anion present in the interlayer. This method is comparable to the widely studied cation exchange of cationic clays, but in HTs anions are exchanged. However, the ion exchange in HTs is more difficult than in smectite-type clays, their cationic counterpart, due to the higher charge density of HTs in comparison to smectites,  $4\text{e}/\text{nm}^2$  to  $1\text{e}/\text{nm}^2$ , respectively [2, 25, 35]. Therefore anions with high charge density are needed. Inorganic as well as organic ions can be exchanged. Next to the fundamental necessities, mentioned above, there are several other factors concerning the applicability of this method. The anion present in the HT must be easily exchangeable. Therefore carbonated HTs are only of very limited use for the classical ion exchange as carbonate is not easy exchangeable and its destruction by diluted mineral acids can lead simultaneously to the destruction of the HT [27, 40]. Hence carbonate free HTs must be used as precursors. The crystal size has also a great influence on the rate of the ion exchange, too big crystals may even inhibit the exchange [27]. For the intercalation of very large anions, like many polyoxoanions, the interlayer space of the HT must be increased before the ion exchange. This can be achieved by keeping the HT in an aqueous suspension, the use of swelling agents such as glycerol, glycol or long chain alcohols or by using HT precursors that contain large organic anions such as terephthalate, p-toluensulphonate or 4-hydroxybenzoate [2, 25, 35, 45].

In the method of structure reconstruction the first step is transformation of the HTs into mixed metal oxides by calcination at temperatures between 250 and 850°C. Such mixed metal oxides derived from HT precursors have a 'memory' of the HT. Due to this

---

'memory effect' the mixed metal oxides prepared from HT precursors can rebuild the HT structure. The memory can be activated in contact with water, water vapour and especially aqueous solutions containing anions [1, 2, 7, 25, 38, 41, 47, 49, 53, 54, 55, 56]. In contrast to the other two methods usually carbonate containing HTs are used as precursors, because of the high volatility of carbonate. It must be pointed out that the reconstruction of the mixed metal oxide to the HT is never complete, because during the formation of the mixed metal oxide a certain amount of a spinel phase is formed which does not reconstruct. The amount of the spinel phase formed generally increases with increasing calcination temperature. Therefore the property of the 'memory effect' is strongly temperature dependent and great care must be taken for keeping the calcination temperature as low as possible [25, 55, 56].

### **1.2.2. Thermal decomposition**

During the heating of HTs three different temperature regions can be found [57]:

100 - 250°C: Water in the interlayer is lost reversibly. The morphology of the HT is maintained. Lost water can be reabsorbed from the air.

250 - 850°C: The brucite-type sheets are dehydroxylated resulting in the formation of a mixed metal oxide. Intercalated anions that are thermally easily destructible, like carbonate and nitrate, are also decomposed. The sheet structure is maintained during the dehydroxylation, no delamination is taking place. Steam and volatiles escape through small and fairly regularly spaced holes in the crystal surface. It appears that the interlaminar forces in the HTs are sufficiently strong even during the heating to prevent intersistal venting, which would result in the delamination of the sheet structure [58]. Investigations concerning a Mg/Al HT calcined at 300°C revealed that a

---

metastable phase is formed, which becomes obscure in a tight sealed silica gel filled desiccator and easily reconstructs to a HT in a humid atmosphere [57]. At temperatures above 500°C the HTs are generally completely transformed into mixed metal oxides. These mixed metal oxides also have the 'memory effect'. The XRD of the mixed metal oxides reveals generally only the presence of a divalent metal oxide phase of low crystallinity.

Studies concerning the structure revealed 3 separate phases [7, 53]. A M(II)O-phase, a M(II)O doped M(III)<sub>2</sub>O<sub>3</sub> phase and a spinel-type phase at their interface, decorating the M(II)O phase. The decoration of the M(II)O phase by the spinel phase is believed to be responsible for the high stability of the materials against heat, steam, sintering and reduction of the M(II)O phase as shown for Ni/Al catalysts derived from HT precursors [6, 7, 53, 59]. With increasing calcination temperature increases the amount of the spinel phase. Due to the fact that the well crystallised spinel phase does not reconstruct the 'memory effect' diminishes with increasing temperature [25, 55, 56]. It has also been shown that the crystallinity of the M(II)O phase increases with increasing calcination temperature resulting in larger M(II)O particles [8, 60].

Above 850°C: The HT is transformed into its final product a mixed metal oxide consisting of well-crystallised stoichiometric spinel and divalent metal oxide phases [25]. Indeed all divalent and trivalent cations that were found to be able to form HTs also give rise to spinel phases. At this final stage of the thermal evolution process, the solids have completely lost the 'memory effect'. They do not reconstruct anymore, due to the stability of the spinel phases [25, 54, 55].

The exact temperatures for the transitions depend qualitatively and quantitatively on several factors. The most important ones are the nature and relative amount of the

metal cations, the nature of the anions and the crystallinity of the HT. For instance results the substitution of  $Mg^{2+}$  or  $Al^{3+}$  ions by transition metal ions such as  $Co^{2+}$ ,  $Cu^{2+}$ ,  $Ni^{2+}$  or  $Fe^{3+}$  in a decrease in the thermal stability of the HT [61, 62, 63]. Another example is that the temperature of the reversible loss of the intersistal water in  $Mg_{1-x}Al_x$  HTs decreases with decreasing amount of Al from 200°C for  $x = 0.33$  to 160°C for  $x = 0.2$  as determined by in situ high temperature XRD [57]. The type of anions can have an even greater effect, e.g. the thermal destruction of bromate in HTs occurs at around 200°C whereas sulphate in the interlayer region decomposes only at temperatures as high as 930-970°C [25]. HT materials with a lower degree of crystallinity show less defined temperature profiles in TG analyses, especially for the first weight loss, which is due to the loss of intersistal water [1, 25, 60]. The ability to reconstruct also depends on the metal composition of the HT precursors. Mg/Al mixed metal oxides derived from HT precursors by calcination at temperatures lower than that required for the formation of a separate spinel readily rehydrate to reconstruct the HT structure, whereas their Ni/Al counterparts calcined at the same temperatures are even stable in hot aqueous NaOH solution at atmospheric pressure. Their reconstruction was only observed upon the energetic stirring of their aqueous suspensions at 250°C at 4 MPa during 12 hours [7, 53].

It must also be pointed out that during the thermal evolution HTs containing variable valence metal ions can lead to the occurrence of other phases than those discussed above. Infra red (IR) investigations concerning Ni/Cr calcined at 450°C in air showed the presence of  $NiCrO_4$  and NiO. The same HT sample calcined at the same temperature, but in vacuum instead of air exhibited no evidence for the oxidation of Cr(III) to Cr(VI) [8, 60]. However NiO and  $NiCr_2O_4$  were the final product of the calcination performed in air and in vacuum. The temperature for the formation of the final product was slightly lower for the sample calcined in air (550°C) than in vacuum

(600°C). For Ni/Al HTs the formation of the final product, spinel and divalent metal oxide phase, was only detected after calcination  $\geq 900^\circ\text{C}$ , showing the great influence of the nature of the trivalent anion on the thermal evolution of the HTs [4, 8, 33, 60].

The calcination temperature has a significant effect on the surface area of the metal oxide systems derived from HT phases (Fig. 2). Their surface area increases upon the reversible loss of interstitial water and the dehydroxylation of the brucite-type metal hydroxide layers up to the point where the HTs are completely transformed into mixed metal oxides. Above this point a steady decrease of the surface area with increasing calcination temperature is observed. The decrease of the surface area may be due to the formation of divalent metal oxide and spinel phases and their improving crystallinity with increasing temperature.

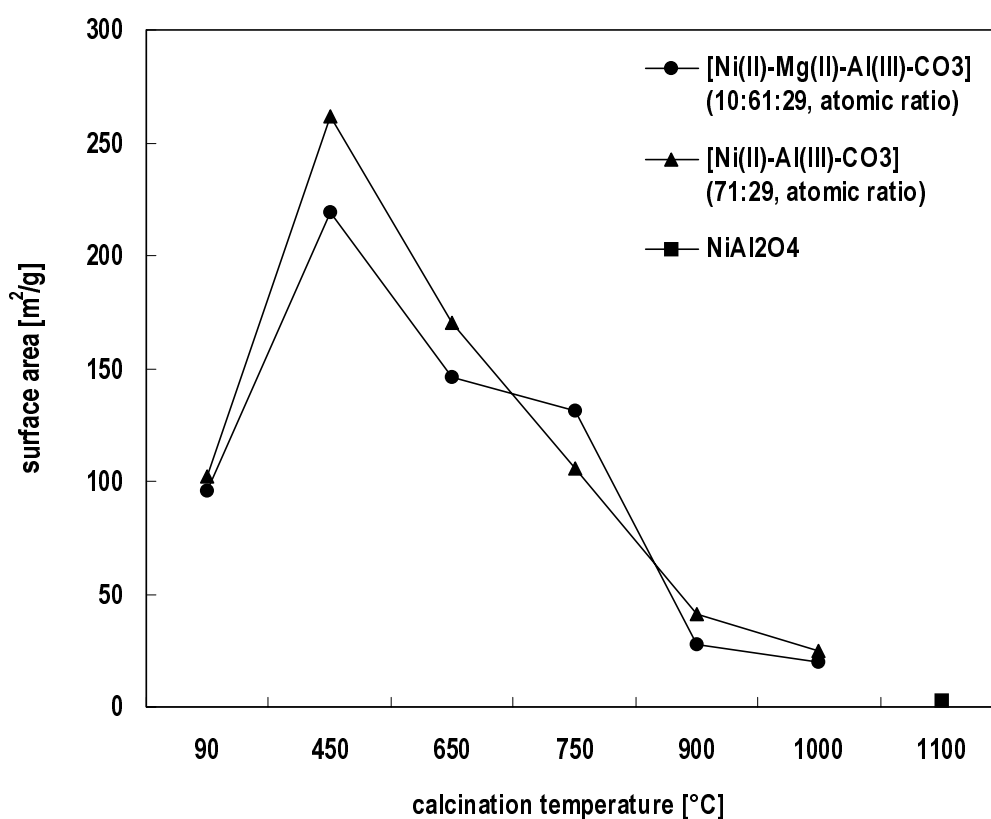


Fig. 2  
Change of surface area during calcination of Ni containing HTs [25]

### **1.2.3. Applications of HTs and HT derived materials**

Because of their interesting properties discussed above HTs and HT derived materials are used for many applications such as waste water treatment, ion exchanger, molecular sieves, halogen free flame retardant, antiacids, stabilisers for polymers, pharmaceuticals and agricultural goods, additive to rubbers, halogen scavenger and heterogeneous catalysts [1, 2, 64].

#### **1.2.3.1. HTs as catalyst precursors in heterogeneous catalysis**

In the field of heterogeneous catalysis HTs themselves are not used, but mixed metal oxides derived from HT precursors are used for various applications (Tab. 4). They have various inherent advantages [1, 2, 7, 25, 53]. HTs can contain basic metal ions like  $Mg^{2+}$ , giving the final catalysts basic properties, hence their wide spread industrial use as solid bases for example. Furthermore HTs have the same structure regardless the composition allowing the substitution of suitable metal ions without changing the morphology and hence structure related properties, like the high surface area found for HT derived catalysts. Another important advantage of HT precursors is the uniform distribution of the metal ions in the brucite-type sheets as this means that the metal ions are evenly mixed in the precursor. By the perfect mixing of the elements synergetic effects between the elements are favoured not only in the HT, but also in the final catalysts. The uniform distribution of the metal ions is also responsible for the formation of well dispersed and stable metal particles as a result of an appropriate calcination and reduction procedure [2, 3, 65]. HT derived catalysts generally exhibit a high thermal stability, crucial for any high temperature applications.

Tab. 4: Composition of the HT catalyst precursor and their catalytic application [1]

Composition	Catalytic application
$\text{Mg}_6\text{Al}_2\text{CO}_3(\text{OH})_{16} \cdot 4 \text{H}_2\text{O}$	dehydration, catalyst support
$\text{Ni}_6\text{Al}_2\text{CO}_3(\text{OH})_{16} \cdot 4 \text{H}_2\text{O}$	methanation, hydrogenation, dealkylation
$\text{Ni}_3\text{Mg}_3\text{Al}_2\text{CO}_3(\text{OH})_{16} \cdot 4 \text{H}_2\text{O}$	hydrogenation, dealkylation, cracking
$\text{Co}_3\text{Mg}_3\text{Al}_2\text{CO}_3(\text{OH})_{16} \cdot 4 \text{H}_2\text{O}$	hydrogenation
$\text{Co}_6\text{Al}_2\text{CO}_3(\text{OH})_{16} \cdot 4 \text{H}_2\text{O}$	hydrogenation
$\text{Ni}_{0.9}\text{Co}_{0.75}\text{Cu}_{0.35}\text{Mg}_4\text{Al}_2\text{CO}_3(\text{OH})_{16} \cdot 4 \text{H}_2\text{O}$	hydrogenation, dehydrogenation
$\text{Cu}_3\text{Mg}_3\text{Al}_2\text{CO}_3(\text{OH})_{16} \cdot 4 \text{H}_2\text{O}$	dehydrogenation of secondary alcohols to ketons, hydrogenation of nitro groups
$\text{Cu}_6\text{Al}_2\text{CO}_3(\text{OH})_{16} \cdot 4 \text{H}_2\text{O}$	isomerisation, hydrogenation of nitro groups, dehydrogenation of secondary alcohols to ketons
$\text{Cu}_3\text{Zn}_3\text{Al}_2\text{CO}_3(\text{OH})_{16} \cdot 4 \text{H}_2\text{O}$	dehydrogenation of secondary alcohols to ketons
$\text{Ni}_3\text{Zn}_3\text{Al}_2\text{CO}_3(\text{OH})_{16} \cdot 4 \text{H}_2\text{O}$	hydrogenation
$\text{Ni}_3\text{Mg}_3\text{Al}_{1.8}\text{Cr}_{0.2}\text{CO}_3(\text{OH})_{16} \cdot 4 \text{H}_2\text{O}$	hydrogenation

It is well known that the metal cations present in the brucite-type sheets of the HTs play a key role for the catalytic properties of the final catalyst as the catalytic behaviour depends greatly on the chosen metals as the catalytic centres [1]. However, also the anions present between the layers of the HTs can have an important influence on the catalytic properties. The anions present in the HT can also have an effect on other properties like the crystal size of the catalyst. Ni/Al derived from HTs containing carbonate showed smaller crystallite sizes of the NiO and metallic Ni particles and also generally higher activities than those containing nitrate and especially chloride [4, 42, 59, 66]. Nitric oxides, formed upon the calcination of nitrate containing HTs and

---

chloride enhance sintering of the NiO particles. Chloride is also a poison for the catalytic activity of Ni. However, the sintering due to the nitric oxides has been suggested to be avoidable by the fast removal of the nitric oxide gases by a stream of air. Fine crushing of the sample further assists the fast removal during calcination [4, 59, 66]. It was also pointed out that under such conditions also water is quickly removed. Water also leads to sintering of NiO particles. Schaper et al. also reported that the effect of Ni particle sintering due to the evolution of nitric oxide gases can be avoided by carrying out the calcination in a flow of hydrogen by which the nitric oxides should be reduced to nitrogen or ammonia [66]. Also adsorbed species can influence the catalytic behaviour. For example catalysts derived from HTs prepared from sodium containing solutions can contain Na salts due to insufficient washing of the HTs after coprecipitation. Na ions are a poison for steam reforming and methanisation catalysts [1, 4, 59].

The HT derived mixed metal oxides can be doped with any additional metal ions by impregnation methods [1, 25]. For metal ions that are not suitable for the preparation or the intercalation of HTs this is the only way of their introduction to the catalyst. The 'memory effect' can be activated by contact with water and even more by aqueous solutions containing anions. Therefore impregnation is best performed in anhydrous solvents such as anhydrous ethanol, which are able to dissolve many metal salts but do not activate the 'memory effect' [67].

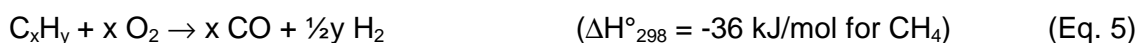
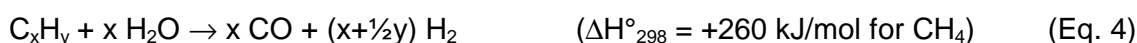
For many technical applications a good mechanical stability of the catalysts is crucial. The mechanical stability of the mixed metal oxides derived from HT precursors can be improved by using a support. Silicates, hydrated aluminium, aluminium-, zirconium- and titanium oxide as well as graphite are suitable supports [1]. Two different procedures have been used for the preparation of supported HTs [1, 5, 6, 66]. Most

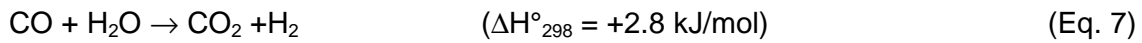
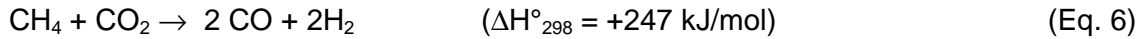


commonly the HTs are directly precipitated onto the support. The HTs are afterwards calcined together with the support yielding the supported mixed metal oxide catalyst. The second method is deposition-precipitation on preformed pellets of theta and gamma alumina, successfully applied in the synthesis of Ni/Al catalysts [66]. Pellets of alumina are impregnated with a solution containing only of the M(II) salt. An initially high pH value is used to dissolve part of the aluminium ions of the support, e.g. as  $[\text{Al}(\text{OH})_4]^-$ . This way the support provides the aluminium ions, which then react with the M(II) ions of the solution, forming HT phases on the support surface and inside the pores upon lowering the pH value. Noteworthy, that this method was not successful using alpha alumina pellets, which has been attributed to the low surface area and the stability of this support material against hydroxide ions.

### 1.3. Production of hydrogen and syngas using hydrocarbon feedstock

Industrial processes designed to produce hydrogen or syngas are mainly based on the conversion of hydrocarbons to syngas a mixture of CO and H<sub>2</sub> with steam (Eq. 4), or with oxygen (Eq. 5). On a much smaller scale also CO<sub>2</sub> reforming of methane is used (Eq. 6). Steam reforming and CO<sub>2</sub> reforming are highly endothermic processes, whereas the partial oxidation is slightly exothermic. To maximise the production of hydrogen or to adjust the CO/H<sub>2</sub> ratio the reversible water gas shift reaction is used (Eq. 7). As hydrogen and syngas are produced in the same manner their production processes will be discussed together.





The production of syngas using coal as feedstock was discovered already at the end of the 18<sup>th</sup> century [68]. Coal gasification is a well-established commercial technology. Modern processes for the coal gasification are autothermal processes [68]. The heat needed to drive endothermic conversion of the coal to syngas by steam is provided by the exothermic in-situ oxidation of part of the coal by oxygen. However, it is only competitive where oil and natural gas is expensive, e.g. South Africa and China [16].

### 1.3.1. Steam reforming

Steam reforming of hydrocarbons (STR) is up to date the dominant process for the hydrogen and syngas production [11]. Methane, light and heavier paraffins as well as naphtha can be used as feedstock. It is the most hydrogen efficient process, it is well established and it has been optimised over the last decades. Nevertheless it faces several drawbacks especially the large net energy input needed to drive the endothermic reaction. The heat required for the reaction is provided by external burning of fuel leading to a complex and bulky reactor installation and gaseous emissions of  $\text{NO}_x$  and  $\text{SO}_2$  [11, 69]. Industrial catalysts used in the steam reforming are based on supported Ni [10, 11, 17, 18]. Co and several noble metals are also active catalysts, but more expensive. Even though coke formation, being the main reason for catalyst deactivation, is significantly smaller over noble metals than over Ni catalysts, Ni catalysts are still the most cost effective. This trend should increase due to the dwindling world reserves of the noble metals [70]. The Ni catalysts are activated by reduction prior to the reaction. The reaction conditions in the steam reformer are

---

generally reaction temperatures  $\geq 800^{\circ}\text{C}$ , pressures about 15-40 bar and steam to carbon ratios of 2-5 [10, 11, 17, 18, 71]. Due to the severe reaction conditions only thermoresistant supports are used, commonly  $\alpha$ -alumina, magnesium oxide, magnesia aluminium spinel or zirconia [17]. The supports and the catalysts need to be silica free because  $\text{SiO}_2$  is volatile under the reaction conditions. Hydrated silica escaping from the catalyst would deposit downstream the reactor damaging the equipment [17].

Coke formation is the main problem in the STR process [10, 11, 17, 18, 72, 73, 74, 75, 79]. Coking may not only lead to the deactivation or the mechanical destruction of the catalyst, but may also cause partial or total blockage of the reactor. The tendency for coking of the used feedstock increases in the order methane < light paraffins < higher paraffins < naphtha. In order to avoid excessive carbon formation high steam to carbon ratios are used that facilitate gasification of carbon deposits [17, 72, 74]. Addition of basic elements such as alkali and alkaline earth elements are well known to minimise carbon formation by enhancing the gasification of carbon deposits with steam. As shown by Borowiecki et al. also a high Ni dispersion of the catalyst reduces the carbon formation in the STR process [74, 75].

The Topsoe SPARG process has focused on minimising coke formation in the STR of methane by ensemble size effect on the Ni surface [17, 18, 72, 76, 77]. In this process traces of sulphur are added to the feed. Sulphur adsorbs reversibly on the surface in a regular array blocking part of the Ni sites. It was suggested that 3-4 Ni atoms are needed for the steam reforming reaction, but 6-7 for the formation of coke. Tests on industrial scale showed that using this process carbon formation was essentially eliminated. As the adsorption of sulphur is reversible it has to be added constantly to the feed. Very careful control of the sulphur levels in the feed is essential, as too small amounts do not prevent coking and too large amounts lead to the total deactivation of

---

the catalyst. A further disadvantage is that the adsorption of sulphur does not only decrease the rate of coke formation but decreases the rate of steam reforming too.

Another new approach to control coke formation in the STR of methane is based on the idea of preventing coke formation by the use of metal dopants, which react with Ni inhibiting carbide formation [18, 72]. Ag, Sn, Pb, As, Sb, Bi and Zn were found to reduce coke formation significantly, but they also reduced the rate of steam reforming over the catalyst. The reasons for the reduction of coke formation are not clear yet, but all the metals that had a positive effect on coking also form clusters on the surface with Ni. This may indicate ensemble size control like in the passivation with sulphur [18, 78]. Also the addition of small amounts of Mo a Ni/Al catalyst were found to reduce the rate of coking in the STR of n-butane. Also here the exact reason is not yet clear [79].

Natural gas consists next to methane to a considerable part of light paraffins, especially ethane and also propane, generally 3-30% [11]. Since higher paraffins could lead to coke accumulation in the methane steam reformer, pre-reformers are used in the STR of natural gas [11, 17]. As the light paraffins are more reactive than methane the pre-reformer works at lower temperatures than the actual steam reformer. In the pre-reformer also Ni catalysts are used. It is noteworthy that the Ni catalysts in the pre-reformer are not prepared by impregnation as conventional normal steam reforming catalysts but by coprecipitation or deposition precipitation because such catalysts are more active [17].

The formulation of catalysts used for the steam reforming of light paraffins ( $C_2H_6 - C_4H_{10}$ ) and higher hydrocarbons especially naphtha is more complicated than for methane because of their greater tendency to form coke deposits. Excessive coke formation can be suppressed by basic additives to the catalyst as already mentioned.

---

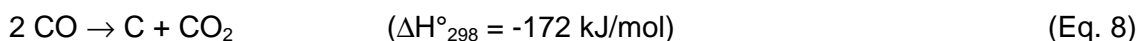
Unlike for the STR of methane, which is generally performed over  $\alpha$ - $\text{Al}_2\text{O}_3$  supported Ni catalysts, for the STR of light paraffins only basic supports are suitable such as  $\text{MgAl}_2\text{O}_4$ ,  $\text{CaAl}_2\text{O}_4$ ,  $\text{BaAl}_2\text{O}_4$ ,  $\text{SrAl}_2\text{O}_4$ ,  $\text{ZrO}_2$ - $\text{Al}_2\text{O}_3$  or  $\text{Al}_2\text{O}_3$  containing rare earth metal oxides [17]. For higher aliphatic feedstock the addition of alkali metal oxides to the catalyst is necessary to prevent excessive carbon formation. However, the reduction of the catalytic activity by alkali metal oxides and the continuous removal of the alkali metals with time-on-stream are major problems [17, 18].

### 1.3.2. Other processes for syngas production

The other major pathway for the production of syngas and hydrogen is the non-catalytic partial oxidation of fossil fuels often also referred to as gasification [10, 11]. A key advantage of this process is that it accepts all sorts of refinery feedstock including such as heavy distillation fractions and petroleum coke that are not suitable for steam reforming. Furthermore it is an exothermic reaction, but as it is not a catalysed process high reaction temperatures are needed ( $\sim 1300^\circ\text{C}$ ). The large amounts of coke produced in the process have to be regularly removed from the reactor walls.

An alternative approach to the non-catalysed partial oxidation and the steam reforming is the autothermal reforming [10, 11]. In this process the exothermic non-catalytic partial oxidation is combined with the endothermic steam reforming. The advantage is that it uses the energy surplus of the partial oxidation reaction to run the steam reforming, using only a single reactor and no outer heating. Typically, in the top of the reactor the non-catalytic partial oxidation reaction takes place providing the heat for the endothermic steam reaction over Ni based catalyst placed downstream the reactor.

The production of hydrogen by CO<sub>2</sub> reforming has no importance because of the high energy input needed and the low H<sub>2</sub>/CO ratio. However the low H<sub>2</sub>/CO ratio available in this process can be beneficial for the Fischer-Tropsch synthesis of products with a lower H/C ratio like olefins and oxygenated products [17, 77, 80, 81, 82, 83, 84, 85]. CO<sub>2</sub> reforming has found industrial application in the reduction of iron ore (Fe<sub>2</sub>O<sub>3</sub>) by synthesis gas, because CO<sub>2</sub> reforming yields syngas containing less water compared to the other processes. The most economic solutions of this reduction process involve a minimum content of water in the reformer effluent gas [17]. As in the steam reforming process suitable catalysts for the CO<sub>2</sub> reforming are based on several noble metals and Ni [11, 17, 77, 80, 83, 84, 86, 87, 88, 89]. The main problem is the catalyst deactivation by coking, which is more pronounced in this process than in the STR because of the higher amount of CO produced, which leads to a shift the Boudouard reaction favouring coke formation (Eq. 8).



As in the STR process noble metal catalysts are more resistant against coking Ni catalysts, but Ni based catalysts are preferred because of their lower costs. Some Ni catalysts supported on magnesium aluminate, MgO or mixtures of  $\alpha$ -aluminium and calcium oxide have been reported to exhibit good stability.

#### 1.4. Catalyst deactivation

The three most common deactivation processes in heterogeneous catalysis are poisoning, thermal degradation and coking (or fouling) [17, 71, 72, 73]. Poisoning is the loss of activity due to the blocking of the catalyst's active sites by impurities (poisons)

---

contained in the feed. In the steam reforming process over Ni catalysts for example  $\text{H}_2\text{S}$ ,  $\text{AsH}_3$ , chlorine and other halogen are known poisons. These compounds form inactive Ni species and must therefore be removed from the feed stream before entering the reactor. Thermal degradation is usually due to sintering or catalyst-support reactions leading to new phases for instance as a result of overheating. As many solid-solid reactions are highly activated thermal deactivation is especially important for high temperature reactions such as the processes for the production of syngas described above. A typical example is the transformation of  $\gamma$ -aluminium oxide to  $\alpha$ -aluminium oxide at high temperatures which is accompanied with a decrease of the surface area from  $\sim 200 \text{ m}^2$  for  $\gamma$ -aluminium oxide to  $\sim 2 \text{ m}^2$  for  $\alpha$ -aluminium oxide upon heating to  $\sim 1100^\circ\text{C}$  [72]. Such phase changes can result in the collapse of pores and the encapsulation of the active phase within the new lattice or the coalescence of active sites. Another example is the formation of  $\text{NiAl}_2\text{O}_4$  from NiO on  $\text{Al}_2\text{O}_3$  if steaming is carried out in the absence of  $\text{H}_2$  above  $700^\circ\text{C}$ . The spinel is not active in the steam reforming process and more difficult to reduce. The most common and often most important cause for the deactivation of the catalysts is coking. Coking can result in the mechanical destruction of the catalyst, its deactivation by blockage of the active sites or the blockage of the reactor. Even partial blockage of the reactor is deteriorating as it results in uneven flow distributions causing overheating, which causes irreversible damage to the reactor.

#### 1.4.1. Coking

The terms 'coke' and 'coking' are generic descriptions for a variety of carbonaceous deposits. Coke is formed at relatively high temperatures and its chemical nature can vary widely from graphitic carbon to condensed polymers and metal carbides [17, 18, 71, 72, 90, 91, 92]. Which type of coke is formed depends greatly on the type of the

reaction, e.g. gas phase or liquid phase process, and the presence of catalytic elements, e.g. metallic surfaces or acidic centres. The properties of common forms of coke are summarised in Table 5.

Tab. 5: Various types of coke [72]

Type	Origin	Temperature of formation [°C]	C/H ratio	Gasification
C	atomic carbon adsorbed on surfaces	>200		easy
C	polymeric amorphous film	>300	8	possible
whisker	whisker carbon usually with a metal particle on top	>300	8	reasonably easy
carbides	metal carbides	>300		reasonably easy
surface	deposited on non catalytic or catalytic surfaces	>300	50	difficult
gas phase	formed in the gas phase	>500	8	difficult
liquid phase	deposited from heavy oils in the liquid phase	~400	1	difficult
graphite		>1000	high	difficult

The tendency to form coke depends on the hydrocarbon feedstock. The tendency of hydrocarbon feedstock is generally characterised by their boiling point. Although certain hydrocarbon structures can have a particularly high coking effect depending on the catalyst, fractions with a higher boiling point are more prone to coking [24, 91]. For each hydrocarbon type, the boiling point increases with the molecular weight. Also the reaction temperature plays an important role in the formation of carbon deposits.



---

Hydrocarbons are generally less stable at higher temperatures and low pressure with regard to their decompositions into the elements, whereas in reactions such as steam reforming or partial oxidation coke formation is less favoured at higher temperatures, because of the overall thermodynamics of these processes. The temperature and the reaction conditions also play a key role in the formation of the type of coke formed. As already discussed is coke formation the main cause of catalyst deactivation in the processes for the syngas and hydrogen. In these processes coke can be formed by gas phase reactions and by gas-solid reactions.

#### **1.4.1.1. Coking in gas phase reactions**

Coke formation in the gas phase is complicated because of the interaction with surfaces, even if they are not catalytic. Reactions in the gas phase are free radical in nature and occur at relatively high temperatures [18, 71, 72]. The sequence of events is still unknown, but high molecular weight compounds (tars) are built up by a series of polymerisation-condensation reactions. Their vapour pressure is low, even at high temperatures, and they may nucleate to form a droplet in the gas phase or condense on any relatively cool surface. Subsequent dehydrogenation and ordering reactions can lead to carbon whether or not the surface is catalytic [72, 90]. Catalyst deactivation can result from both the tars and the carbon formed. Tars are less deteriorating to the catalytic activity, because they tend not to form a continuous layer over the surface, however neither of these forms is desirable.

Control of coking always depends on a balance between coke formation and coke removal. As radical polymerisations are favoured by high temperatures and high-pressure the coke formation can be minimised by keeping the pressure and the temperature as low as possible. However, this is not always favourable for the whole

process. For example the power requirements for the methanol synthesis from syngas can be almost halved by increasing the pressure of the syngas from 10 to 80 bar [10] and higher temperatures allow generally minimising the size of the reactor [72]. If the temperature and the pressure cannot be minimised, the residence time in the gas phase should be minimised by careful engineering of the design of the whole process equipment. As coking by gas phase reactions is a radical polymerisation reaction, coke formation can generally also be minimised by keeping the radicals apart using diluents. Inert diluents such as  $N_2$  and He as well as reactive ones such as  $H_2$ ,  $O_2$ ,  $CO_2$  or steam may be used [18, 71, 72]. However, also the use of diluents depends on the pressure requirements, considering the costs of compression of the diluent [10]. Reactive diluents minimise the coke formation not only by dilution of the feed but also by gasification of coke or coke intermediates by reactions such as  $C + 0.5 O_2 \rightarrow CO$  ;  $C + H_2O \rightarrow CO + H_2$  ;  $C + CO_2 \rightarrow 2 CO$  ;  $C + 2 H_2 \rightarrow CH_4$ . Gases like hydrogen may also act to trap radicals,  $R^\cdot + H_2 \rightarrow RH + H^\cdot$ . If the radicals hit the surface, the coking sequence may be interrupted before coke is formed,  $H^\cdot + H^\cdot + Surface \rightarrow H_2 + Surface$ . As a result it is an incentive to increase the surface to volume ratio in order to retard gas phase radical reactions.

#### 1.4.1.2. Coking in gas-solid catalytic reactions

The catalysts themselves may also be centres of coke formation. Here coking may occur on metal particles and acid centres [17, 71, 72, 91, 92]. The polymerisation of alkenes or alkynes is suspected to be the main reaction involved on acidic catalysts. If not present in the feed, alkenes and alkynes can be readily produced especially in high temperature processes by thermal cracking.

---

On metal surfaces various types of coke can be formed. For example on Ni surfaces in the steam reforming process catalytic results from the dissociative adsorption of hydrocarbons ( $C_xH_y \rightarrow x C + y/2 H_2$ ) and disproportionation of CO by the Boudouard reaction ( $2 CO \rightarrow C + CO_2$ ) both resulting in reactive  $C_\alpha$  coke. If  $C_\alpha$  is gasified, for example by steam in the steam reforming process, then the desired CO and  $H_2$  are the products. However,  $C_\alpha$  may react further either by polymerisation to form  $C_\beta$  or by dissolution in the metal [17, 71, 72, 90, 92]. It is uncertain whether only  $C_\alpha$  or also  $C_\beta$  dissolve in the metal. Once the carbon is dissolved it may form metal carbide and diffuse through the metal particle to precipitate out a grain boundary. Continuation of the process leads to the growth of a filament, a so-called whisker, with a metal particle on the top of the whisker. As a result the metal particle is still accessible to the gas and the catalytic activity is generally not decreased [72, 90]. Though the formation of carbon whiskers does not necessarily decrease the catalytic activity, it is nevertheless deteriorating for the process because it can cause partial or total blockage of the reactor. This results in uneven flow distributions causing overheating, which finally results in irreversible reactor damage [10, 17, 18]. Polymerisation of  $C_\alpha$  to  $C_\beta$  followed by possible ordering of the carbon can lead to the accumulation of the surface deposits forming encapsulating carbon. In this case metal surface area is generally lost and the catalyst deactivates. The whole scheme of carbon deposition in steam reforming is depicted in Figure 3. The minimisation of coke in gas-solid depends on the reaction itself and on the particular catalyst. For example, as already pointed out above are noble metal catalysts much less prone to coking than Ni based catalysts in the steam reforming process. Concepts like the addition of basic promoters to the catalyst to minimise coke formation in the steam reforming and the  $CO_2$  reforming over Ni catalysts have already been discussed above.

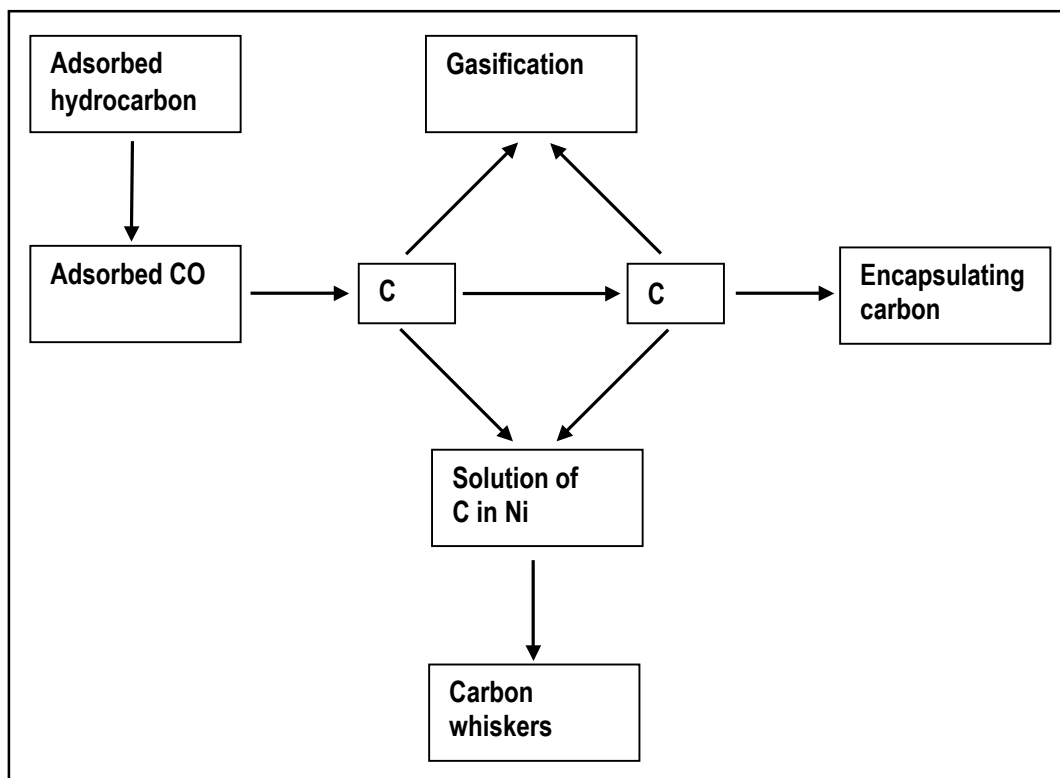


Fig. 3  
Scheme of the formation of carbon deposits during steam reforming

### 1.5. Catalytic partial oxidation

Though the catalytic partial oxidation of methane (CPOM) has not yet been used on an industrial scale the large number of publications and patents issued recently show the great interest in this process [10]. Research in this field has been focused almost exclusively on methane as feedstock. Different catalysts containing group VIII metals (group 8-10) and Cu were studied [9, 10, 22, 23, 65, 69, 93, 94, 95, 96, 97, 98, 99, 100, 101, 102, 103, 104, 105, 106, 107, 108, 109, 110, 111, 112]. As in the steam reforming and the  $\text{CO}_2$  reforming, several noble metals, Co and Ni catalyse the reaction. Ni and Rh containing catalysts were found to be the most active catalysts for CPOM.

### 1.5.1. Catalytic partial oxidation of methane over Ni catalysts

The thermodynamic calculations show that in the partial oxidation of CH<sub>4</sub>, CO and H<sub>2</sub> are the main products at higher temperatures, H<sub>2</sub>O and CO<sub>2</sub> being the only considerable by products (Tab. 6) [9, 107].

Tab. 6: Approximate thermodynamic values of the CH<sub>4</sub> conversion and selectivity of CO and H<sub>2</sub> for a reaction mixture of CH<sub>4</sub>/O<sub>2</sub>/He (2/1/4) [9]

	500°C	600°C	700°C	800°C	900°C
CH <sub>4</sub> conversion	28%	60%	83%	95%	98%
CO selectivity	41%	65%	91%	96%	99%
H <sub>2</sub> selectivity	61%	81%	83%	97%	99%

As in the steam reforming and the CO<sub>2</sub> reforming Ni catalysts are also likely to be used for the partial oxidation of hydrocarbons on an industrial scale as they are active and inexpensive. However the reaction scheme of the CPOM over Ni catalysts is still under discussion. Generally two extremes and combinations of them are considered (Fig. 4). In the one extreme CO and H<sub>2</sub> are the primary products of the oxidation of CH<sub>4</sub>. Reactions leading to the thermodynamically most stable reaction mixture containing next to CO and H<sub>2</sub> also H<sub>2</sub>O and CO<sub>2</sub> are secondary reactions. If this scheme was valid it would be possible to achieve CO and H<sub>2</sub> yields higher than predicted by the overall process thermodynamics by suppressing the secondary reactions leading to the equilibration. In the other possible extreme first all O<sub>2</sub> is consumed in the total oxidation of part of the CH<sub>4</sub>, yielding H<sub>2</sub>O and CO<sub>2</sub>. H<sub>2</sub>O and CO<sub>2</sub> then react in the second step with the remaining CH<sub>4</sub> yielding CO and H<sub>2</sub>. The overall thermodynamics present the maximum CO and H<sub>2</sub> yields achievable.

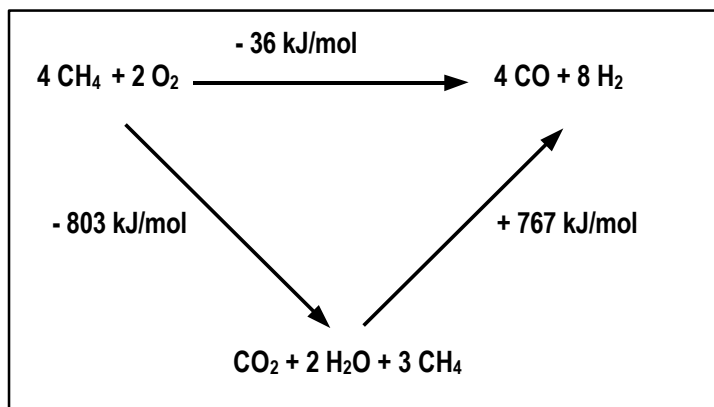


Fig. 4  
Scheme of the two extreme reaction pathways for the partial oxidation of  $\text{CH}_4$

#### 1.5.1.1. Direct syngas formation

Choudhary et al. proposed that CO and  $\text{H}_2$  are the primary products over Ni catalysts [10, 104]. They studied CPOM over Ni catalysts at high space velocities and undiluted feed and found that the selectivities towards CO and  $\text{H}_2$  were higher than those predicted by the thermodynamics of the overall process including side products. They concluded that this was due to the fact that CO and  $\text{H}_2$  are primary products and that at short enough contact times the equilibration of the gas mixture is not possible. Other authors showed that under the applied conditions huge temperature gradients exist and that the local temperature in the catalyst can be more than  $300^\circ\text{C}$  higher than the measured one [9, 69, 109]. Therefore it is difficult to draw any comparison of these results with thermodynamic data. Qin et al. also observed a rise in the temperature due to the partial oxidation reaction for reaction mixtures diluted by 57 vol%  $\text{N}_2$  [94]. Basile et al. also observed a considerable temperature rise in the reactor upon increasing the GHSV, even at a dilution of the feed by 87 vol% He [9].

### 1.5.1.2. Total oxidation followed by reforming

Prettre et al. were in 1946 among the first to study the CPOM over Ni catalysts [10, 107]. They observed an exothermic reaction in the entry of the catalyst bed, which was followed by an endothermic reaction. The composition of the gas mixture at the outlet corresponded to thermodynamic predictions considering side products. On the basis of these results they proposed a two step reaction scheme. The exothermic reaction at the entry of the catalyst's bed was attributed to the complete deep oxidation of 25% of the  $\text{CH}_4$  by 100% of the  $\text{O}_2$  yielding  $\text{CO}_2$  and  $\text{H}_2\text{O}$ . The subsequent following endothermic reaction was believed to be the reforming of the remaining  $\text{CH}_4$  by  $\text{CO}_2$  and  $\text{H}_2\text{O}$  formed previously. Heitnes et al., Dissanayake et al. and Basile et al. observed the same general temperature profile [9, 97, 107]. Looji et al. compared CPOM to the reforming of the same reaction mixture where all the  $\text{O}_2$  was consumed in the total combustion step prior to the reforming over the Ni catalyst at rather long contact times [109]. They observed no differences between the two reactions and also proposed the reaction mechanism total combustion followed by the combined steam and  $\text{CO}_2$  reforming (mixed reforming).

Though the observations made by the authors are strong evidence for the possibility of such a reaction scheme, the only mechanistic studies here are the comparison of the CPOM with the mixed reforming. However the experiments were performed at long contact time. It might be that the contact time was long enough for both reactions to achieve the same result. Studies concerning the CPOM and the mixed reforming at different contact times or other mechanistic studies were not performed.

### 1.5.1.3. Pyrolysis mechanism

Au et al. performed CPOM pulse experiments over Ni/SiO<sub>2</sub> using CH<sub>4</sub> and CD<sub>4</sub> [101]. They observed a normal isotope effect with regard to methane conversion (higher CD<sub>4</sub> than CH<sub>4</sub> conversion) and no changes in the CO/CO<sub>2</sub> ratio. No data were presented concerning H<sub>2</sub> and water. From these results they concluded that the activation of CH<sub>4</sub> is the rate-determining step in CPOM. They furthermore observed that when the CH<sub>4</sub> flow was stopped and only O<sub>2</sub> pulsed that CO and CO<sub>2</sub> were evolved and their amount decreased with the number of O<sub>2</sub> pulses [102]. They attributed this finding to the existence of surface carbon formed by the CH<sub>4</sub> pyrolysis (CH<sub>4</sub> → C + 2 H<sub>2</sub>). Surface carbon formed on Ni catalysts under the reaction conditions was also observed by Dissanayake et al. [107].

On this basis the authors advocated a so-called pyrolysis mechanism as the possible reaction scheme for the partial oxidation of CH<sub>4</sub> over Ni catalysts (Fig. 5). According to this mechanism, carbon deposits on the catalyst surface are the active carbon source. CO and CO<sub>2</sub> selectivities are mainly governed by the relative rates of the CO desorption and oxidation on the catalyst surface. A possible mechanism concerning the formation of hydrogen and water was not presented.

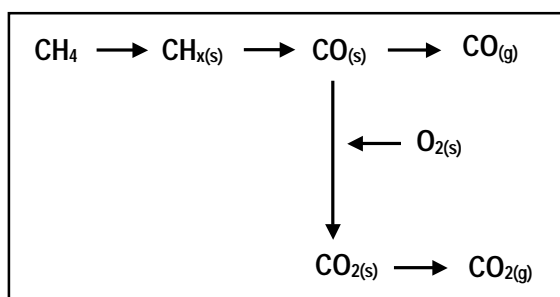


Fig. 5  
Pyrolysis reaction scheme for the partial oxidation of CH<sub>4</sub> (s = surface, g = gas phase)



#### 1.5.1.4. Parallel pathways

Qin et al. investigated the partial oxidation, steam reforming, CO<sub>2</sub> reforming and the mixed reforming of CH<sub>4</sub> by steady state experiments over MgO supported Ru, Pd, Pt, Ir, Rh and to a lesser extent Ni catalysts [94]. Additionally they performed temperature programmed reactions over the Rh/MgO catalyst. In all steady state experiments the same GHSV was used, allowing a direct comparison of the results for the different reactions. In the steady state experiments they observed CH<sub>4</sub> conversions near the equilibrium only for CPOM, whereas in the other reactions the CH<sub>4</sub> conversions were considerably lower. They noted a significant temperature rise in CPOM, despite the dilution of the feed stream by N<sub>2</sub> (57 vol%). They did neither record it nor decrease the heating power of the furnace to compensate it. As the CH<sub>4</sub> conversion was highest in CPOM they excluded a reaction mechanism of the form total oxidation followed by reforming as the main reaction pathway. In the temperature programmed reaction they observed that partial oxidation and the mixed reforming reactions are starting at very similar temperatures. Therefore they assumed that these reactions take place simultaneously and proceed by the same oxygen reaction intermediate, which they assumed to be adsorbed atomic oxygen O<sub>ad</sub> bound to the metal surface in the form M-O. They regarded the strength of the M-O bond to be the key factor for the activity and the selectivity of the catalysts. First, the formation of M-O assists the decomposition of O<sub>2</sub>, H<sub>2</sub>O and CO<sub>2</sub>, generating adsorbed atomic oxygen. Hence M-O bond strength is favourable. Weaker bond strength is required to allow M-O bond cleavage without high activation energy, crucial to form CO with adsorbed carbon species formed upon the adsorption of CH<sub>4</sub>. However, a too weak M-O bond enhances atomic oxygen desorption. Desorbed atomic oxygen is a very strong and non-selective oxidation reagent thus increasing the amount of the products of the total oxidation. The correlation of the M-O bond strength with the CO formation rate revealed that metals

---

with a low or high M-O bond strength, e.g. Pt and Ru respectively, showed a lower CO formation rate than those with a rather intermediate M-O bond strength such as Ni. This trend is also in quite good agreement with the results of the group of Schmidt et al. [93, 98, 100]. The same correlation made for steam reforming revealed that the CO formation rate increased with the M-O bond strength. They explained this with the need for a higher M-O bond strength in the steam reforming process, as H<sub>2</sub>O is more difficult to activate than O<sub>2</sub>, according to the authors.

Qin et al. compared the various reforming reactions with the partial oxidation but did not account for the higher reaction temperature in the partial oxidation, due to the exothermic reaction(s). Hence their conclusion that the direct partial oxidation is the predominating reaction is not conclusive, as the higher CH<sub>4</sub> conversions in the CPOM might be due the higher reaction temperature. For the same reason the correlation of the strength of the M-O bond and the activity of the catalyst in the CPOM is also not completely reliable. Furthermore the authors performed temperature programmed reactions only for the Rh catalyst but assumed that the result, similar onset temperatures for all the different reactions, is valid for all catalysts.

#### **1.5.1.5. Activation of the catalyst**

Reduction is necessary to activate the Ni catalysts in the CPOM. Dissanayake et al. [107], Looji et al. [109, 110] and Nichio et al. [108], observed in CPOM over unreduced Ni catalysts below 700°C no complete conversion of O<sub>2</sub> and very low conversions of CH<sub>4</sub>. The reactions products were exclusively CO<sub>2</sub> and H<sub>2</sub>O. Upon rising the reaction temperature to about 700°C all three observed a sudden sharp increase in the CH<sub>4</sub> conversion and almost complete O<sub>2</sub> conversion, the products were now predominantly CO and H<sub>2</sub>. CO<sub>2</sub> and H<sub>2</sub>O the only considerable side products. The behaviour was

---

comparable to the catalysts that were reduced prior to the reaction. Therefore the great enhancement of the catalytic activity was attributed to the reduction of the catalyst under the reaction conditions. This was also backed by Dissanayake et al. who observed that the composition of the catalyst bed was comparable to that of the catalyst reduced prior to the reaction under the same reaction conditions. Consequent decrease of the temperature had no effect on the O<sub>2</sub> conversion and led to a moderate decrease in the CH<sub>4</sub> conversion and the selectivities towards CO and H<sub>2</sub> as predicted by thermodynamics. The observed CH<sub>4</sub> conversions were still much higher over these at least partially reduced catalysts than over the non-reduced ones. Upon the further decrease of the temperature down to about 400°C the catalysts lost their enhanced activity and the former low active state was restored. Similar results were also obtained by Au et al. [101, 102], who performed pulse experiments over NiO/SiO<sub>2</sub> and Ni/SiO<sub>2</sub> catalysts.

#### **1.5.1.6. State of the active catalyst**

To gain information about the state of the active catalyst in CPOM several authors investigated the state of catalysts after a certain time on stream and under simulated reaction conditions.

Looji et al. [110] conducted in-situ high temperature XRD and semi-in-situ XPS on an Ni/SiO<sub>2</sub> catalyst under different reaction conditions and performed additional temperature programmed surface reactions (TPSR) experiments. They assumed a total combustion followed by reforming mechanism. According to this mechanism the CH<sub>4</sub>/O<sub>2</sub> ratio should increase along the catalyst bed as first all O<sub>2</sub> is consumed in the total oxidation of CH<sub>4</sub>, before the formed H<sub>2</sub>O and CO<sub>2</sub> react with the remaining CH<sub>4</sub> yielding syngas as discussed above. Therefore they investigated their catalyst under

different  $\text{CH}_4/\text{O}_2$  inlet ratios. They observed that at low  $\text{CH}_4/\text{O}_2$  inlet ratios, corresponding to  $\text{O}_2$  conversion levels of 0 and 25%, the reaction mixture is net oxidising for the reduced Ni catalyst resulting in the formation of NiO. For higher ratios, 60-85%  $\text{O}_2$  conversion, no oxidation of bulk Ni was observed, but partial oxidation of the surface Ni atoms, which was greater at 60%  $\text{O}_2$  conversion than at 85%. They showed by the TPSR experiments with Ni catalysts of different oxidation degrees, that the catalysts only mildly passivated were more active in the total combustion of  $\text{CH}_4$  than the fully oxidised ones.

Dissanayake et al. investigated an industrial Ni/Al steam reforming catalyst after CPOM by means of XRD and XPS [107] and Basile et al. a hydrotalcite-type derived Ni/Mg/Al catalyst after CPOM employing XRD and Scanning electron microscopy energy dispersive spectroscopy (SEM-EDS) [9]. Both authors found that Ni in the head of the catalyst was completely oxidised and in the tail of the catalytic beds they both found Ni only in the metallic state. However, they observed different Ni phases in the middle part of the bed. Basile et al. observed NiO and Ni, whereas Dissanayake et al. observed surface NiO on  $\text{Al}_2\text{O}_3$ , which they regarded to be catalytically more active than  $\text{NiAl}_2\text{O}_4$  found in the Head, The low activity of  $\text{NiAl}_2\text{O}_4$  was also reported by Choudhary et al. [105, 106]. Dissanayake et al. also observed that the proportion of the 3 sections of the catalyst bed (head, middle and tail) changed with the reaction temperature and also the contact time. The amount of the tail (metallic Ni) decreases with decreasing reaction temperature and also by decreasing contact time, whereas the head ( $\text{NiAl}_2\text{O}_4$ ) and the middle ( $\text{NiO}/\text{Al}_2\text{O}_3$ ) increased. A catalyst consisting only of  $\text{NiAl}_2\text{O}_4$  was the final result of even further decrease of the temperature.

The results show that the phase composition of the catalyst changes along the catalyst bed due to the oxidative character of the reaction mixture. The authors linked this to the

decrease in the  $O_2$  due to its consumption by the formation of  $H_2O$  and  $CO_2$ . However, they did not discuss the possibility that the oxidative character of the mixture may not only be changed by reduction of the  $O_2$  content, but also by the simultaneous formation of reducing  $CO$  and  $H_2$  (direct syngas formation, pyrolysis mechanism and parallel pathway).

#### 1.5.1.7. Influence of the reaction conditions

Dissanayake et al. investigated their Ni catalyst at different  $CH_4/O_2$  ratios [107]. They found that the catalyst is transformed to its low activity oxidised state at ratios  $\leq 1.25$ , where the ratio of 2 corresponds to the stoichiometric value. At ratios  $\geq 2$  large amounts of carbon were formed that filled the catalysts pores and caused the disintegration of the catalyst granules. At a ratio of 1.78 they observed a steady-state contraction of surface carbon of about 1 monolayer, which caused no observable decrease in the activity of the catalyst during 50 h on stream. Schmidt et al. investigated the CPOM over Rh, Ni, Pt and Ir coated catalysts at  $CH_4/O_2$  ratios of between 1.7 and 2 in autothermal reactors. Hence the reaction temperature could differ remarkably between the different catalysts by more than  $300^\circ C$  and between the  $CH_4/O_2$  ratio over one catalyst by about  $150^\circ C$  [93]. The  $O_2$  conversion was almost complete in all experiments, whereas the  $CH_4$  conversion and the temperature decreased with increasing  $CH_4/O_2$  ratio.  $CO$  and  $H_2$  were always the main products, regardless the  $CH_4/O_2$  ratio.

The influence of the gas hourly space velocity (GHSV), the inversion of the contact time, is more complicated to evaluate. This is firstly due to the fact that it can be expressed as  $\text{volume(gases)} \cdot \text{h}^{-1} \cdot \text{volume(catalyst)}^{-1}$  if the density of the catalyst is known or as  $\text{volume(gases)} \cdot \text{h}^{-1} \cdot \text{weight(catalyst)}^{-1}$ . The first definition gives normally higher

numbers as the density of solid catalysts is generally  $> 1$ . Also is it most often impossible to convert the first definition into the other, because in none of the publications referred to in this work the density of the catalysts was stated. Therefore no actual numbers may be stated in this section. Basile et al. observed that the reaction temperature increased with increasing GHSV, accounting for the observed higher activity of the catalyst [9]. Dissanayake et al. and Looij et al. showed that at sufficiently high GHSV the activity of the catalyst decreases [107, 109]. The final result of further increase of the GHSV is the total oxidation of the catalyst and hence the loss of activity.

The experiments performed by Schmidt et al. show clear tendencies for the influence of the  $\text{CH}_4/\text{O}_2$  ratio, but it must be kept in mind that the reaction temperature was higher in the experiments with a lower  $\text{CH}_4/\text{O}_2$  ratio. Due to the temperature differences it is difficult to determine in how far the higher  $\text{CH}_4$  conversions were due to the lower  $\text{CH}_4/\text{O}_2$  ratio or to the higher reaction temperature. Increasing GHSV may result in the oxidation of the catalysts by the reaction mixture that is more oxidative due to the lower conversion of  $\text{O}_2$ .

#### **1.5.1.8 Stability of the catalysts**

Deactivation of Ni catalysts with time-on-stream was reported in several cases. Like in the steam reforming and the  $\text{CO}_2$  reforming the deactivation is due to the formation of carbon deposits [10]. Basile et al. tested Ni/Mg/Al containing catalysts derived from hydrotalcite-type precursors with varying Ni and Mg content [9]. They observed that the pure Ni/Al catalyst and the catalyst with a high Ni/Mg ratios ( $\sim 6:1$ ) deactivated very fast due to coking. The catalysts with a lower Ni/Mg ratio, 3:4 and 1:6 showed good stability, according to the authors these two catalysts showed no signs of deactivation

during 500 hours time-on-stream. The positive effect of Mg was also reported by Sokolovskii et al. who found that coprecipitated Co/Mg/Al catalysts with Co/Mg ratio of 1:1 and 1:3 were stable for hundreds of hours on stream [96]. Though coke formation is the main problem, also the oxidation of the Ni particles to NiO was reported to have a deteriorating effect on the conversion and the selectivities of the catalyst in CPOM as already discussed. These oxidised Ni catalysts can be further damaged due to solid state reactions of NiO with the support. Choudhary et al. and Torniaainen et al. reported the formation of  $\text{NiAl}_2\text{O}_4$  and  $\text{NiSiO}_3$  for Ni catalysts on alumina and silica, respectively, under the conditions of CPOM at higher temperatures [93, 105, 106]. Both compounds were reported to be inactive in CPOM and are more difficult to reduce than NiO, thus causing severe damage to the catalyst. Choudhary et al. reported that it was possible to avoid the formation of  $\text{NiAl}_2\text{O}_4$  and  $\text{NiSiO}_3$  by precoating the support with different alkaline and rare earth metal oxides ( $\text{MgO}$ ,  $\text{CaO}$ ,  $\text{SrO}$ ,  $\text{BaO}$ ,  $\text{Sm}_2\text{O}_3$  and  $\text{Yb}_2\text{O}_3$ ) and calcining the precoated support prior to the impregnation with NiO [105, 106]. They found distinct differences in the  $\text{CH}_4$  conversions and selectivities to syngas depending on the precoating agent. MgO precoated catalyst exhibited the best results and SrO and BaO the worst. On the basis of the results of the temperature programmed reduction (TPR) of the different precoated catalysts they claimed that sintering of the Ni particles was responsible for the differences in the activities. MgO precoated catalyst showed the lowest degree of reduction, but the highest degree of Ni dispersion after reduction. The authors attributed the stronger resistance of the MgO precoated catalyst against reduction and sintering to the formation of a solid NiO-MgO solution.

### 1.5.2. Catalytic partial oxidation of higher hydrocarbons

In contrast to the catalytic partial oxidation of methane only very limited work has been presented concerning the catalytic partial oxidation of hydrocarbon feedstock other

than methane. Schmidt and his co-workers have performed most of the work. They investigated the partial oxidation of the C<sub>2</sub>-C<sub>6</sub> alkanes [20, 21, 22, 23]. Their studies have been limited to Pt, Rh and Pd containing monoliths using different carbon/oxygen ratios and various GHSVs under autothermal conditions, hence the reaction temperatures could differ quite drastically. In the catalytic partial oxidation of the C<sub>2</sub>-C<sub>6</sub> feedstock over Rh they observed that syngas was the main product regardless the C/O ratio whereas over Pt the selectivity was shifted to olefins with increasing C/O ratio. The Pd based catalyst deactivated rapidly due to coking even at low C/O ratios. They also found that the O<sub>2</sub> conversion was always high if not complete in the conversion of C<sub>2</sub>-C<sub>4</sub> alkanes over all the active catalysts. In the partial oxidation of C<sub>5</sub> and C<sub>6</sub> feedstock the O<sub>2</sub> conversions were considerably lower, even at high C/O ratios O<sub>2</sub> breakthrough was observed. The changes of the temperature and the alkane conversion as a function of the C/O ratio were presented only for Pt. The temperature and the alkane conversion decreased with increasing C/O ratio.

### **1.6. The scope of this work**

The aim of this work was to study the catalytic performance and the possibility of application of different Ni/Mg/Al catalysts derived from hydrotalcite-type precursors in the partial oxidation of C<sub>3</sub>H<sub>8</sub> to CO and H<sub>2</sub>. The main focus of investigations was the influence of the catalyst composition on their activity, selectivity, stability and coking in relation to the Ni dispersion and the basicity. Dispersion and basicity are known to be the main factors influencing the catalytic performance of Ni containing catalysts in the related reactions (steam reforming, CO<sub>2</sub> reforming, partial oxidation of CH<sub>4</sub>). The catalysts were further to be compared with a conventional steam reforming catalyst to scale their effectiveness. More detailed studies were devoted to the choice of optimum reaction conditions for the best catalyst. Further attention was also paid to the effect of



---

the calcination temperature on the catalyst's performance. More detailed mechanistic studies were not planned as the partial oxidation of propane is expected to be more complex than the catalytic partial oxidation of methane, where the reaction mechanism is still under discussion.

### 1.6.1. Methodology

In order to find an optimal catalyst and to study the influence of the Ni and Mg content a set of Ni/Mg/Al catalysts was prepared derived from hydrotalcite-type precursors. The hydrotalcite-type precursors were prepared by coprecipitation at low supersaturation at constant pH as it is regarded in the literature as the most successful method of synthesis. The Ni and Mg content ranged from pure Mg/Al to pure Ni/Al. The Al content was kept constant as it can only vary in a narrow range (25 – 33 metal atom%).

Extensive characterisation of the physicochemical properties of the as prepared HT materials was performed by means of inductively coupled plasma atomic emission spectroscopy (ICP-AES) for the determination of the metal composition, C and N analysis to measure the amount of  $\text{CO}_3^{2-}$ ,  $\text{NO}_3^-$ , thermogravimetry coupled with mass spectroscopy (TG-MS) to determine the amount of intercalated  $\text{H}_2\text{O}$ , X-ray powder diffraction (XRD) for the phase composition, TG-MS and differential scanning calorimetry (DSC) for the analysis of the thermal degradation process of the HTs.

The as-synthesised hydrotalcite-type solids were then transformed into mixed metal oxides by calcination at  $900^\circ\text{C}$  using a slow heating program and under a constant stream of air for the fast removal of the volatile decomposition products.  $900^\circ\text{C}$  was chosen as calcination temperature for three reasons. Firstly, because in the catalytic partial oxidation of  $\text{CH}_4$  rising the reaction temperature above  $800^\circ\text{C}$  had no significant

---

influence anymore. Since  $\text{CH}_4$  is thermodynamically more stable at higher temperatures than  $\text{C}_3\text{H}_8$  and also more difficult to activate [113],  $800^\circ\text{C}$  was also regarded as the highest reasonable reaction temperature for the partial oxidation of  $\text{C}_3\text{H}_8$ . As the partial oxidation of  $\text{C}_3\text{H}_8$  is an exothermic reaction, a possible overheating of the catalyst surface at least locally must be taken into account. In order to avoid structural changes of the catalyst due to this effect they were calcined  $100^\circ\text{C}$  above the maximum reaction temperature. Secondly, because in the partial oxidation of  $\text{C}_3\text{H}_8$  considerable amounts of  $\text{H}_2\text{O}$  can be produced which may lead to the reconstruction of the former HT structure during the catalytic tests. HT derived catalysts calcined at temperatures  $\geq 900^\circ\text{C}$  are much more resistant against the reconstruction of the former HT structure than those calcined at lower temperatures. Thirdly, because higher calcination temperatures were regarded as undesirable because of negative effects such as the loss of surface area.

To investigate the structural composition of the catalysts XRD was employed and scanning electron microscopy (SEM) for studies of their morphology. As the surface area can be an important factor it was determined by BET measurements. In order to study the reduction process and to find a suitable reduction method, which is crucial in the activation of the catalysts, temperature programmed reduction (TPR) was performed. The resistance of the reduced catalysts against oxidation was studied by temperature programmed oxidation (TPOx). The Ni dispersion of the catalysts was estimated basing on TPR results as the relative amount of reducible Ni after passivation of the reduced catalysts. The dispersion of the catalysts is not only important for its activity, but has also been reported to be important for the coke resistance of the catalysts in the related steam reforming process. In order to investigate the reducibility of the  $\text{Ni}^{2+}$  ions in the different phases of the catalyst and as

---

well as the influence of the substitution of  $\text{Ni}^{2+}$  by  $\text{Mg}^{2+}$  reduction combined with in-situ high temperature XRD measurements was additionally performed.

From the processes that are related to the intended partial oxidation of  $\text{C}_3\text{H}_8$  it is known that the basicity is an important factor in the coke resistance of the catalysts. For the determination of the basicity of solids three methods are generally used: Hammett measurements, temperature programmed desorption of probe molecules and test reactions. Hammett measurements involve the adsorption of indicators from suitable non-aqueous solutions, where the solvent does not interact with the catalyst acid or basic sites, the acidity or basicity of the catalysts is determined from the colour change of the indicator [114]. As the studied catalysts change their own colour with the Ni/Mg ratio, from white for pure Mg/Al catalyst to darkish green for the pure Ni/Al catalyst Hammett indicators were regarded as not suitable for the measurement of the basicity.

Basicity can also be determined by temperature programmed desorption (TPD) of specific molecules adsorbed in a controlled manner prior to the desorption process. For the measurement of the basicity  $\text{CO}_2$  has been repetitively employed [49, 89, 115, 116, 117].  $\text{CO}_2$  can adsorb on basic sites of oxide surfaces to form a superficial carbonate. Various TPD of  $\text{CO}_2$  experiments were systematically performed in order to find optimal test conditions.

The basicity or acidity of solids can also be characterised by the certain reactions that are either only catalysed by acidic or basic centres or that form different products over basic centres than acidic centres. From several test reactions in the gas phase reported in the literature two were chosen for the purpose of the scaling of the basicity of the catalysts. The first test reaction is the transformation of isopropanol (2-propanol) to propene and/or to acetone [48, 89, 116, 117, 118, 119, 120]. Generally speaking,

---

isopropanol is transformed to acetone by basic sites of the catalyst and to propene by acidic sites. The second test reaction is the aldol condensation of acetone leading to  $\alpha,\beta$ -unsaturated carbonyl compounds over basic and to hydrocarbons over acid site [116]. The basicity of the catalysts can be scaled by the selectivity of the products formed over basic sites to the ones formed over acidic sites.

In order to study the influence of the catalyst composition on conversion, selectivity, stability and the tendency towards coke formation and to find the best catalyst for further studies, all Ni containing catalysts were reduced in-situ at 800°C and tested for 240 minutes time on stream. The reduction temperature was chosen on the basis of the TPR results, 240 min time on stream were chosen for two reasons. Firstly, because it was found to be long enough to analyse the catalytic performance under steady state conditions. Secondly, because it resulted in sufficient amounts of carbon deposits in order to study the catalyst tendency towards coking by temperature programmed combustion (TPC) of the carbon deposits using TG-MS. The results were compared with a conventional steam reforming catalyst Ni/Al<sub>2</sub>O<sub>3</sub> (20% NiO, 2% K<sub>2</sub>O) tested under the same reaction conditions. The catalytic tests were performed at 700 and 800°C as these were reported to be suitable reaction temperatures in the related reactions. The reaction was performed in 25% O<sub>2</sub> surplus compared to the stoichiometric value in order to avoid excessive coke formation, which could lead to the complete deactivation of the catalysts and the disintegration of the catalyst particles as reported for the partial oxidation of CH<sub>4</sub>. In order to improve the heat transfer necessary to minimise possible overheating of the catalyst surface He was used as a diluent because of its high thermal conductivity. Most of the catalytic tests were repeated to verify the reproducibility of the results.

Additional catalytic tests were performed in order to quantify the effectiveness of the reduced catalysts using the empty reactor, SiO<sub>2</sub> wool (used to hold the catalyst) and the not reduced catalyst, Ni free as well as NiO containing. In order to find an optimum calcination temperature experiments catalytic tests were performed with catalysts calcined at various temperatures. And finally to optimise the reaction conditions the influence of changes in the gas hourly space velocity (GHSV) and the effect of variations of the O<sub>2</sub>/C<sub>3</sub>H<sub>8</sub> ratio of the feed were investigated.

## 2. Experimental

### 2.1. Synthesis of the hydrotalcite-type solids

$\text{Ni}^{2+}$  is like  $\text{Mg}^{2+}$  and  $\text{Al}^{3+}$  a suitable metal ion for the preparation of HT materials. In fact the naturally occurring mineral takovite  $\text{Ni}_6\text{Al}_2(\text{OH})_{16}(\text{CO}_3) \cdot 4\text{H}_2\text{O}$ , is isomorphous to hydrotalcite ( $\text{Mg}_6\text{Al}_2(\text{OH})_{16}(\text{CO}_3) \cdot 4\text{H}_2\text{O}$ ). The successful synthesis of Ni/Al HTs was reported for Ni/Al ratios of 2/1 – 3/1 ( $\text{Ni}_{0.67}\text{Al}_{0.33}$  –  $\text{Ni}_{0.75}\text{Al}_{0.25}$ ). At higher Ni contents the formation of free  $\text{Ni}(\text{OH})_2$  next to the HT phase was observed, at lower Ni contents free  $\text{Al}(\text{OH})_3$  next to a HT phase was formed [4, 6, 7]. No limitations for the Ni/Mg ratio for the synthesis of Ni/Mg/Al HTs were reported in the literature [1, 9, 42, 43, 46]. Synthetic Ni containing HTs are generally prepared under the conditions of low supersaturation at  $\text{pH } 8 \pm 0.1$  to  $\pm 0.2$  [1, 7, 8, 9, 43, 46, 53, 60]. A pH value  $\geq 10$  during the precipitation is not recommendable, because of the possible dissolving of  $\text{Al}^{3+}$  ions and the difficult removal of sodium salts from HTs prepared at  $\text{pH} \geq 10$  [4, 66]. Basic alkali containing solutions are generally used in the preparation of HTs, frequently also basic ammonium containing solutions. Metal nitrates are almost exclusively used as metal precursors and only rarely metal chlorides.

The preparation was carried out at low supersaturation at  $\text{pH } 8 \pm 0.2$  at 60-70°C. Metal nitrates were chosen as metal salt precursors and NaOH and  $\text{NaHCO}_3$  as bases. In order to be able to tolerate small derivations in the  $(\text{Ni}^{2+} + \text{Mg}^{2+})/\text{Al}^{3+}$  ratio, a ratio of 2.57 corresponding to the formula  $\text{Ni}_x\text{Mg}_{72-x}\text{Al}_{28}$  was chosen. To improve the degree of crystallinity the coprecipitated solids were hydrothermally treated at moderate temperature (60-70°C) for 2 hours.

For coprecipitation at low supersaturation a system was build, which is depicted in Figure 6.

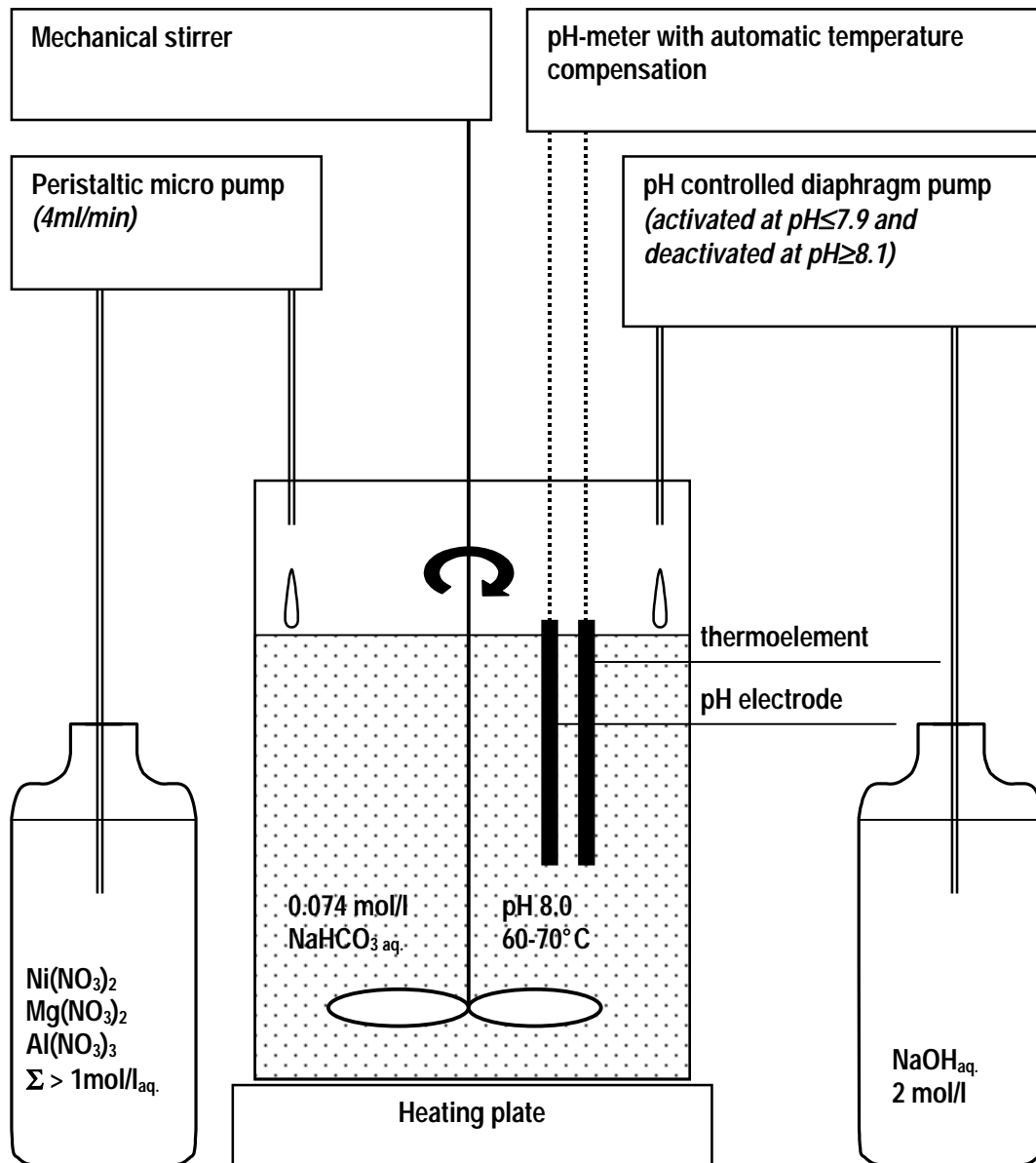


Fig. 6  
Set up for the preparation of hydrotalcite-type solids at low supersaturation

The following preparation procedure was developed and strictly followed for every preparation of HTs. The reaction vessel was filled with 500 ml of a freshly prepared

0.074 mol/l  $\text{NaHCO}_3$  solution (p.a., POCh, Poland) providing the carbonate ions necessary for the synthesis of carbonate containing HTs. Considering the general formula of the desired HTs  $\text{M(II)}_{2.6}\text{M(III)}_{1.0}(\text{OH})_{3.6}\text{CO}_3$  the solution contained a slight excess of carbonate of about 5% [67]. It was also found that the solution of  $\text{NaHCO}_3$  in the reaction vessel before the coprecipitation is advantageous in order to keep the pH value stable in the beginning, when the first precipitate is formed. The freshly calibrated pH meter (Eurosensor, Poland) and the thermoelement (DHN, Poland), both connected to the pH controller (Cole-Parmer, USA) were submerged into the solution. The pH controller automatically compensated the influence of the temperature on the pH value. The solution was stirred vigorously by a mechanical stirrer with a glass propeller and heated up to 60-70°C. Just before the start of the coprecipitation, the amount of water lost due to evaporation was added by adding water to the level marked before heating up. The pH was adjusted to 8.0 by addition of small amounts of diluted  $\text{HNO}_3$  (POCh, Gliwice, Poland) and if necessary also of a freshly prepared 2 M NaOH solutions (p.a., POCh, Poland).

Altogether 0.5 mol of  $\text{Mg}(\text{NO}_3)_2 \cdot 6 \text{H}_2\text{O}$  (99%, Aldrich),  $\text{Ni}(\text{NO}_3)_2 \cdot 6 \text{H}_2\text{O}$  (Crystal, Aldrich) and  $\text{Al}(\text{NO}_3)_3 \cdot 9 \text{H}_2\text{O}$  (99.997, Aldrich) were dissolved in 500 ml distilled water. The exact ratio of their amounts reflected the desired metal composition of the final HT. Due to their hydrate water the volume of the resulting metal nitrate solution was in all experiments about 600 ml, hence the metal concentration of the metal nitrate solution < 1 mol/l. After the reaction temperature was reached and the pH adjusted, the metal nitrates containing solution was continuously added dropwise to the reaction vessel by a peristaltic micro pump (Zalimp, Poland) at a speed of approximately 4 ml/min. The decrease in the pH value caused by the addition of the acidic metal nitrate solution was compensated by the pH controlled dropwise addition of a freshly prepared 2 M NaOH solution using a diaphragm pump (Cole Parmer, USA). The diaphragm pump was



automatically activated by the pH controller as soon as the pH value reached 7.9 and deactivated at pH 8.1. Following this procedure it was possible to keep the pH-value constant at  $\text{pH } 8 \pm 0.2$  during all coprecipitations. During the whole addition, which typically last 150 min the reaction mixture was stirred vigorously and the temperature kept at 60-70°C by a conventional 6 stage heating plate.

After the addition the coprecipitated solid was aged by keeping the solution under energetic stirring for 120 min at 60-70°. Afterwards the suspension was allowed to settle and to cool down to 30°C before being filtered under water pump vacuum. For the effective removal of all the sodium salts ( $\text{NaNO}_3$ ,  $\text{NaHCO}_3$  and especially less soluble  $\text{Na}_2\text{CO}_3$ ) possibly present in the precipitate, it was suspended in 500 ml distilled water under vigorous stirring and filtered again. As all these sodium salts are basic, the changes in the pH value of the filtrate with each washing cycle were used to monitor their removal. This procedure consisting of filtration and suspension was repeated until the pH value of two consecutive filtrates did not change. In all syntheses 3 washing cycles were necessary. After the final filtration the resulting solids were dried at 100°C for about 24 hours.

## 2.2. Preparation of the catalysts

The dried hydrotalcite-type solids were transformed into metal oxides by calcination in a tubular furnace (Barnstead | Thermolyne, USA). The furnace consisted of an innermost segment with a heat stability of  $\pm 0.2^\circ\text{C}$ , according to the producer. The quartz boat was placed in this innermost segment allowing uniform calcination conditions. The catalysts were calcined at the desired temperature (700-1000°C) for 16 hours. The furnace was heated up and cooled down by a temperature ramp of 10°C/min. During the calcination a constant flow of air, generated by a water pump,

through the furnace was maintained. The hydrotalcite-type solids were powdered before the calcination to allow an even calcination and to assist the fast removal of the gases evolved during the calcination process.

The use of the catalyst as a fine powder as received after the calcination process can lead to the blockage of the reactor due to the too fine particles, therefore larger particles must be used. However to avoid local variations of the velocities in a plug flow reactor (inner diameter 4mm) the reactor diameter should be at least 10 times larger than the particle size [121]. In order to fulfill these criteria the catalyst powder obtained after the calcination process was pressed at 5 bar and the resulting pellet crushed and sieved. The sieve fraction 0.2-0.385 mm was used.

A conventional steam reforming catalyst prepared by the 'Institute of Fertilisers' in Puławy, Poland, was used as a reference catalyst. The catalyst consisted of 20% NiO supported on  $\text{Al}_2\text{O}_3$  and contained additionally 2%  $\text{K}_2\text{O}$ . The surface area of the  $\text{Al}_2\text{O}_3$  support was  $30.5 \text{ m}^2/\text{g}$ . It was delivered as pellets after calcination at  $450^\circ\text{C}$  for 4 hours, reduction for 4 hours at  $800^\circ\text{C}$  and passivation. Before the catalytic tests it was crushed, sieved and reduced like the normal catalysts.

### 2.3. Elemental and structural analysis

The metal content of all hydrotalcite-type solids was determined employing inductively coupled plasma atomic emission spectroscopy (ICP-AES, Perkin-Elmer P400). The carbon and nitrogen content was analysed by an elemental analyser (Carlo-Erba elemental analyser 1106). The amount of intercalated water was determined from the first weight loss during the calcination, measured by thermogravimetry coupled with

---

mass spectroscopy (TG-MS) (Mettler Toledo Star TGA/SDTA 851<sup>e</sup> - Balzer GSD 300T3).

The structure of all coprecipitated and all calcined solids was studied by means of X-ray powder diffraction (XRD) (Siemens D500 diffractometer) using CuK $\alpha$  radiation ( $\lambda=0.15418$  nm). A range from 8° to 70° was investigated at a scanning speed of 0.030°/s. The morphology of selected calcined samples was investigated by scanning electron microscopy (SEM) at 20keV (Joel JSM 6300).

A detailed characterisation of the calcination process of all coprecipitated solids was performed by thermogravimetry combined with on-line analysis of the evolved gases by mass spectroscopy (TG-MS, described above) and by differential scanning calorimetry (DSC) (Mettler Toledo Star DSC 821<sup>e</sup>). TG was performed in a flow of air up to 1100°C and DSC in a flow of Ar up to 600°C, both at a heating rate of 5°C/min.

The BET surface area of the calcined samples was calculated from 3 point N<sub>2</sub> adsorption isotherm measured using Ankersmit Quantasorb Jr., employing mixtures of 10, 20 and 30% He in N<sub>2</sub>. The response factor for each mixture was calibrated for each measurement. Each sample was dried at 347°C for 2 hours in a flow of 10% He in N<sub>2</sub> prior to the measurement. The correlation coefficient for the N<sub>2</sub> adsorption isotherm was in all measurements between 0.99985 and 1.00000.

#### **2.4. Temperature programmed reduction and oxidation**

The reduction, oxidation and the Ni dispersion was studied by temperature programmed reduction (TPR) and temperature programmed oxidation (TPOx). The Ni dispersion was expressed as the amount of reducible Ni after passivation to the total

amount of reducible Ni<sup>2+</sup> ions. In order to investigate all properties for one sample, first the calcined catalyst was reduced, then passivated, reduced again and finally oxidised.

The set up used for the TPR experiments consisted of the reactant feed system, the reactor and the analytical unit. In the reactant feed system two mass flow controllers (Brooks, USA) were used to control the gas flows. One mass flow controller was used for inert gases, the other one for reactive gases, in these studies 5 vol% H<sub>2</sub>/Ar (Linde) and 5 vol% O<sub>2</sub>/He (Linde) mixtures. Each individual gas supply line could be opened and closed by toggle valves placed before the mass flow controllers. Only stainless steel or copper tubing was used outer diameter 3.2 mm (1/8"). The reactor was heated by an electrical furnace, controlled by a temperature controller (Chinotherm, Hungary, model LP-849). The reactor itself consisted of a quartz tube, inner diameter 4 mm, outer diameter 6 mm, in which the catalyst was placed on a quartz wool bed. The actual temperature of the catalyst was measured by a type-K thermocouple placed in a quartz capillary, which was positioned in the middle of the catalyst bed. The second thermocouple (type-K) necessary for the control of the heating element of the furnace was placed near the heating element of the furnace. Both thermocouples were connected to the thermocontroller, which controlled the heating power of the furnace. Changes in the composition of the reaction gas mixture, corresponding to the reaction rate were measured by a thermal conductivity detector (Valco, USA). A personal computer continuously recorded the temperature in the reactor and the detector signal.

A sample of 5 mg of each calcined catalyst was heated up in a linear temperature program of 5°C/min up to 950°C in the flow of the reduction mixture (8.5 ml/min). After the reduction the catalyst was cooled down to 40°C in the flow of the reduction mixture to avoid any possible oxidation of the catalyst. As soon as the temperature was below 40°C the reduced catalyst was passivated for 30 minutes in a flow of the oxidation

mixture. After the passivation the sample was reduced again up to 850°C at a constant heating rate of 10°C/min. Afterwards the catalyst was cooled down to room temperature in the flow of the reduction mixture and then heated up to 950°C in the flow of the oxidation mixture at a constant heating rate of 10°C/min. Before starting each measurement the baseline was allowed to stabilise and adjusted to zero. A stable baseline was also used as indicator for the absence of any leaks.

For the TPR measurements a H<sub>2</sub>/Ar mixture was employed because of the large thermal conductivity differences between H<sub>2</sub> and Ar. The amount of reducible Ni<sup>2+</sup> ions was determined from the consumption of H<sub>2</sub> from the 5 vol% H<sub>2</sub>/Ar mixture. Water formed during the reduction did not influence the detector signal because its thermal conductivity is very similar to that of Ar. For the TPOx an O<sub>2</sub>/He mixture was employed because of the large thermal conductivity differences between O<sub>2</sub> and He. The thermal conductivity of the gases is listed in Table 7.

Tab. 7: Thermal conductivity of relevant gases [122].

Gas	Thermal conductivity ( $\lambda$ ) at 120°C [(Cal· s <sup>-1</sup> · cm <sup>-1</sup> · °C <sup>-1</sup> )x10 <sup>-6</sup> ]
Ar	45.46
H <sub>2</sub>	471.11
H <sub>2</sub> O	46.70
He	376.07
O <sub>2</sub>	68.19

### 2.5. In-situ reduction combined with high temperature XRD

In-situ reduction experiments employing high temperature XRD were performed at temperature steps chosen on the results of the TPR experiments. Additionally XRD

spectra were also recorded at room temperature before and after the completed reduction to compare the spectra before and after the reduction process without distortions of the  $2\theta$  values of the reflections and the height of the amplitudes due to the temperature differences at the recording.

The set up consisted of a high temperature camera (Anton Paar, Austria) in combination with a Philips diffractometer PW3710 X'PERT, using  $\text{CuK}\alpha$  radiation ( $\lambda=0.15418$  nm). A range from  $10^\circ$  to  $70^\circ$  was investigated at a scanning speed of  $0.020^\circ/\text{s}$  for Ni30C900 and  $0.010^\circ/\text{s}$  for Ni72C900. The samples were placed on an electrically heated Pt ribbon and kept throughout the experiments in a flow of the reduction mixture (5 vol%  $\text{H}_2/\text{Ar}$ , Linde). Both samples were heated up at a linear heating rate of  $5^\circ\text{C}/\text{min}$  and cooled down at  $10^\circ\text{C}/\text{min}$ . The samples were scanned at room temperature, at 300, 600 and  $900^\circ\text{C}$  and again after cooling down to room temperature. During the scans the temperature was kept constant.

## 2.6. Temperature programmed desorption of $\text{CO}_2$

For the temperature-programmed desorption of  $\text{CO}_2$  (TPD- $\text{CO}_2$ ) the same set up was employed as for the TPR experiments described above apart from two modifications.  $\text{CO}_2$  (technical grade, Polgaz) was used as reactive gas and He as inert gas for desorption. He (99.9999%, Praxair) was used because of the large difference of the thermal conductivity of He and  $\text{CO}_2$ ,  $376.07 \times 10^{-6}$  and  $43.81 \times 10^{-6}$  ( $\text{Cal} \cdot \text{s}^{-1} \cdot \text{cm}^{-1} \cdot ^\circ\text{C}^{-1}$ ) respectively [122]. The other modification is that the  $\text{CO}_2$  stream was dried by a moisture trap containing silica gel. This was necessary as technical grade  $\text{CO}_2$  was used for the experiments. The colour change from blue (dry) to pink (hydrated) was used as indicator for the reactivation of the moisture trap.

---

In the TPD-CO<sub>2</sub> experiments a sample of 50 mg of each calcined catalyst was used instead of 5 mg like in the TPR experiments, because of the lower effect of the CO<sub>2</sub> desorption on the detector signal. The samples were degassed up to 620°C in the flow of He. After desorption of contamination the sample was cooled down in a flow of He to the desired adsorption temperature (100-200°C). CO<sub>2</sub> adsorption was performed in a flow of pure CO<sub>2</sub> for 1, 3 or 15 hours. After the adsorption the flow was switched to He and the baseline was allowed to stabilise and adjusted to zero before performing the CO<sub>2</sub> desorption up to 620°C at a heating rate of 10°C/min.

### **2.7. Test reactions for determination of basicity**

The transformation of isopropanol and the aldol condensation were performed using a simple catalytic reactor set up that consisted of the reaction feed system, the reactor and the analytical system. In the reactant feed system two mass flow controllers were used for controlling the gas flows. One was used for controlling the He flow passing through a saturator containing the liquid substrate (isopropanol, acetone, p.a., POCh, Poland), the other one to adjust the flow of He to dilute the saturated He stream or to control the flow of air. The saturator consisted of two parts. In the first part the He stream was saturated with the vapour of the liquid at room temperature by bubbling it through the liquid. To ensure a constant concentration of the vapour, in the second stage the gas stream was equilibrated at 0°C using a condensator cooled by a water-ice mixture. To avoid condensation of less volatile products the tubing after the reactor was heated by heating tape. The quartz plug flow reactor, the electric furnace and the temperature control was similar to the one described in the temperature programmed reaction experiments. The product stream was analysed by the analytical unit consisting of a gas chromatograph with flame ionisation detector (GC-FID) (Shimadzu, Japan, model GC-14A) equipped with a Porapack Q column, 5· 1/8' in stainless steel

(Macherey-Nagel). Samples were taken automatically using a GC controlled 6 port equipped with a sample loop. The catalysts (50 mg) were activated prior to the reaction by heating in a flow of air up to 600°C/30min and cooled down to the starting reaction temperature in a flow of He. The reactions were from 200 to 280°C for isopropanol, step size 10°C, and from 270 to 310°C for acetone, step size 20°C. For each experiment a fresh catalyst sample was used.

## 2.8. Catalytic partial oxidation of propane

### 2.8.1. Catalytic reactor set up

The set up used for the catalytic tests, depicted in Figure 7, consisted of three general parts: the reactant feed system, the reactor and the analytical unit.

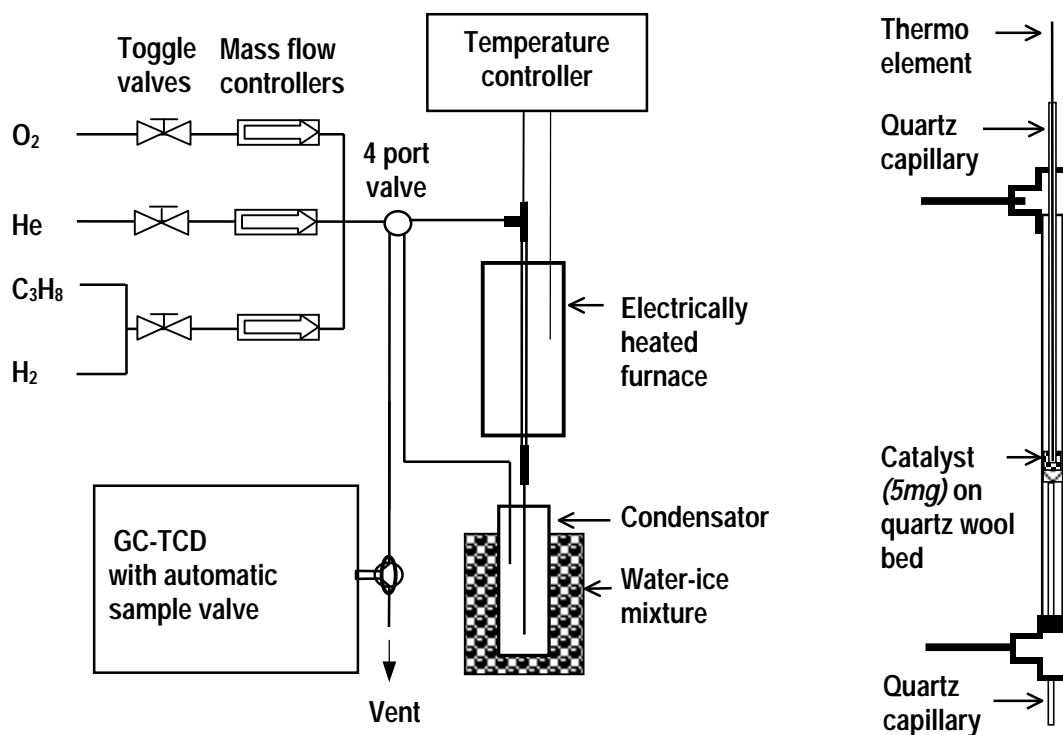


Fig. 7  
Schematic drawing of the apparatus set up used in the catalytic tests (left) and of the packed micro flow reactor (left)



---

The gas flows were controlled by 3 mass flow controllers (Brooks, USA), one used for reductive gases: propane (Aldrich, 98%+) or H<sub>2</sub> (generated by a gas generator (Domnik Hunter, England, model DHG 500), one used for O<sub>2</sub> (technical grade, Poligaz) and the last one for the inert gas (He, 99,999%+, Praxair, Poligaz). Helium was further purified by a heated high capacity gas purifier (Supelco). Each individual gas supply line could be opened and closed by a toggle valve placed before the mass flow controllers. Before the toggle valves copper as well as stainless steel tubing was used whereas after the toggle valves only stainless steel tubing, the tube diameter was in all cases 3.2 mm (1/8"). After the mass flow controllers the gases were allowed to mix. A 4 port valve allowed choosing whether the gas mixture flew through the reactor or bypassing it. Bypassing the reactor allowed faster calibration and was essential for checking any leaks in the reactor by comparing the flow rates through the reactor and through the bypass.

As in the temperature programmed reactions and the test reactions the reactor consisted of a quartz tube, inner diameter 4 mm, outer diameter 6 mm, in which the catalyst was placed on a quartz wool bed, the whole reactor set up is depicted in Figure 7. The quartz wool bed was replaced for each experiment. It was observed that the quartz wool bed and the catalysts could be pushed down the reactor by the flowing gas mixture. To avoid this the quartz wool bed was held by a quartz capillary from beneath. Otherwise the reactor set up is identical with the one used for the catalytic test reactions and the temperature programmed reactions described above. The temperature of the reactor was controlled by a temperature controller identical to the one used in the temperature programmed reactions. Water was separated from the product stream by a glass condensator at 0°C using a water-ice mixture.

After the condensation of water the gases were analysed by the analytical unit consisting of a gas chromatograph (GC-TCD) (Varian, USA, model Star 3400CX) equipped with thermal conductivity detector and Carboxen 1004 micropacked porous carbon column, 2· 1/16' in stainless steel (Supelco). Samples were taken automatically using a GC controlled 6 port valve equipped with a sample loop. Helium was used as carrier gas.

The comparison of the flow rates bypassing the reactor and through the reactor was used to check whether the reactor was leak free before starting each experiment. Conventional leak detectors based on liquids producing bubbles in case of a leak had proven not to be suitable for the detection of small leaks at atmospheric pressure. A portable thermal conductivity detector (TCD) was also not sufficient. The reactor was assumed leak free only if the difference in the flow rate between bypassing the reactor and through the reactor was  $\leq 0.1\%$  ( $\leq 0.04$  ml/min at a total flow rate of 40ml/min). Only if this criterion was fulfilled the catalytic tests were reproducible.

The peak area of the TCD signal was calibrated for all reactants and products by one-point calibration except for  $H_2$ ,  $C_3H_4$  and  $C_3H_6$ .  $O_2$  and  $C_3H_8$  were calibrated using the not reacted substrate feed, for  $C_3H_4$  and  $C_3H_6$  the same calibration coefficients were assumed as for  $C_3H_8$ .  $CO$ ,  $CO_2$ ,  $CH_4$ ,  $C_2H_2$ ,  $C_2H_4$ ,  $C_2H_6$  were calibrated from a calibration mixture each compound at  $\sim 1\%$  in  $N_2$  (Scott). Due to the closeness of the retention times of  $CO$  and  $N_2$  and the large amount of  $N_2$  in the calibration mixture ( $\sim 94\%$ ), it was not possible to achieve a sufficient separation of the  $CO$  and  $N_2$  peak using the Carboxen 1004 column. Therefore  $CO$  and  $N_2$  were separated using a freshly activated Molsieve 5A column. The peak area of  $CO$  for the Carboxen column was calculated from the ratio of the well separated  $CO$  and  $N_2$  peak area using the molsieve

5A column and the total area of the not sufficiently resolved N<sub>2</sub>-CO peak over the Carboxen column according to:

$$\frac{\text{Area CO}_{\text{Molsieve 5A}}}{\text{Area (CO + N}_2\text{)}_{\text{Molsieve 5A}}} = \frac{\text{Area CO}_{\text{Carboxen 1004}}}{\text{Area (CO + N}_2\text{)}_{\text{Carboxen 1004}}}$$

As N<sub>2</sub> was never present in the catalytic tests the problem of the separation of N<sub>2</sub> and CO occurred only during the calibration.

Since H<sub>2</sub> has a non-linear thermal conductivity behaviour in He, which was used as carrier gas, for the calibration of the H<sub>2</sub> response signal 18 points were used ranging from 3.9 to 45% H<sub>2</sub>/He. A calibration curve was fitted to the experimental points by a polynomial function of the 6<sup>th</sup> degree using Microsoft Excel software.

### 2.8.2. Procedure

The performance of the catalysts was tested in a standardised procedure to ensure to reproducibility and the comparability of the results. In each catalytic test 5 mg of catalyst were placed on a quartz wool bed in the quartz reactor. The catalyst was heated up to the reduction temperature in a flow of 40 ml/min He. This way adsorbed compounds like water and CO<sub>2</sub> were desorbed prior to the reduction. The reduction of the catalysts was performed in-situ prior to the reaction at the desired temperature in a flow 40 ml/min of pure H<sub>2</sub> for two hours. This rather high flow was used to ensure constantly high partial pressure of H<sub>2</sub> and to remove any H<sub>2</sub>O formed during the reduction, which has been reported to be beneficial [59]. The reduction was started after the temperature was constant for at least 5 min. H<sub>2</sub> was added and the He flow

switched off after the H<sub>2</sub> flow was stable. Changes in the temperature at the beginning of the reduction were compensated by changes of the heating power of the temperature controller. After 2 hours of reduction a flow of 40 ml He was added and the H<sub>2</sub> flow switched off as soon as the He flow was stable. The reactor was purged with He and the temperature adjusted to the desired reaction temperature in the flow of He.

The catalytic test was carried out by continuously passing the gaseous reaction mixture consisting of He, C<sub>3</sub>H<sub>8</sub> and O<sub>2</sub> over the catalyst. In order to avoid any oxidation of the catalyst prior to the reaction first C<sub>3</sub>H<sub>8</sub> was added to the existing flow of He and allowed to stabilise before adding O<sub>2</sub> to the feed. The standard catalytic test was carried out by passing continuously 75 ml/min of the reaction mixture over the catalyst resulting in a gas hourly space velocity (GHSV) of 900 dm<sup>3</sup>·h<sup>-1</sup>·g(cat)<sup>-1</sup> measured at room temperature and atmospheric pressure. The reaction mixture consisted of C<sub>3</sub>H<sub>8</sub>, O<sub>2</sub> and He in a ratio of 16/30/54. The temperature rise observed at the beginning of the reaction was automatically compensated by decreasing the heating power of the furnace. The reaction temperature had to be stable at the set temperature for at least 5 min before the first analysis. After the stabilisation of the temperature the reaction temperature had to be constant within 2°C of the set temperature otherwise the experiment was rejected. After 240 min on stream the reaction was stopped by switching off first the O<sub>2</sub> and then C<sub>3</sub>H<sub>8</sub> flow in order to avoid oxidation of the carbon deposits or of the catalyst. The catalyst was cooled down in a flow of He and separated from the quartz wool bed for further the determination of the amount of coke formed during the reaction.

Experiments with different C<sub>3</sub>H<sub>8</sub>/O<sub>2</sub> ratios were performed by increasing or decreasing the O<sub>2</sub> flow. The total flow and hence the GHSV were kept constant by adjusting the helium flow accordingly. Experiments carried out at different GHSVs were performed

by using the same ratio of the gases as under the standard test reaction but changing the total flow rate while keeping the amount of the catalyst constant. This was done because the length of the catalyst bed can influence the performance of the catalyst even at the same GHSV [121]. The flow rates of the gases were measured using the same bubble flow meter as in the leak checks.

The carbon content of the spent catalyst was measured as mass lost during the temperature programmed combustion (TPC) in air up to 1100°C in the TG-MS a linear heating rate of 20°C/min. The mass gain due to oxidation of reduced Ni particles, which overlapped with the combustion of the carbon deposits was taken into account by considering that all Ni particles reducible in the temperature programmed reduction were in the metallic state after the catalytic tests and oxidised to NiO during the temperature programmed combustion.

The catalysts' relative deactivation rate was measured as the relative decrease of the C<sub>3</sub>H<sub>8</sub> conversion with time on stream divided by the time from the first to the last analysis. The relative decrease of the C<sub>3</sub>H<sub>8</sub> conversion was calculated from the linear trend line using Microsoft Excel software.

The C<sub>3</sub>H<sub>8</sub> and O<sub>2</sub> conversion values (X) were calculated according to:

$$X_{\text{C}_3\text{H}_8} = \frac{F_{\text{C}_3\text{H}_8 \text{ in}} - F_{\text{C}_3\text{H}_8 \text{ out}}}{F_{\text{C}_3\text{H}_8 \text{ in}}}$$

$$X_{\text{O}_2} = \frac{F_{\text{O}_2 \text{ in}} - F_{\text{O}_2 \text{ out}}}{F_{\text{O}_2 \text{ in}}}$$

$$F_{i\text{out}} = x_i \times F_{\text{totalout}}$$

where F is the flow (ml/min) measured at room temperature and atmospheric pressure and x is the volume fraction as calculated from the calibrated peak area

The total outlet flow rate changed due to the reaction and was calculated from the helium balance:

$$F_{\text{Heout}} = F_{\text{Hein}} = 40 \text{ ml/min}$$

$$x_{\text{Heout}} = 1 - \sum x_{i\text{out}}$$

$$F_{\text{totalout}} \times x_{\text{Heout}} = F_{\text{outHe}} = F_{\text{Hein}} = 40 \text{ ml/min}$$

$$F_{\text{totalout}} = \frac{40 \text{ ml/min}}{x_{\text{Heout}}}$$

$$F_{i\text{out}} = x_i \times F_{\text{totalout}}$$

The quantities of water formed were determined from the oxygen atom balance:

$$F_{\text{H}_2\text{O}} = 2 \times F_{\text{O}_2\text{in}} - 2 \times F_{\text{O}_2\text{out}} - 2 \times F_{\text{CO}_2\text{out}} - F_{\text{COout}}$$

The selectivities (S) were calculated as hydrogen selectivity for H<sub>2</sub> and H<sub>2</sub>O and as carbon selectivity for all carbon containing products according to:

$$S_{H_2} = \frac{2 \cdot F_{H_2}}{\sum_i (N_{Hi} \cdot F_i)}$$

$$S_{H_2O} = \frac{2 \cdot F_{H_2O}}{\sum_i (N_{Hi} \cdot F_i)}$$

$$S_{\text{carbon containing product } i} = \frac{N_{Ci} \cdot F_i}{\sum_i (N_{Ci} \cdot F_i)}$$

where  $N_{Hi}$  is the number of hydrogen atoms of product molecule  $i$

and  $N_{Ci}$  is the number of carbon atoms of product molecule  $i$

The yield ( $Y$ ) was calculated according to:

$$Y_i = X_{\text{propane}} \cdot S_i$$

### 2.8.3. Modification of the furnace

Considerable temperature gradients in the catalyst bed must be avoided as much as possible when catalysts are tested. Otherwise the temperature measured may not be representative for the whole system and the catalytic tests would have only limited validation. A reactor with a small temperature gradient may also provide that the gas stream is preheated to the reaction temperature before it gets in contact with the catalyst, hence minimising any temperature gradient, especially at the beginning of the catalyst bed. Therefore it is of great importance that a furnace is used that provides such an isothermal zone in the reactor (no temperature gradient). A long isothermal

zone is also beneficial if larger amounts of catalysts are employed (long catalyst bed), ensuring a negligible temperature gradients due to the reactor itself. The temperature gradient of a given reactor in the absence of a reaction is determined by the furnace. Therefore a furnace must be chosen that provide no or little temperature gradients under the reaction conditions. The original furnace consisted of a cylindrical electrical heating element hollow in the middle (outer diameter 4.4 cm, inner diameter 1.6 cm). The heating element consisted of a ceramic element and a heating wire. The whole element itself was surrounded for electrical and thermal isolation by a thin layer of synthetic kaolinite wool and suited in a metal container (Fig. 8).

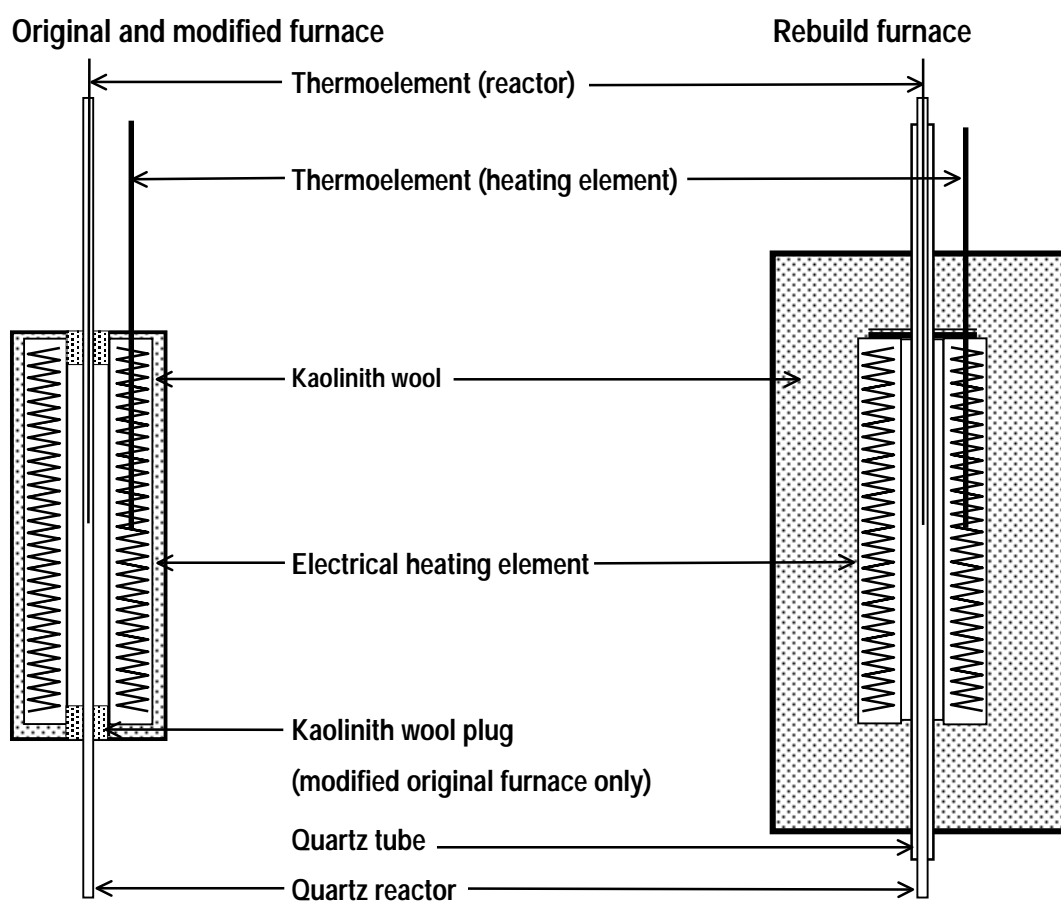


Fig. 8  
Proportional drawings of the original, the modified and the rebuild furnace



The reactor (outer diameter 6 mm, inner diameter 4 mm) was placed in the middle of the furnace. The temperature profile of the original furnace exhibited a strong temperature gradient (Fig. 9). From the middle of the furnace to 3 cm downstream, the temperature decreased by 162°C, from the middle to 1 cm downstream 35°C. Due to this large temperature gradient the furnace was regarded as not suitable for the purpose of the catalytic tests and therefore modified.

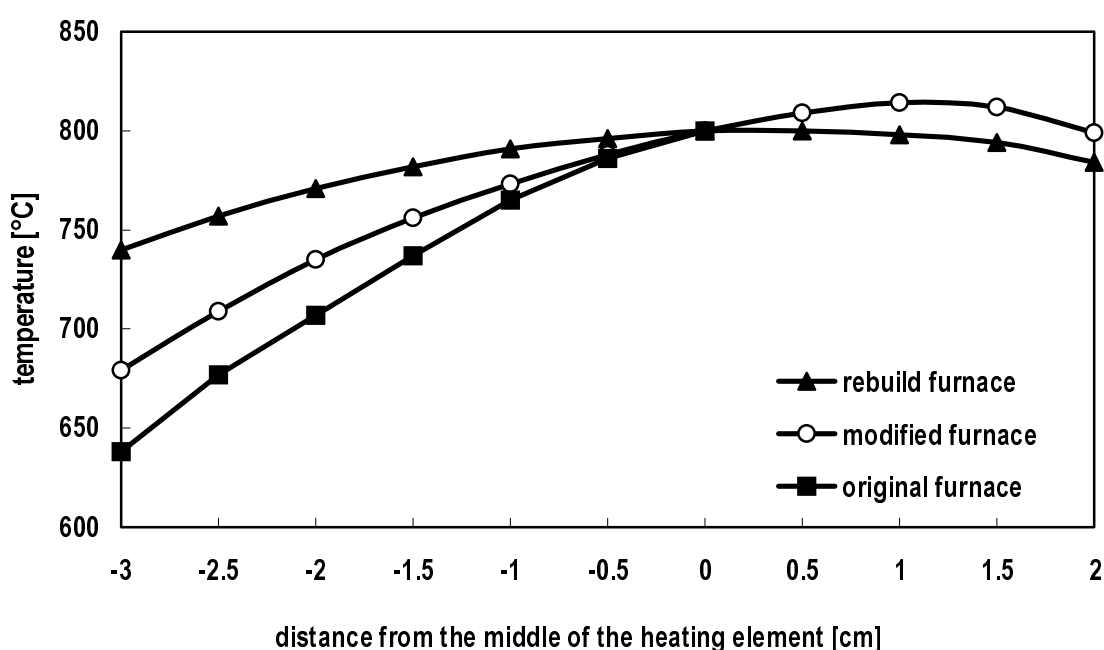


Fig. 9  
Temperature profiles of the original, the modified and the rebuild furnace

Since cold air circulating between the furnace and the reactor like in a chimney is suspected to be the main reason for the large temperature gradient, the top and bottom ends of the void between the furnace and the reactor were plugged with kaolinite wool (Fig. 8). This improved the temperature profile considerably. A short almost isothermal zone was found ca. 1 cm upstream the middle of the reactor. Nevertheless the furnace was still considered to be insufficient for various reasons. The temperature gradient in

the 1 cm long isothermal zone was still 5°C. Furthermore, the hottest zone in the reactor at which the catalyst bed must be placed was shifted upstream by about 1 cm. This means shortening of the time for the feed stream to heat up to the reaction temperature, which might be important when using high flow rates as demanded for the catalytic tests. A sufficient preheat of the feed stream had also to be questioned on the basis of the sloping shape of the temperature profile of the furnace (Fig. 9). A further problem is that it cannot be guaranteed that the kaolinite wool plug is always of the same thickness and shape, both factors that may change the temperature profile and hence the catalytic performance.

To further minimise the total temperature gradient over the whole reactor and to improve the isothermal zone especially, the furnace was rebuilt using the same electrical heating element (Fig. 9). A wider and longer metal container with a tightly fitting lid was used in which the furnace was placed. The free space between the metal container and the heating element was filled with insulating kaolinite wool enlarging the furnace dimensions and the heated zone. Furthermore a straight quartz tube was inserted between the furnace and the reactor reducing the space through which cold air can circulate. The 3 way T-junction which hold the reactor was placed on the top of the insert. This way the T-junction also plugged the top end of the insert, hence avoiding the need for an additional kaolinite wool plug. This way the reactor could also be placed without any complications in the same position in every experiment. The rebuilding of the furnace improved the temperature profile remarkably (Fig. 9). As the hottest zone was only shifted upstream by 0.3 cm and the temperature gradient in the innermost 1 cm of the hottest zone was reduced to 2°C. Also the whole temperature profile was found to be much narrower. Therefore the furnace was regarded as suitable.

The temperature measurements were performed at 800°C in a flow of 50 and 100 ml/min He in order to resemble the reaction conditions as much as possible. Helium was used for the measurements, because of its good thermal conductivity ensuring accurate temperature readings. The actual temperature at different positions was measured by an additional external thermocouple system. Each measurement was performed twice. The reproducibility for each experiment at each point was within  $\pm 1^\circ\text{C}$ . The flow rate had no considerable influence on the temperature ( $\pm 2^\circ\text{C}$ ) or the temperature profiles.

### 3. Results and discussion - catalyst preparation and characterisation

#### 3.1. Catalyst precursors

##### 3.1.1. Elemental analysis

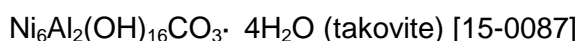
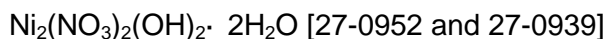
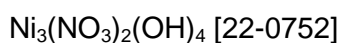
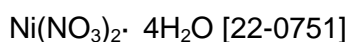
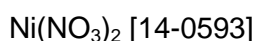
The coprecipitated solids are labelled according to their Ni content (expressed as metal atom%) as Ni0, Ni5, Ni10, Ni15, Ni30, Ni50 and Ni72 (Tab. 8). The measured amount of  $\text{CO}_3^{2-}$  and  $\text{NO}_3^-$  reflected the amount of anionic charge needed to compensate the additional charge due to the substitution of  $\text{Mg}^{2+}$  by  $\text{Al}^{3+}$ . The theoretical value of the total weight loss was calculated taking into account the amount of intercalated water, the destruction of the intercalated anions and the dehydroxylation of the metal hydroxides.

Tab. 8: Chemical composition of the coprecipitated solids (int. = intended, obs. = observed, cal. = calculated)

Sample	Composition [metal atom%]						$\text{CO}_3^{2-}$ [mol %]	$\text{NO}_3^-$ [mol %]	Total weight loss [%]	
	Ni		Mg		Al				cal.	obs.
	int.	obs.	int.	obs.	int.	obs.				
Ni0	—	—	72.0	72.0	28.0	28.0	0.09	0.13	45.47	45.46
Ni5	5.0	5.0	67.0	66.0	28.0	29.0	0.10	0.16	46.89	46.74
Ni10	10.0	9.4	62.0	61.6	28.0	29.1	0.08	0.16	44.47	43.03
Ni15	15.0	15.7	57.0	55.8	28.0	28.5	0.08	0.16	44.76	45.23
Ni30	30.0	30.1	42.0	41.8	28.0	28.1	0.10	0.12	40.16	42.04
Ni50	50.0	50.3	22.0	21.4	28.0	28.3	0.06	0.16	38.19	39.23
Ni72	72.0	73.2	—	—	28.0	26.8	0.08	0.13	33.80	36.43

### 3.1.2. Structural analysis

The XRD spectra of the coprecipitated and dried solids are presented in Figure 10. The diffraction patterns were compared to the 3 strongest reflections of Mg, Ni and Al hydroxides, nitrates, carbonates and mixtures of them using a continuously upgraded JCPDS database. After this first screening the spectra of the coprecipitated solids were carefully compared to the complete diffraction patterns of the following, which exhibited the most similar XRD patterns compounds (the JCPDS catalogue numbers are given in squared brackets).



The comparison showed that well crystallised solids of hydrotalcite-type structure were obtained. The reflections observed correspond to the structures of hydrotalcite ( $\text{Mg}_6\text{Al}_2(\text{OH})_{16}\text{CO}_3 \cdot 4\text{H}_2\text{O}$ ) and takovite ( $\text{Ni}_6\text{Al}_2(\text{OH})_{16}\text{CO}_3 \cdot 4\text{H}_2\text{O}$ ), the Ni derivative of hydrotalcite, the latter found only in Ni72, the pure Ni/Al compound and Ni50, the solid with a high Ni/Mg ratio ( $\sim 5/2$ ).

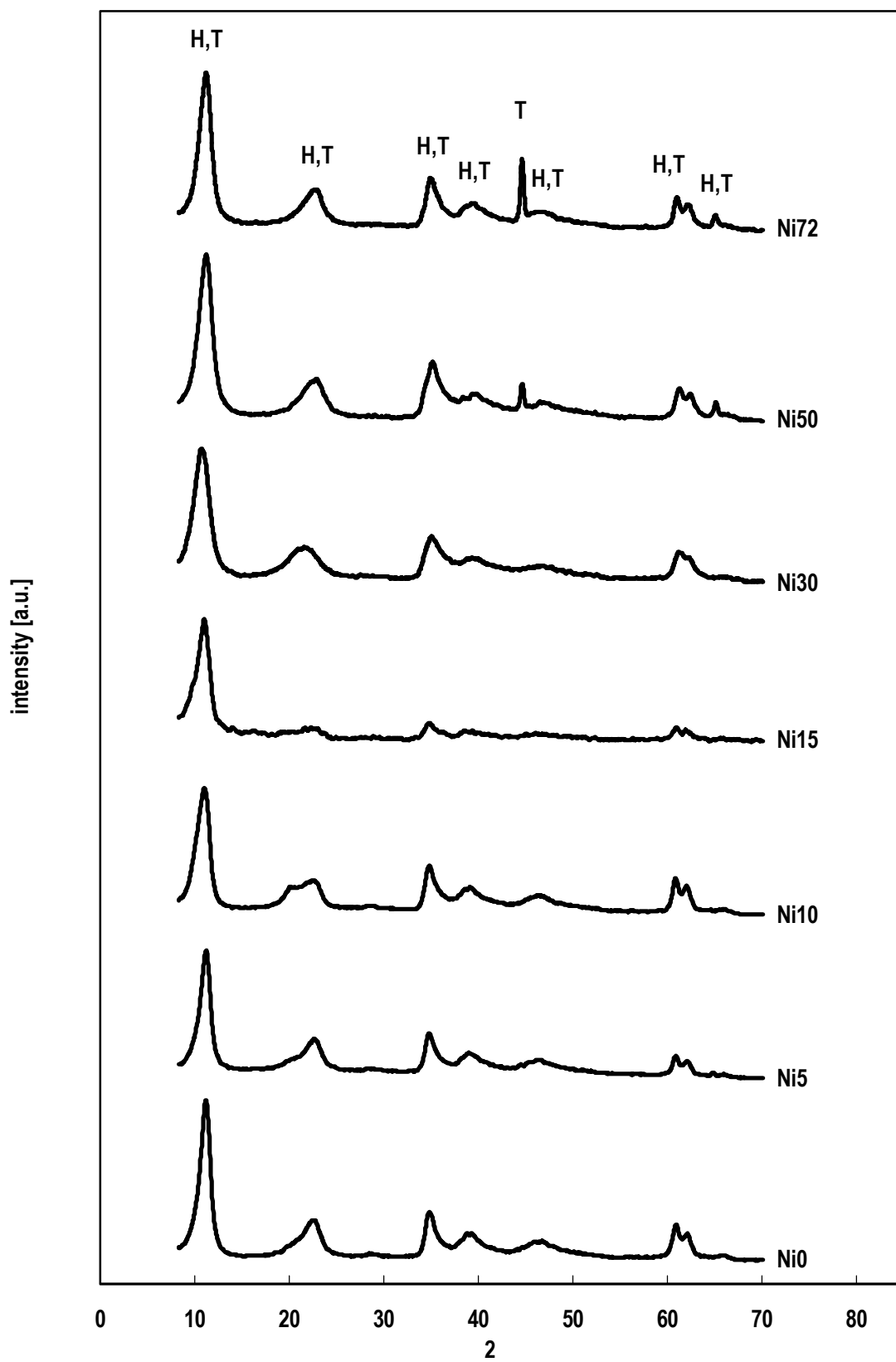
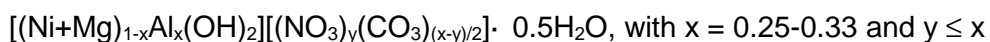


Fig. 10  
XRD spectra of the coprecipitated solids (H = hydrotalcite, T = takovite)

### 3.1.3. Analysis of the thermal degradation

However, as only crystalline phases can be observed by XRD, the presence of amorphous side phases cannot be excluded. Such phases can generally be detected in hydrotalcite-type solids by the study of the thermal degradation process using TG and DSC. The TG profiles with the corresponding DTA curves are presented in Figure 11 and the DSC thermograms in Figure 12. Two endothermic weight losses were observed during the calcination of all samples at about 140 and 360°C. The temperature of the second weight loss increased with decreasing Ni/Mg ratio of the solids from 310°C for Ni72 to 420 for Ni0. Depending on the sample composition, the first weight loss accounted for about 8-15% mass loss and the second one for about 15-35%.

The temperature, the amount of lost weight and the shape of the curves are typical for HT materials. On the basis of the on-line analyses of the volatiles by MS and the literature (see chapter 1.2.2.), the first weight loss should be attributed to the loss of the interlayer water, the latter to the elimination of the carbonate and nitrate anions in the interlayer and the dehydroxylation of the metal hydroxide. The results show that the thermal stability of the hydrotalcite-type solids decreases with increasing substitution of  $Mg^{2+}$  by  $Ni^{2+}$ . The analysis of the structure and the thermal degradation process proofs that coprecipitation yielded well crystallised solids of hydrotalcite-type structure their composition and phase composition is presented in Table 9. The composition of the solids matches well with the idealised formula found in the literature for synthetic Ni/Mg/Al solids of hydrotalcite-type structure [6, 33, 42, 43, 46]:



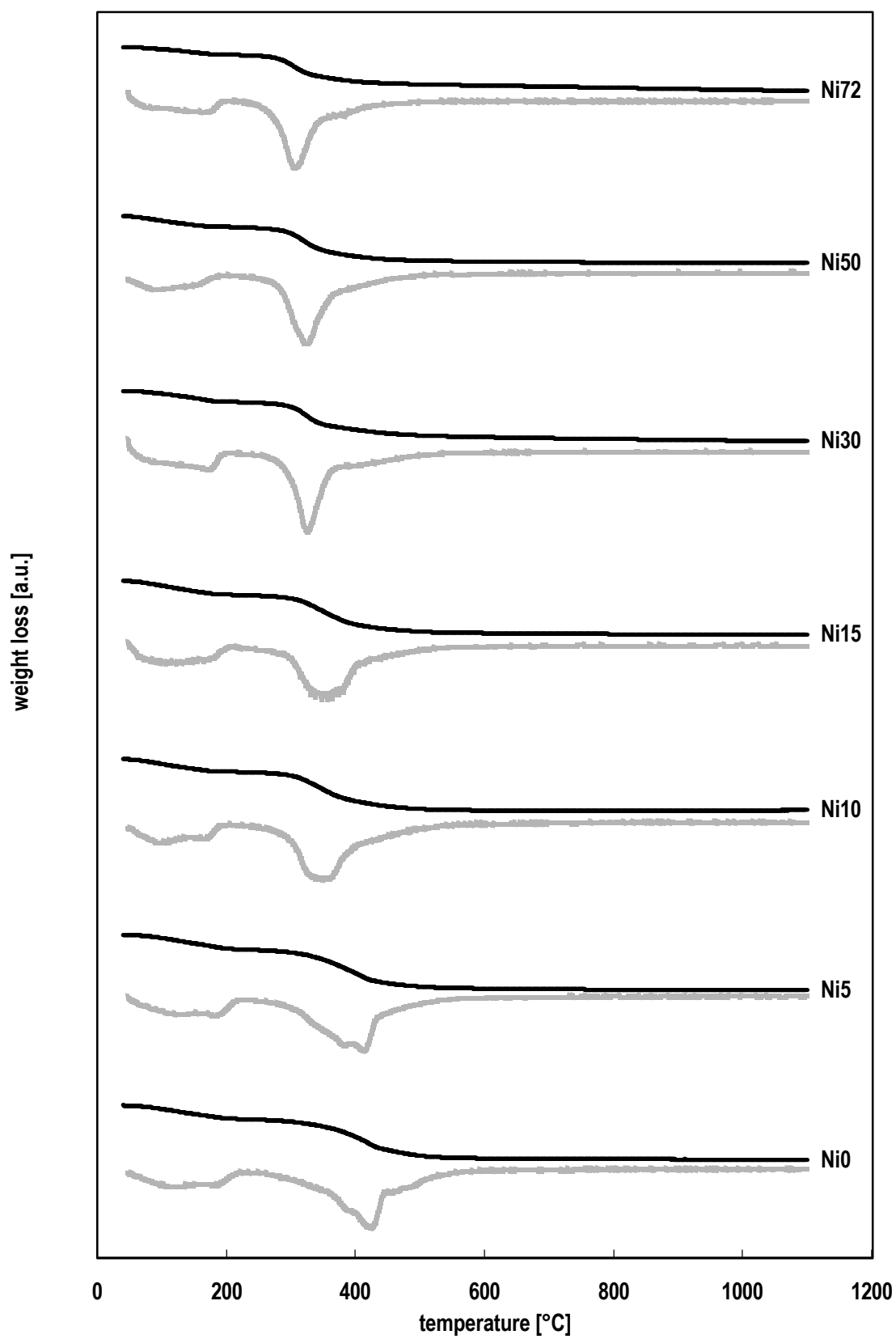


Fig. 11  
TG profiles (black) and DTG profiles (grey) of the coprecipitated solids



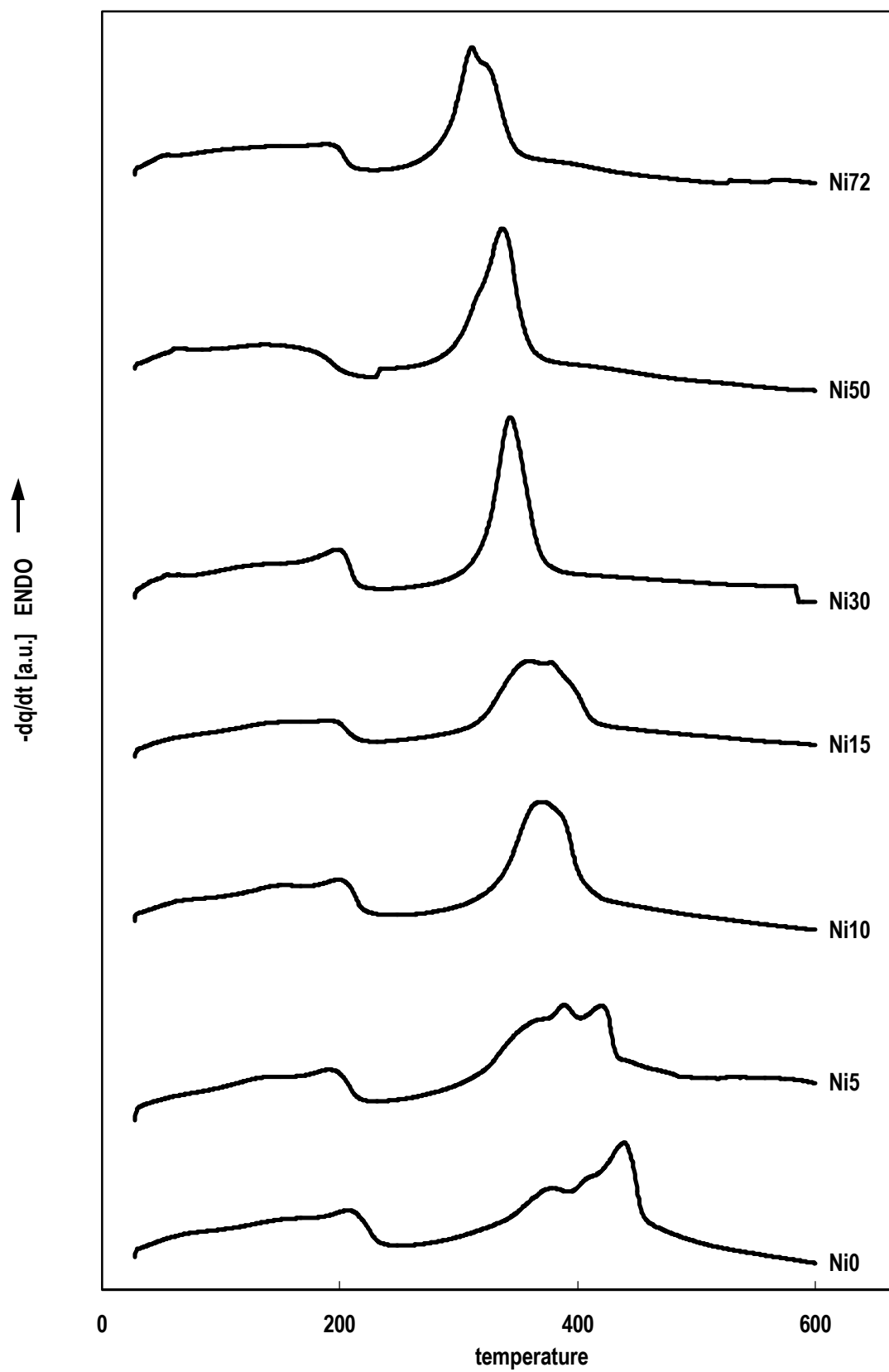


Fig. 12  
DSC thermograms of the coprecipitated solids

Tab. 9: Formula and structure of the coprecipitated solids

Sample	Chemical composition	Structure
Ni0	$[\text{Mg}_{0.720}\text{Al}_{0.280}(\text{OH})_2][(\text{NO}_3)_{0.121}(\text{CO}_3)_{0.079}] \cdot 0.52 \text{ H}_2\text{O}$	hydrotalcite
Ni5	$[\text{Ni}_{0.050}\text{Mg}_{0.660}\text{Al}_{0.290}(\text{OH})_2][(\text{NO}_3)_{0.131}(\text{CO}_3)_{0.080}] \cdot 0.61 \text{ H}_2\text{O}$	hydrotalcite
Ni10	$[\text{Ni}_{0.094}\text{Mg}_{0.616}\text{Al}_{0.291}(\text{OH})_2][(\text{NO}_3)_{0.149}(\text{CO}_3)_{0.071}] \cdot 0.50 \text{ H}_2\text{O}$	hydrotalcite
Ni15	$[\text{Ni}_{0.157}\text{Mg}_{0.558}\text{Al}_{0.285}(\text{OH})_2][(\text{NO}_3)_{0.141}(\text{CO}_3)_{0.072}] \cdot 0.57 \text{ H}_2\text{O}$	hydrotalcite
Ni30	$[\text{Ni}_{0.301}\text{Mg}_{0.418}\text{Al}_{0.281}(\text{OH})_2][(\text{NO}_3)_{0.109}(\text{CO}_3)_{0.086}] \cdot 0.44 \text{ H}_2\text{O}$	hydrotalcite
Ni50	$[\text{Ni}_{0.503}\text{Mg}_{0.214}\text{Al}_{0.283}(\text{OH})_2][(\text{NO}_3)_{0.164}(\text{CO}_3)_{0.059}] \cdot 0.52 \text{ H}_2\text{O}$	hydrotalcite, takovite
Ni72	$[\text{Ni}_{0.732}\text{Al}_{0.268}(\text{OH})_2][(\text{NO}_3)_{0.121}(\text{CO}_3)_{0.073}] \cdot 0.36 \text{ H}_2\text{O}$	takovite

## 3.2. Catalysts

### 3.2.1. Preparation

For the use as catalysts the prepared HTs were transformed into mixed metal oxide catalysts by calcination at 900°C. The HT Ni10 was also calcined at different temperatures (700, 800, 900 and 1000°C) to study the influence of the calcination temperature on the catalytic behaviour of the final catalyst. In the following the catalysts will be denoted according to their metal atom percentage of Ni and their calcination temperature, e.g. Ni10C900: catalyst precursor Ni10 calcined at 900°C.

### 3.2.2. Structure and morphology

The XRD spectra of the HT precursors calcined at 900°C are presented in Figure 13 and the spectra of Ni10 calcined at various temperatures in Figure 14. The analysis

was performed analogously to the coprecipitated solids. The spectra of the calcined catalysts were carefully compared to the complete diffraction patterns of the following compounds (again the JCPDS catalogue numbers are given in squared brackets):

MgO (periclase) [04-0829]

NiO (bunsenite) [04-0835]

Mg<sub>0.4</sub>Ni<sub>0.6</sub>O [34-0410]

MgNiO<sub>2</sub> [03-0999]

MgAl<sub>2</sub>O<sub>4</sub> [21-1152]

NiAl<sub>2</sub>O<sub>4</sub> [10-3339]

Al<sub>2</sub>O<sub>3</sub> [13-0373]

Al<sub>2</sub>O<sub>3</sub> [34-0493]

Mg<sub>6</sub>Al<sub>2</sub>(OH)<sub>16</sub>CO<sub>3</sub>·4H<sub>2</sub>O (hydrotalcite) [41-1428]

Ni<sub>6</sub>Al<sub>2</sub>(OH)<sub>16</sub>CO<sub>3</sub>·H<sub>2</sub>O (takovite) [15-0087]

The comparison showed that the HTs calcined at 900°C consist of well crystallised divalent metal oxide and spinel phases. Depending on the composition various spinel phases (e.g. MgAl<sub>2</sub>O<sub>4</sub>, NiAl<sub>2</sub>O<sub>4</sub>) and various divalent metal oxide phases (Mg<sub>x</sub>Ni<sub>1-x</sub>O) with periclase or bunsenite structure and could be formed. As bunsenite is the Ni derivative of periclase these divalent metal oxide phases will be referred to in the following as divalent metal oxide phases with periclase structure. In case of Ni5C900 also hydrotalcite-type phase was detected, which is attributed to partially surfacial reconstruction.

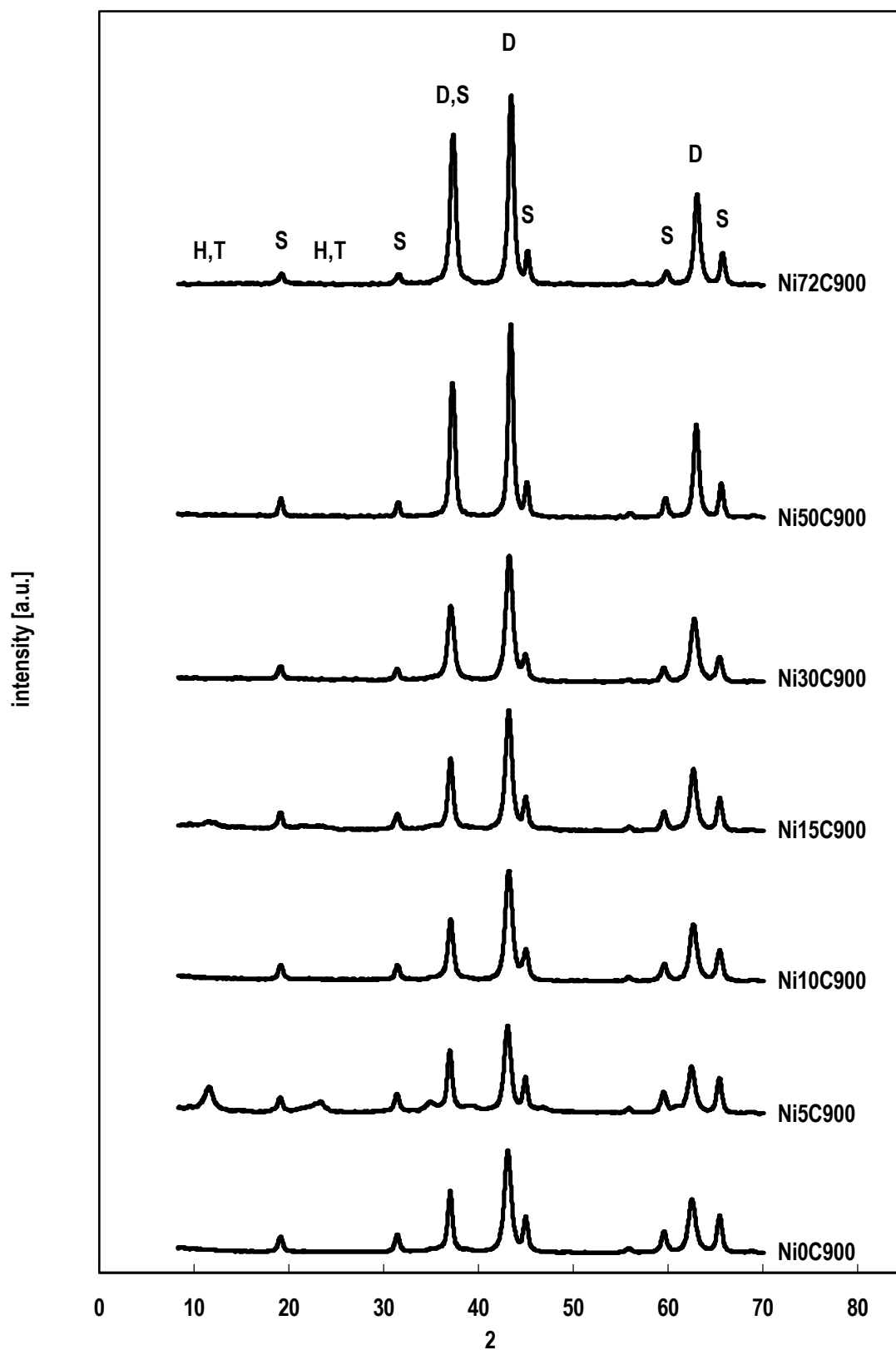


Fig. 13

XRD spectra of the catalysts calcined at 900°C (D = divalent metal oxide phase with periclase structure, S = spinel phase, H = hydrotalcite-type phase, T = takovite-type phase)

The XRD spectra of Ni10 calcined at the different temperatures reveal that at temperatures  $\geq 900^\circ\text{C}$  the catalysts consist of well crystallised spinel phases and divalent metal oxide phases with periclase structure. Upon calcination at temperatures  $\leq 800^\circ\text{C}$  only poorly crystallised spinel phases and divalent metal oxide phases with periclase structure were observed next to a hydrotalcite-type phase, which is again attributed to partially surficial reconstruction. Furthermore the crystallinity of all samples increased with increasing calcination temperature as determined by XRD line broadening (Tab. 10). The findings are in good agreement with the existing model concerning the structure of HT derived catalysts. Calcination at temperatures above  $850^\circ\text{C}$  results in the formation of well crystallised divalent metal oxide phases with periclase structure and spinel phases, whereas at temperatures below  $850^\circ\text{C}$  a poorly crystallised divalent metal oxide phase with periclase structure is formed in addition to an amorphous  $\text{Al}_2\text{O}_3$  phase and a spinel phase at their interface [7, 53].

Tab. 10: Crystallite size determined by XRD line broadening

Catalyst	Crystallite size [nm]
Ni10C700	6
Ni10C800	8
Ni10C900	14
Ni10C1000	25

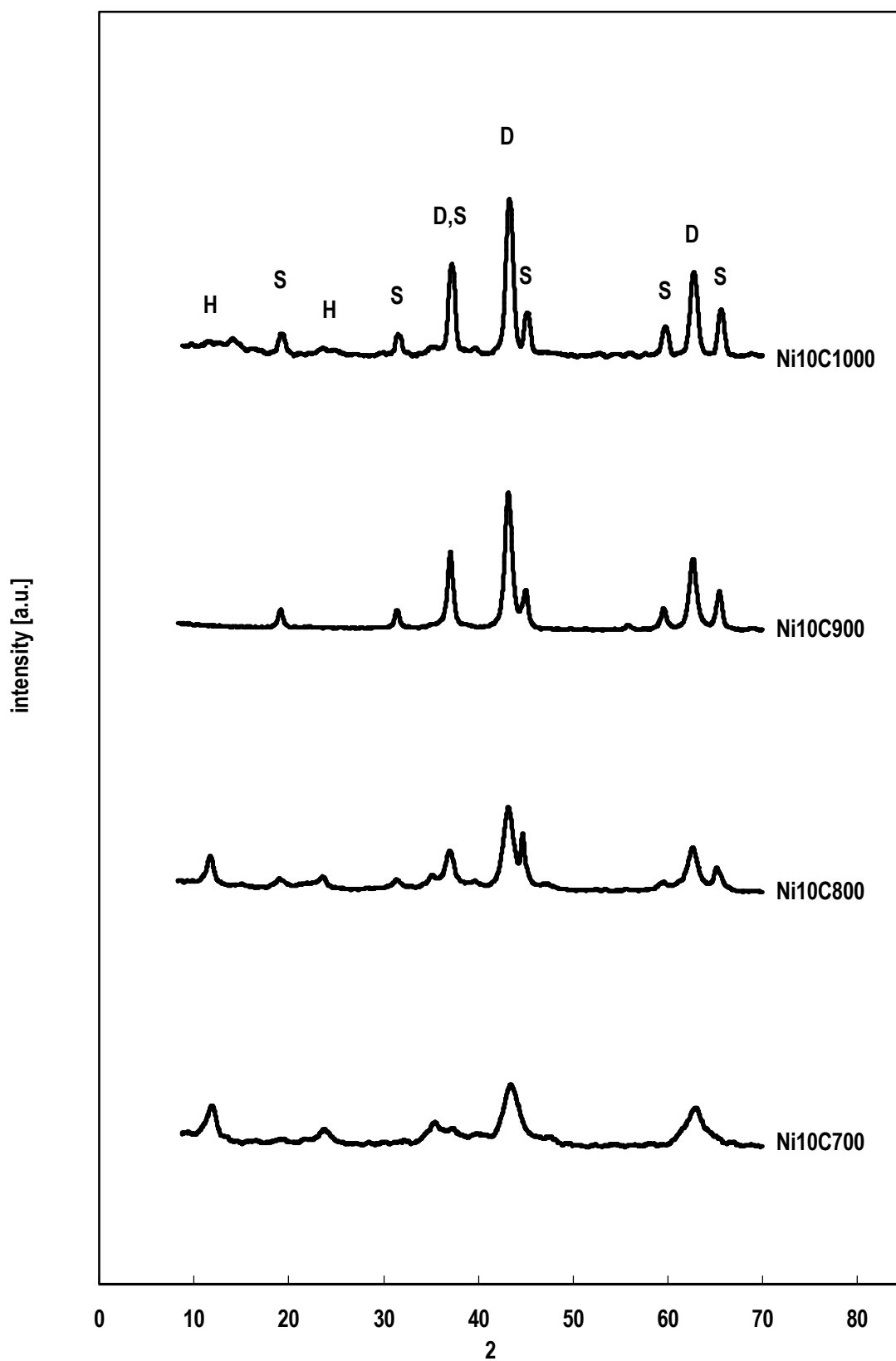


Fig. 14  
XRD spectra of the catalyst precursor Ni<sub>10</sub> calcined at 700, 800, 900 and 1000°C  
(D = divalent metal oxide phase with periclase structure, S = spinel phase,  
H = hydrotalcite-type phase)

The scanning electron microscopy (SEM) images recorded for the catalysts Ni0C900, Ni10C900, Ni30C900, Ni50C900 and Ni72C900 reveal a complex 3 dimensional structure (Fig. 15). Especially the images of Ni0C900, Ni30C00 and Ni50C900 show a rather flat. The craters through which the volatiles are supposed to escape during the calcination process are still visible in particular for the sample Ni50C900 [58].

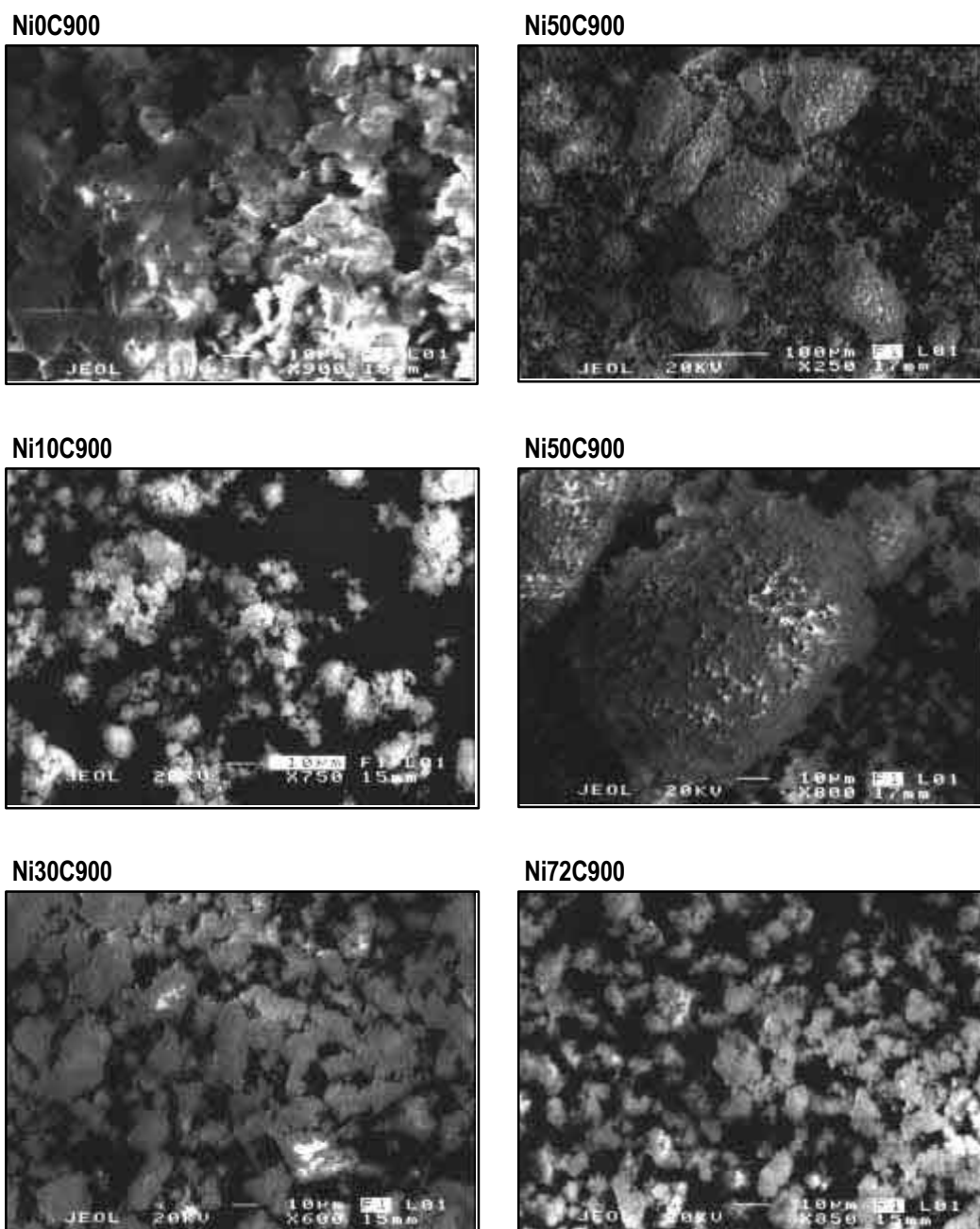


Fig. 15  
SEM images of the catalysts Ni0C900, Ni10C900, Ni30C900, Ni50C900 and Ni72C900

### 3.2.3. BET surface measurements

The surface area of the calcined solids was determined by BET surface measurements for the catalysts Ni0C900, Ni10C900, Ni30C900, Ni50C900 and Ni72C900. The surface area decreased with increasing Ni/Mg ratio of the catalysts up to a ratio of 5/2 (Fig. 16). Basile et al. observed the same trend for very similar Ni/Mg/Al catalysts also derived from HT precursors calcined at 900°C for 16 hours [9, 123]. However, they observed generally a lower surface area (83-27 m<sup>2</sup>/g). Since no specific conditions of the calcination process were mentioned there, it is assumed that static conditions were applied. The remarkably higher surface area for the catalysts especially with a low Ni/Mg ratio indicate that the slow heating rate combined with the fast removal of the gases formed during the calcination using a flow of air is favourable for obtaining catalysts with a high surface area.

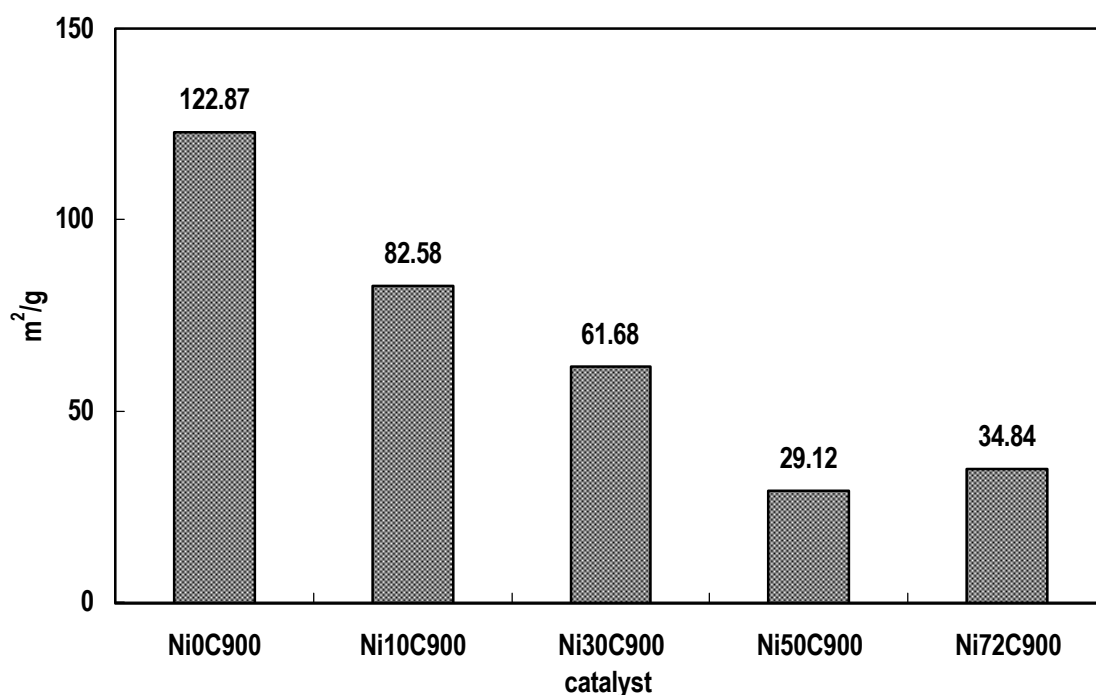


Fig. 16  
BET surface area of the catalysts Ni0C900, Ni10C900, Ni30C900, Ni50C900 and Ni72C900



### 3.2.4. Reducibility

Since Ni catalysts used in the partial oxidation of  $C_3H_8$  (as well as in the other related processes) are activated by reduction, the study of the reducibility of the catalysts was important in order to find a suitable reduction method and to investigate the state of the catalyst after reduction with respect to its composition and structure [124].

#### 3.2.4.1. Temperature programmed reduction

The TPR spectra of the catalysts calcined at  $900^\circ\text{C}$  are presented in Figure 17. In the case of Ni72C900, which does not contain magnesium, two reduction peaks were observed, a large one at  $480^\circ\text{C}$  and a smaller one at  $820^\circ\text{C}$ . The lower temperature reduction peak of Ni72C900 exhibited a shoulder at the lower temperature side. The TPR spectra of the other catalysts did not exhibit such a shoulder. In contrast to the pure Ni/Al catalyst all magnesium containing samples exhibited only one reduction peak, which was shifted from  $480^\circ\text{C}$  for Ni72C900 to  $730^\circ\text{C}$  for Ni50C900 and to even higher temperatures with increasing Mg content. The decrease in the  $H_2$  consumption with decreasing Ni content corresponded to the decreasing total amount of Ni in the catalysts.

The lower temperature peak of the catalyst Ni72C900, the pure Ni/Al catalyst, is attributed to the reduction of  $Ni^{2+}$  ions in the divalent metal oxide phase (NiO) while the higher temperature peak results from the reduction of  $Ni^{2+}$  ions in the spinel phase ( $NiAl_2O_4$ ) [6, 8, 9, 60]. This model for the interpretation of the reduction has been proposed in the literature on the basis of the similarity of the positions of the TPR peaks of HT derived Ni/Al catalysts to those of pure NiO and  $NiAl_2O_4$  [6, 60]. Further evidence was presented by Alzamora et al., who observed by XRD that a Ni/Al HT

derived catalysts consisting of NiO and NiAl<sub>2</sub>O<sub>4</sub> phases after its calcination at 1000°C, still contained NiAl<sub>2</sub>O<sub>4</sub> after subsequent reduction at 600°C in a flow of hydrogen [59].

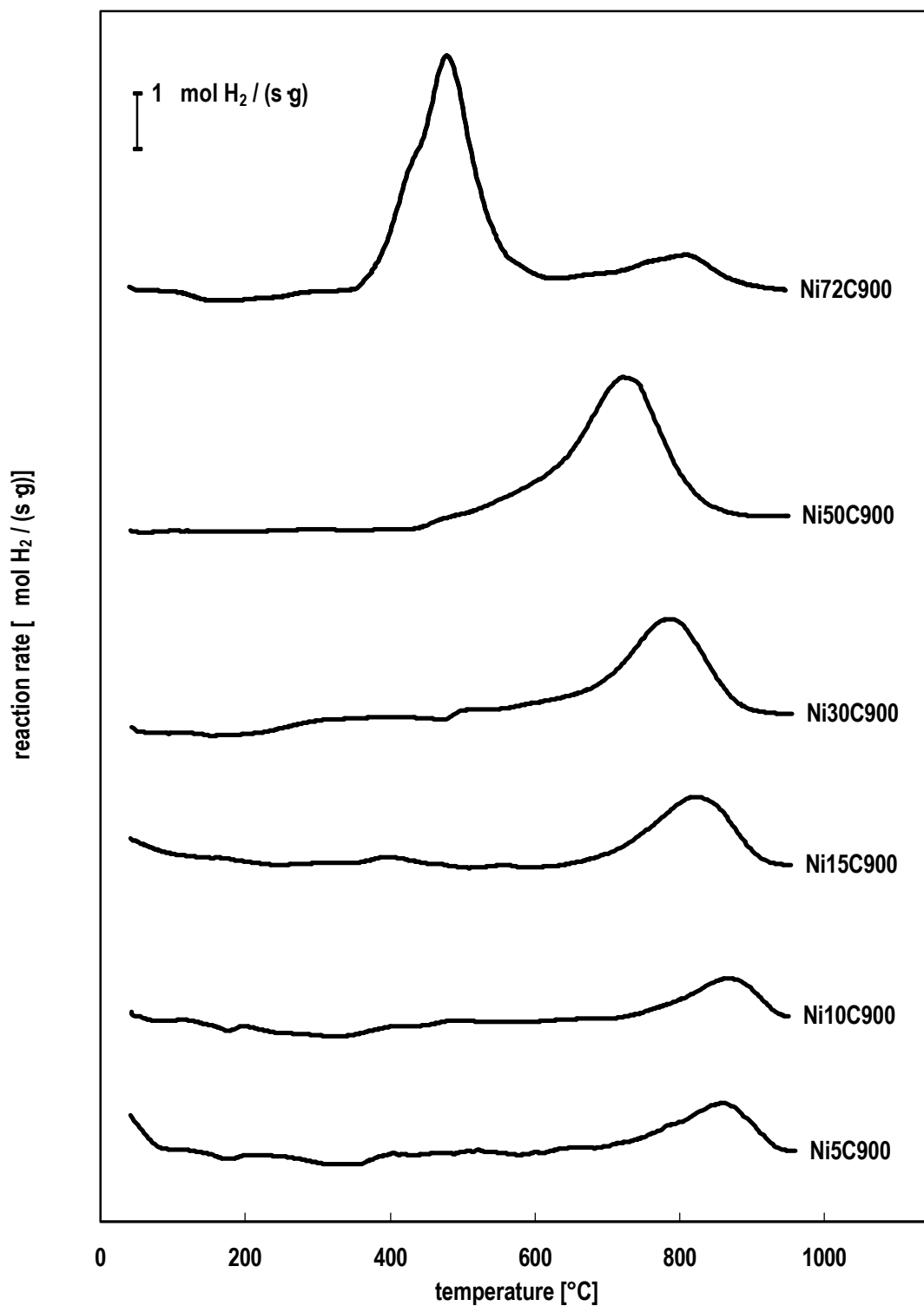


Fig. 17  
TPR profiles of the Ni containing catalysts calcined at 900°C

The reduction peak in the spectra of each Ni/Mg/Al catalyst is attributed to the reduction of the Ni<sup>2+</sup> ions in the divalent mixed metal oxide phase with periclase structure [9]. The total amount of reducible Ni in the divalent metal oxide phase reflected the total Ni/Mg ratio in the samples, suggesting no strong preference of either Ni<sup>2+</sup> or Mg<sup>2+</sup> ions in the formation of the divalent metal oxide phase or the spinel phase. The increase in the reduction temperature with decreasing Ni/Mg ratio shows that the lower the Ni/Mg ratio of the samples the more difficult it is to reduce them. Other authors also reported this general trend for similar HT derived catalysts [9, 125]. This effect is attributed to the substitution of Ni<sup>2+</sup> by Mg<sup>2+</sup> ions leading to the formation of a NiO-MgO solid solution upon calcination, where Ni<sup>2+</sup> ions are stabilised against reduction by an inert MgO matrix. The stabilisation of Ni<sup>2+</sup> ions by an inert MgO matrix has also been reported for solid NiO-MgO solutions [75, 77, 86, 88, 106]. The higher the substitution of Ni<sup>2+</sup> by Mg<sup>2+</sup> ions the more stabilised the Ni<sup>2+</sup> ions are against reduction [9, 86, 88, 106].

The shoulder in the lower temperature peak of Ni72C900 was even better visible when a higher heating rate was applied, 10°C/min instead of 5°C/min (Fig. 18). It may be due to several factors. It could possibly result from the reduction of fine surface particles of NiO not detectable by XRD. It may also be due to a decrease in the accessibility of the NiO surface of the sample [8].

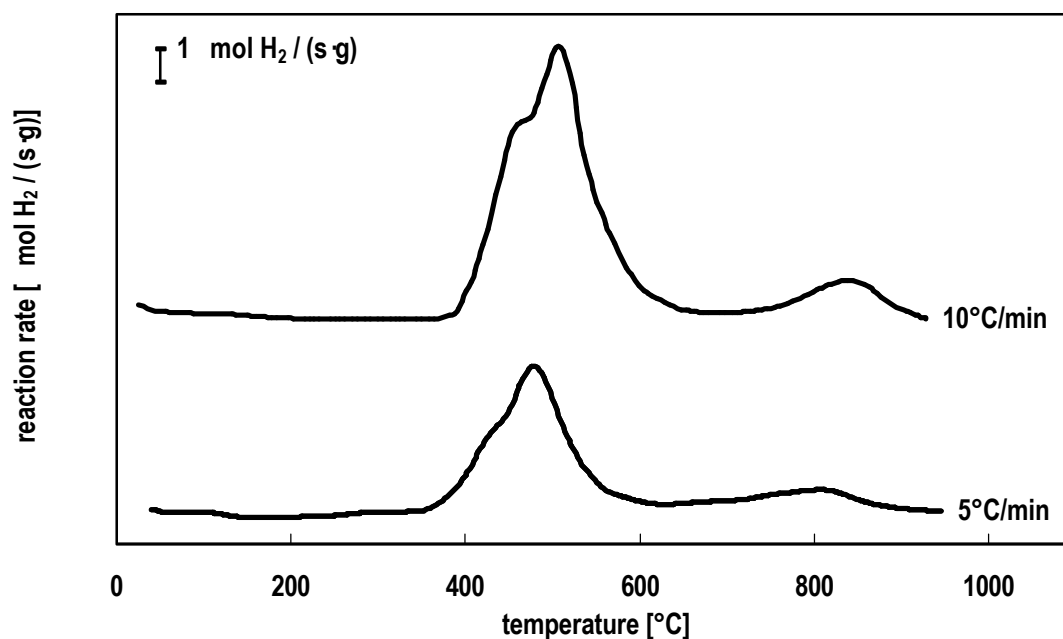


Fig. 18

TPR profiles of Ni72C900 at different heating rates (5 and 10°C/min). The apparent higher amount of reduced Ni at 10°C/min results from the higher heating rate. Integration of the peaks over the time revealed the same amount of reduced Ni for both heating rates

#### 3.2.4.2. Verifications of the existing reduction model

In order to verify the model of the reduction of the catalysts reduction combined with high temperature XRD was employed. The Ni/Al catalyst was used, since it was the catalyst easiest to reduce and it does not contain not reducible MgO and MgAl<sub>2</sub>O<sub>4</sub> phases that would complicate the interpretation of the XRD spectra after the reduction. A catalyst with a medium Ni/Mg ratio (Ni30C900) was additionally investigated. The spectra were recorded before and after the distinct reduction steps to determine the changes in the catalysts caused by the reduction process. XRD spectra were also recorded at room temperature before and after the completed reduction to compare the effect of the reduction process without distortions of the  $2\theta$  values and the intensities caused by the temperature differences during the recording (Fig. 19 and 20).

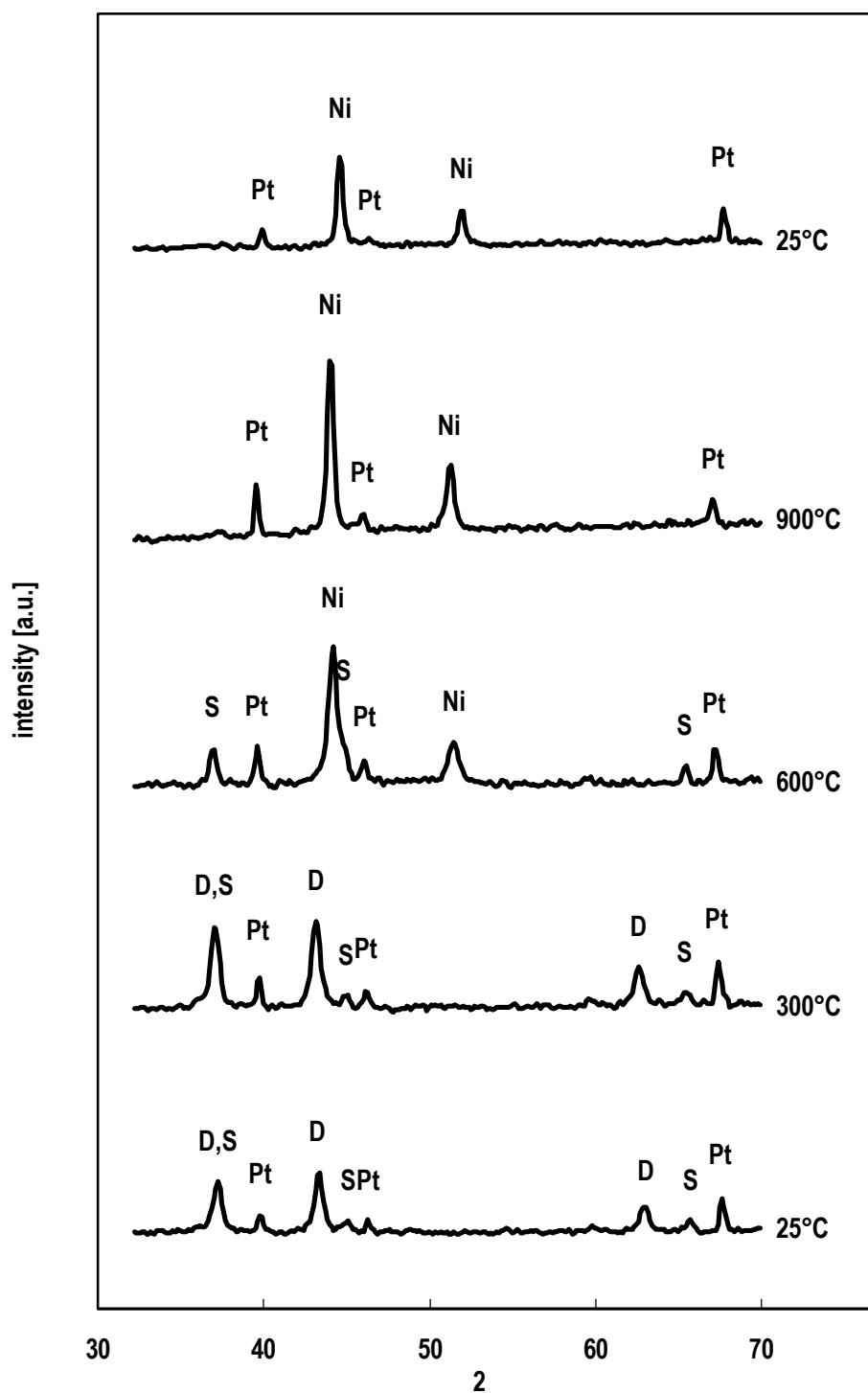


Fig. 19  
High temperature XRD spectra of the reduction process of Ni<sub>72</sub>C<sub>900</sub>C (D = NiO phase with periclase structure (bunsenite), Ni = metallic Ni phase, Pt = platinum (sample holder), S = NiAl<sub>2</sub>O<sub>4</sub> spinel )

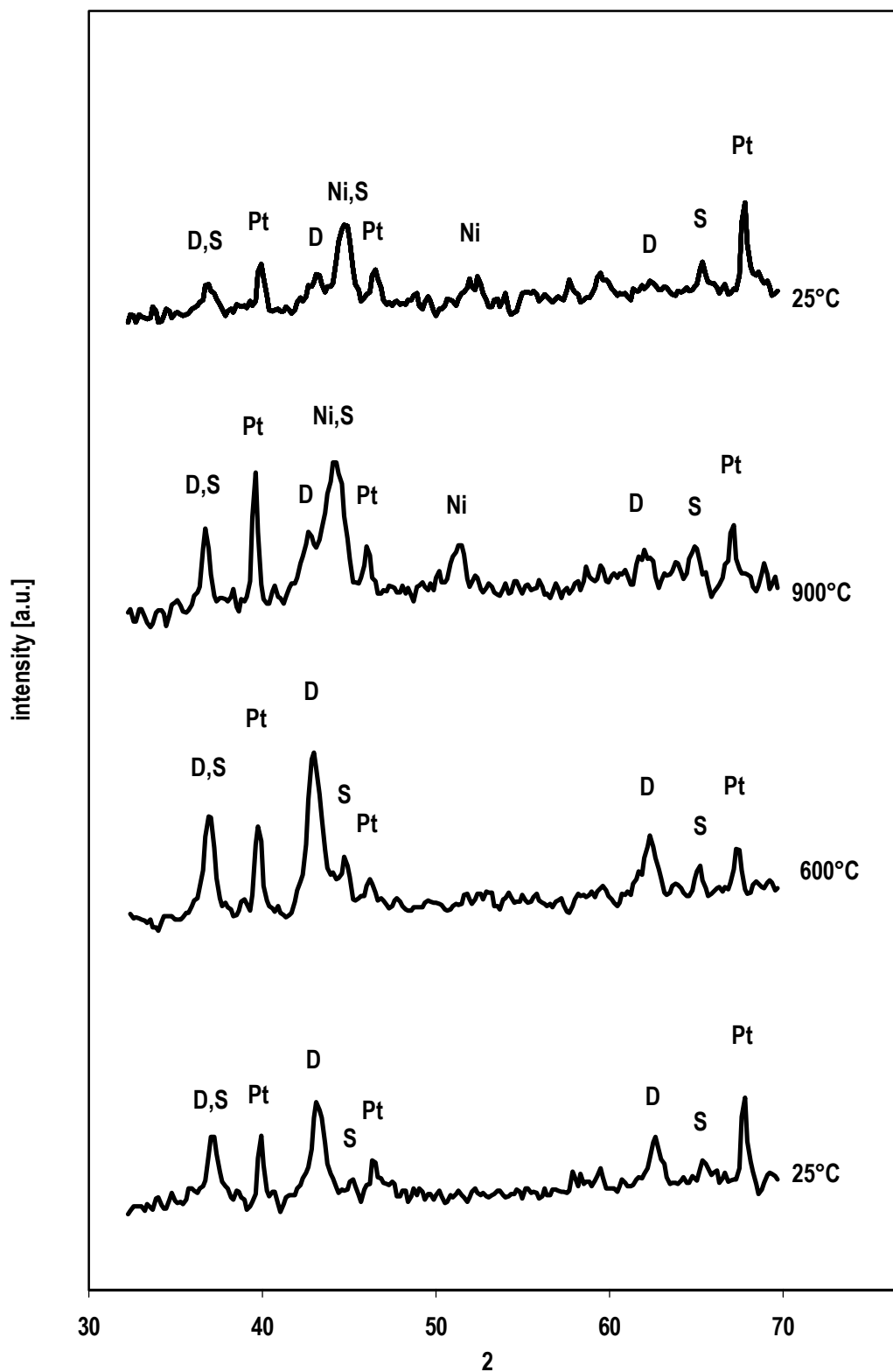


Fig. 20  
High temperature XRD spectra the reduction process of Ni<sub>3</sub>OC<sub>900</sub> (D = divalent metal oxide phase with periclase structure, Ni = metallic Ni phase, Pt = platinum (sample holder), S = spinel phase)

All the spectra exhibited Pt reflections from the Pt ribbon on which the sample was placed and that will not be discussed in the following. Before the reduction process of Ni72C900 only reflections due to NiO and NiAl<sub>2</sub>O<sub>4</sub> were observed. At 600°C only the reflections corresponding to NiO disappeared completely. The reflection that was due to both, NiO and NiAl<sub>2</sub>O<sub>4</sub>, decreased drastically, whereas the reflection due to NiAl<sub>2</sub>O<sub>4</sub> alone seemed to be unchanged. Simultaneously two new reflections of metallic Ni were observed. At 900°C the spectrum exhibited only reflections due to metallic Ni. Although the spectra of Ni30C900 were less intensive a distinction of the different phases was still possible. Before the reduction process of Ni30C900 only reflections due to the divalent metal oxide phase with periclase structure and the spinel phase were observed. At 600°C the spectrum was unchanged. At 900°C the reflections that were entirely due to the divalent metal oxide phase or both phases decreased drastically, whereas the reflection due to the spinel phase alone seemed to be unchanged. Simultaneously two new reflections due to metallic Ni were observed.

The results show that the existing model for the reduction of the Ni/Al and Ni/Mg/Al catalysts is correct, first reduction of the Ni<sup>2+</sup> ions in the divalent metal phase with periclase structure to metallic Ni and second the reduction of Ni<sup>2+</sup> ions in the spinel phase. They also confirm the enhanced resistance of the catalysts against reduction upon the substitution of the Ni<sup>2+</sup> by Mg<sup>2+</sup> ions. The fact that the divalent metal oxide phase did not disappear after reduction at 900°C is attributed to the presence of the not reducible MgO phase. The fact that no reflections of an Al<sup>3+</sup> containing phase were observed, may result from the formation of an amorphous or a poorly crystallised Al<sub>2</sub>O<sub>3</sub> phase not detectable due to the X-ray adsorption by the high amounts of Ar present in the reduction mixture (95%).

### 3.2.5. Ni dispersion

The active surface area of a catalyst (i.e. the surface area of the active phase) is often expressed relatively as the dispersion of the active phase, defined as the ratio of the number of the active sites (or the superficial atoms of the active phase) to the total amount of the atoms of the active phase. This meaning of dispersion should not be confused with that used for characterisation of particle size distribution in a particulate matter. The dispersion of the active phase is an important parameter of the catalyst, related to the total number of the active sites and the average particle size of the active phase that both determine the catalyst's performance. The knowledge of the metal dispersion in the Ni catalysts is important, since it may influence the catalytic activity and selectivity as well as the resistance against coking, as found for the steam reforming process.

In order to estimate the degree of dispersion of the Ni particles after reduction the catalysts were passivated at low temperatures ( $> 40^{\circ}\text{C}$ ) using 5%  $\text{O}_2$  diluted with He. Such a passivation results in the formation of only two or three monolayers of nickel oxide [110]. After passivation the catalysts were reduced again, the results are shown in Figure 21. On the basis of these results it was possible to estimate the dispersion of Ni particles expressed as the ratio of the amount of Ni reduced after passivation to the total amount of reducible Ni after calcination (Fig. 22). For a better comparison the scale of the y-axis is the same as in the TPR profiles of the calcined catalysts.

All passivated catalysts exhibited reduction peaks in the temperature region  $200\text{-}225^{\circ}\text{C}$ . The amount of consumed  $\text{H}_2$  was about 5 - 23% of the amount consumed in the reduction of the calcined catalysts. The dispersion was highest for the catalyst



with a low to medium Ni/Mg ratio with more than 10% and decreased at higher Ni/Mg ratio to 5% at its lowest for Ni72C900 the pure Ni/Al catalyst.

The low reduction temperature and the considerably lower H<sub>2</sub> consumption compared to the TPR of the calcined catalysts confirm that by the passivation process no bulk Ni was oxidised [59]. Borowiecki, who investigated the reducibility and Ni dispersion of alumina supported Ni/Mg steam reforming catalysts also observed a rapid decline in the Ni dispersion at Ni/Mg ratio  $\geq 2.3$ , the same ratio as in the catalyst Ni50C900 [75]. Although such an effect may be expected as the Ni dispersion generally decreases with increasing Ni content due to enhanced sintering of the Ni particles, Choudhary et al. found higher Ni dispersion for a supported catalyst precoated with MgO than precoated with CaO, BaO or Yb<sub>2</sub>O<sub>3</sub> [106]. Therefore it can be concluded that the MgO matrix does not only stabilise the Ni<sup>2+</sup> ions against reduction, but also against sintering, leading to higher reduction temperatures and resulting in a better dispersion of the Ni particles formed.

Furthermore the reduction profiles of the passivated catalysts exhibited no significant temperature shift, which is in contrast to the reduction of the calcined catalysts, where the reduction temperature increased with decreasing Ni/Mg ratio of the catalyst. By the reduction separate metallic Ni particles are formed that are surfacially oxidised by the passivation process. The formed NiO is no longer stabilised against reduction by the MgO matrix. For the formation of a solid solution of NiO with the MgO matrix, the passivation temperature (< 40°C) was much too low. However, it must be pointed out that these dispersion measurements should not be used to draw detailed conclusions about the Ni crystallite size using geometrical models because it was not possible to exactly establish the depth of the surface oxide layer formed by the passivation.

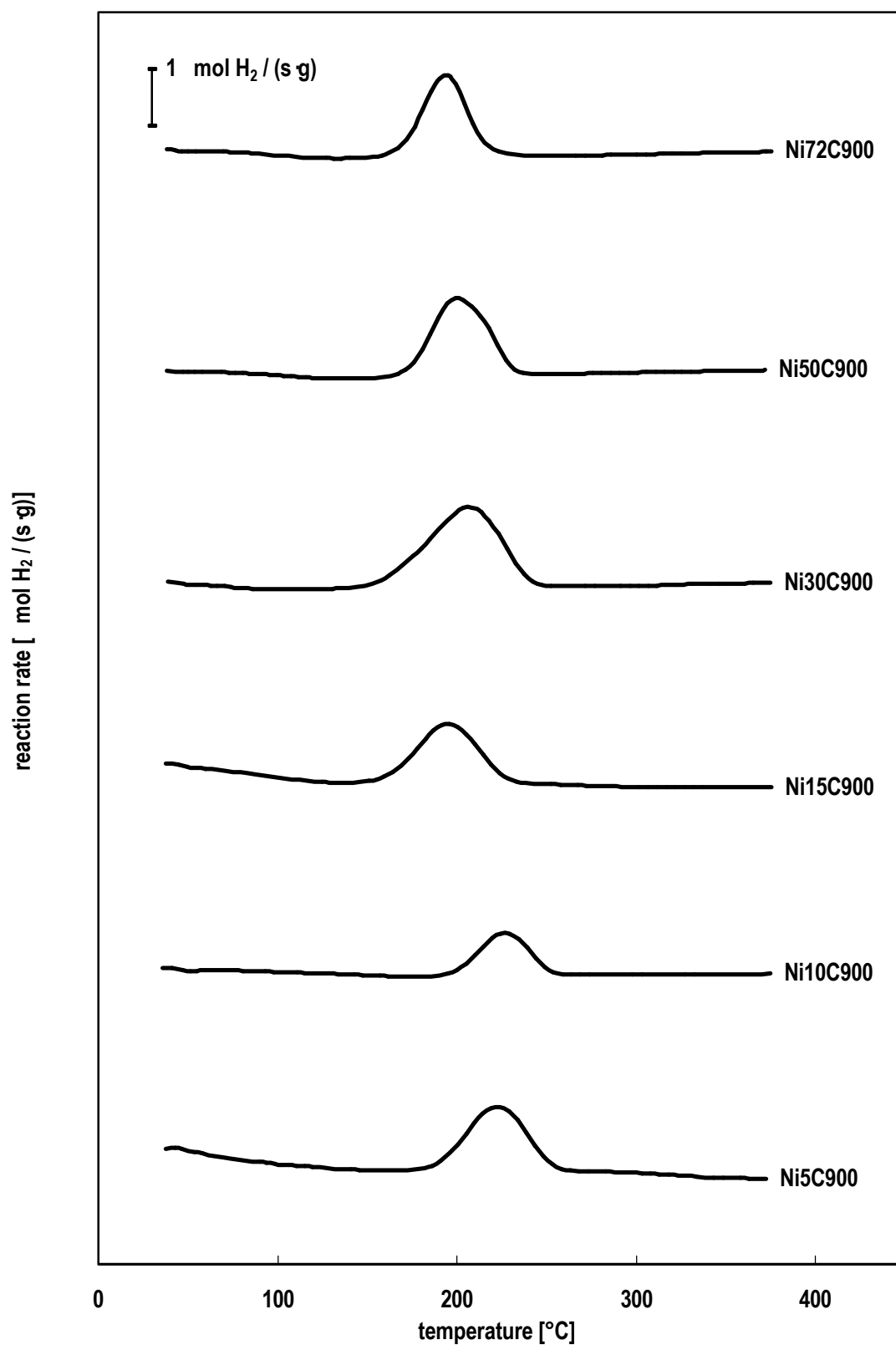


Fig. 21  
TPR profiles of the passivated catalysts. All catalysts were calcined at 900°C, reduced in TPR and passivated below 40°C

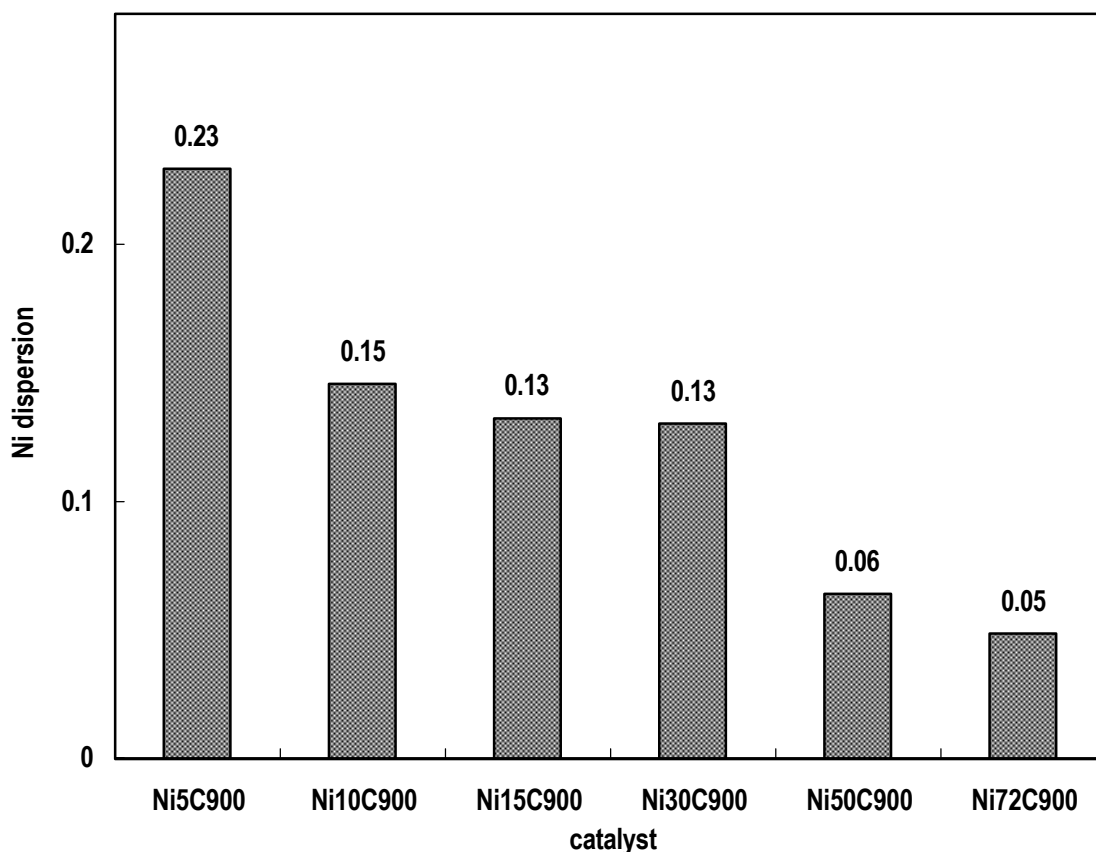


Fig. 22

Ni dispersion of the catalysts estimated from the TPR results

### 3.2.6. Temperature programmed oxidation

The oxidation of the reduced catalysts Ni10C900, Ni30C900, Ni50C900 and Ni72C900 was investigated by temperature programmed oxidation (TPOx). The spectra exhibited broad peaks starting at about 150 – 200°C with maxima between 350-400°C (Fig. 23). In contrast to the reduction temperature the oxidation temperature was almost independent from the Ni/Mg ratio of the catalyst. This again is attributed to the formation of separate metallic Ni particles by the reduction. These are not stabilised against oxidation by the MgO matrix.

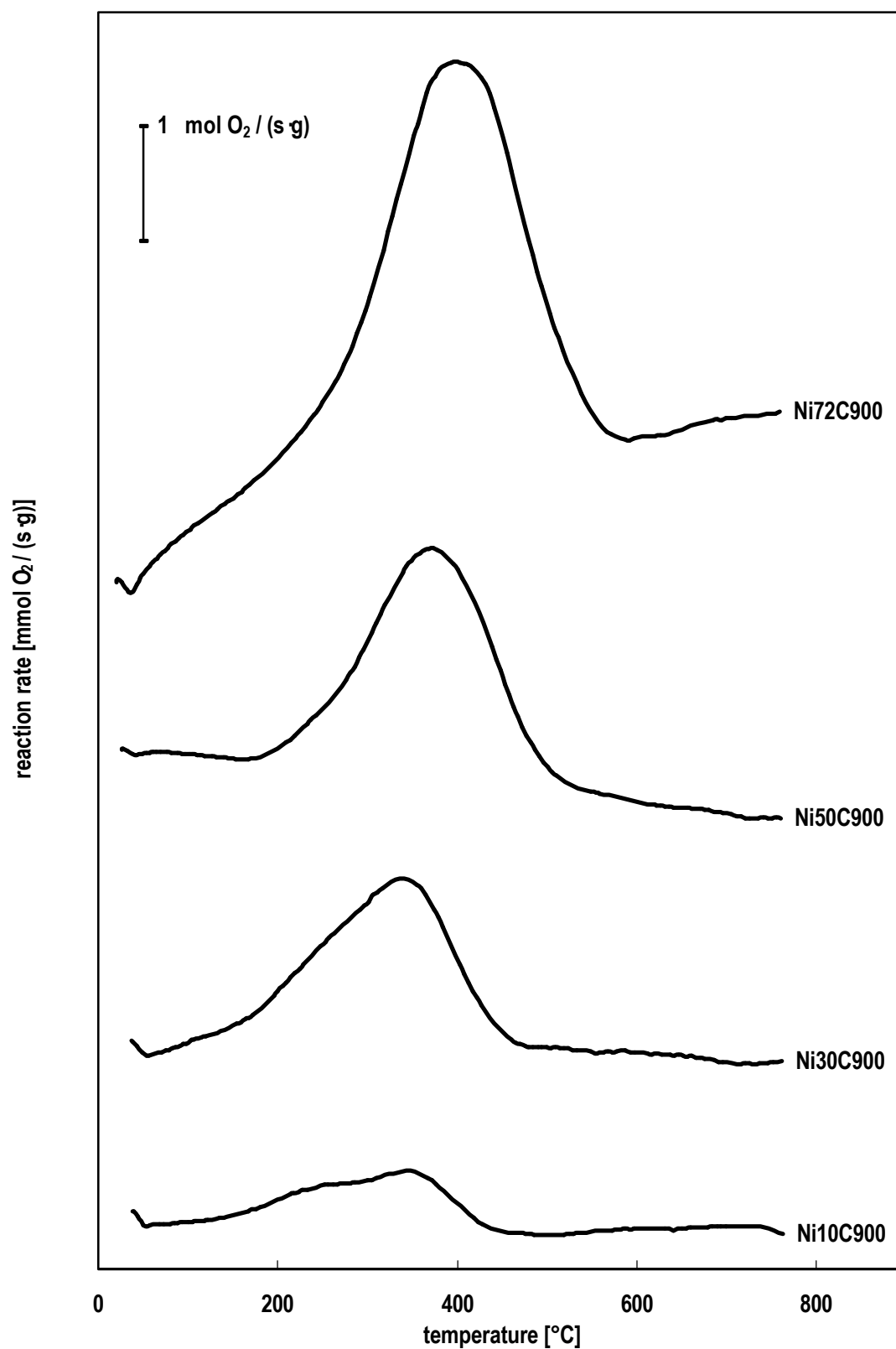


Fig. 23  
TPOx profiles of the catalysts after TPR. All catalysts were calcined at  $900^{\circ}\text{C}$ , reduced in TPR, passivated and reduced again

### 3.2.7. Influence of the calcination temperature on reducibility and Ni dispersion

The catalysts Ni10 calcined at 800, 900 and 1000°C (Ni10C800, Ni10C900 and Ni10C1000) were used to investigate the influence of the calcination temperature on the reducibility and the Ni dispersion (Fig. 24, 25 and 26). The results show a shift in the reduction maxima to higher temperatures with increasing calcination temperature, from about 850°C for Ni10C800 to 900°C for Ni10C1000. The amount of reducible Ni<sup>2+</sup> ions was higher for Ni10C800 than for Ni10C900 and Ni10C1000. The broad not intensive peak in the reduction spectrum of Ni10C800 at about 470°C is attributed to the destruction of the partially reconstructed HT phase in the catalyst. The total amount of passivated Ni was higher for Ni10C800 than for the other catalysts, but the dispersion decreased in the order Ni10C900 > Ni10C1000 > Ni10C800.

The slight increase in the reduction temperature with increasing calcination temperature of the catalysts is attributed to the increasing crystallinity of the catalysts with increasing calcination temperature. The differences in the amount of reducible Ni<sup>2+</sup> are in good agreement of the phase model for hydrotalcite-type derived catalysts. The catalysts calcined at temperatures  $\geq 900^\circ\text{C}$  consist of well crystallised divalent metal oxide phase with periclase structure and spinel phases, where only the Ni<sup>2+</sup> ions in the divalent metal oxide phase are reducible up to the applied reduction temperatures. The catalyst calcined at 800°C consists of a poorly crystallised divalent metal oxide phase with periclase structure, an amorphous Al<sub>2</sub>O<sub>3</sub> phase and a small amount of spinel phase at their interface. This results in the reduction of almost all Ni<sup>2+</sup> ions. Ni10C800 also shows the highest amount of available surface Ni. Nevertheless its dispersion is the lowest, which is attributed to an increase in sintering due to the higher total amount of reduced Ni. The lower Ni dispersion of Ni10C1000 compared to Ni10C900 is attributed to the fact that a higher reduction temperatures had to be applied

(1100°C compared to 950°C) leading to an higher mobility of the Ni atoms formed during the reduction, which results in increased sintering.

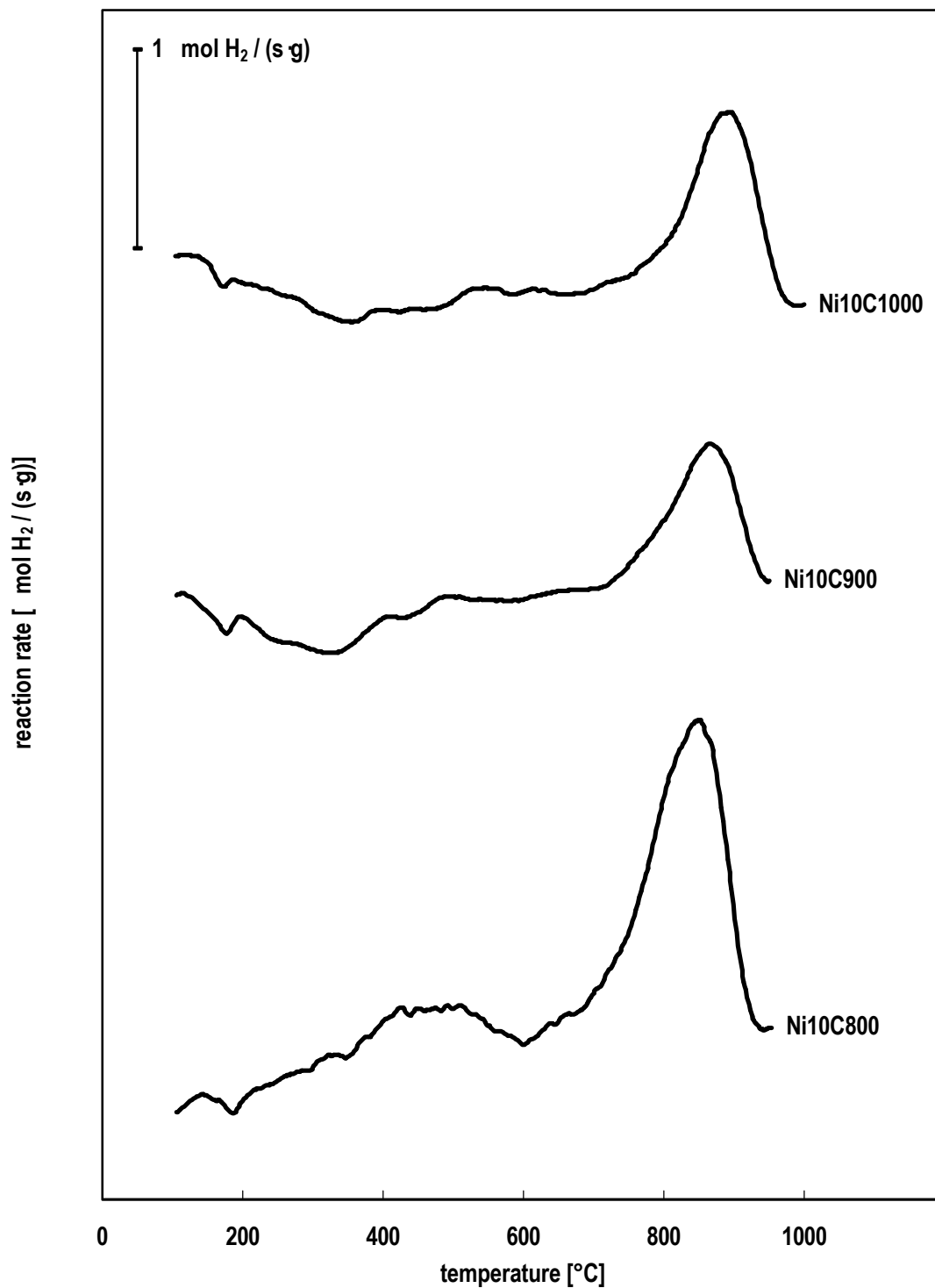


Fig. 24  
TPR profiles of the catalyst Ni10 calcined at 800, 900 and 1000°C

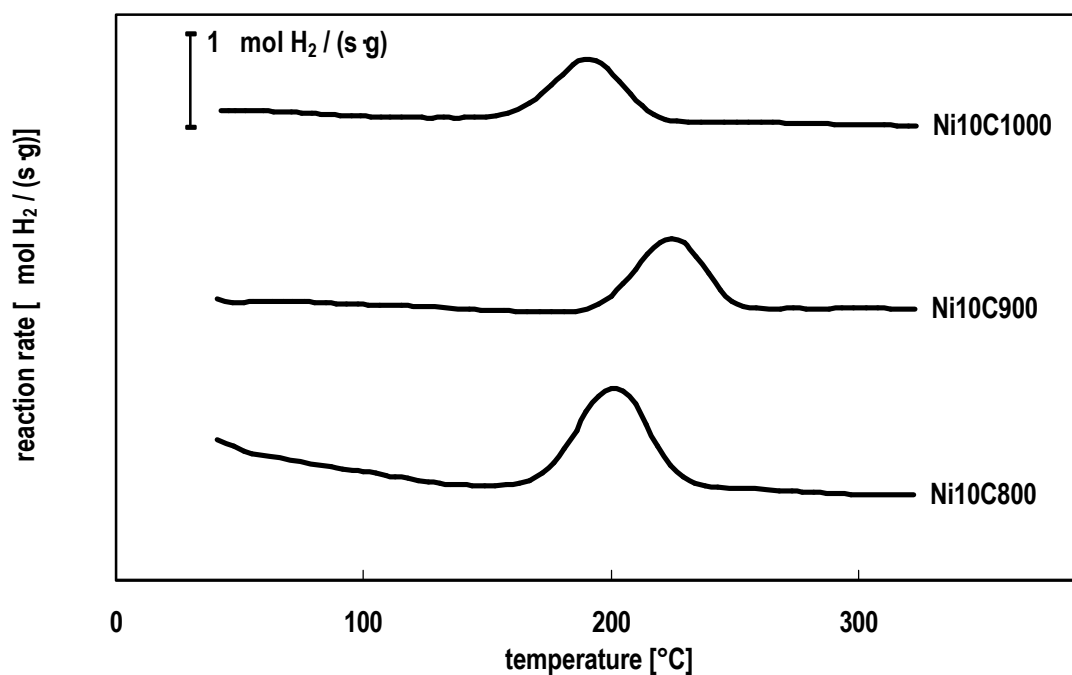


Fig. 25  
TPR profiles after passivation of the catalyst Ni10 calcined at 800, 900 and 1000°C.  
All catalysts were reduced in TPR run and passivated below 40°C

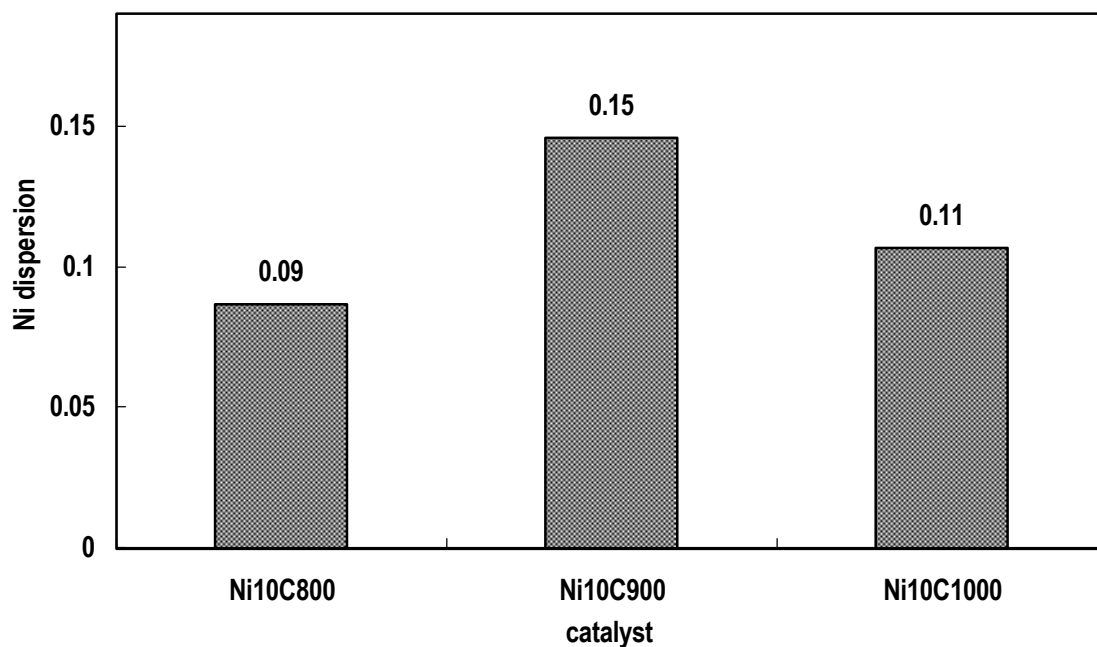


Fig. 26  
Ni dispersion of the catalyst precursor Ni10 calcined at 800, 900 and 1000°C estimated from the TPR results

### 3.2.8. Basicity measurements

For the processes related to the partial oxidation of  $C_3H_8$  (steam reforming,  $CO_2$  reforming, partial oxidation of  $CH_4$ ) it was reported that the basicity can influence the catalytic performance especially the catalyst's stability and the tendency towards coking. For example in the naphtha steam reforming alkali metal oxides must be added to avoid excessive coking of the catalyst. Although the basicity of the studied catalysts can be regarded to increase with increasing Mg content more detailed measurements of the surface basicity were attempted.

#### 3.2.8.1. Temperature programmed desorption of $CO_2$

The catalysts calcined at  $900^\circ C$  were used to investigate the influence of the composition of the catalysts on the basicity by TPD of  $CO_2$  after adsorption at  $100^\circ C$  for 1 hour. The TPR spectra of the catalysts after adsorption at  $100^\circ C/1h$  exhibited one broad peak for each catalyst (Fig. 27). Two trends were observed. With decreasing Ni/Mg ratios of the catalysts increases the total amount of desorbed  $CO_2$  and the position of the maximum is shifted to slightly higher temperatures in the order Ni0C900 > Ni10C900 > Ni30C900 > Ni50C900  $\approx$  Ni72C900. However, specific desorption amount expressed as the amount of desorbed  $CO_2$  divided by the BET surface area, showed hardly any dependence on the composition of the catalysts (Fig. 28). Such results indicated that non specific adsorption of  $CO_2$  on the catalyst surface took place.



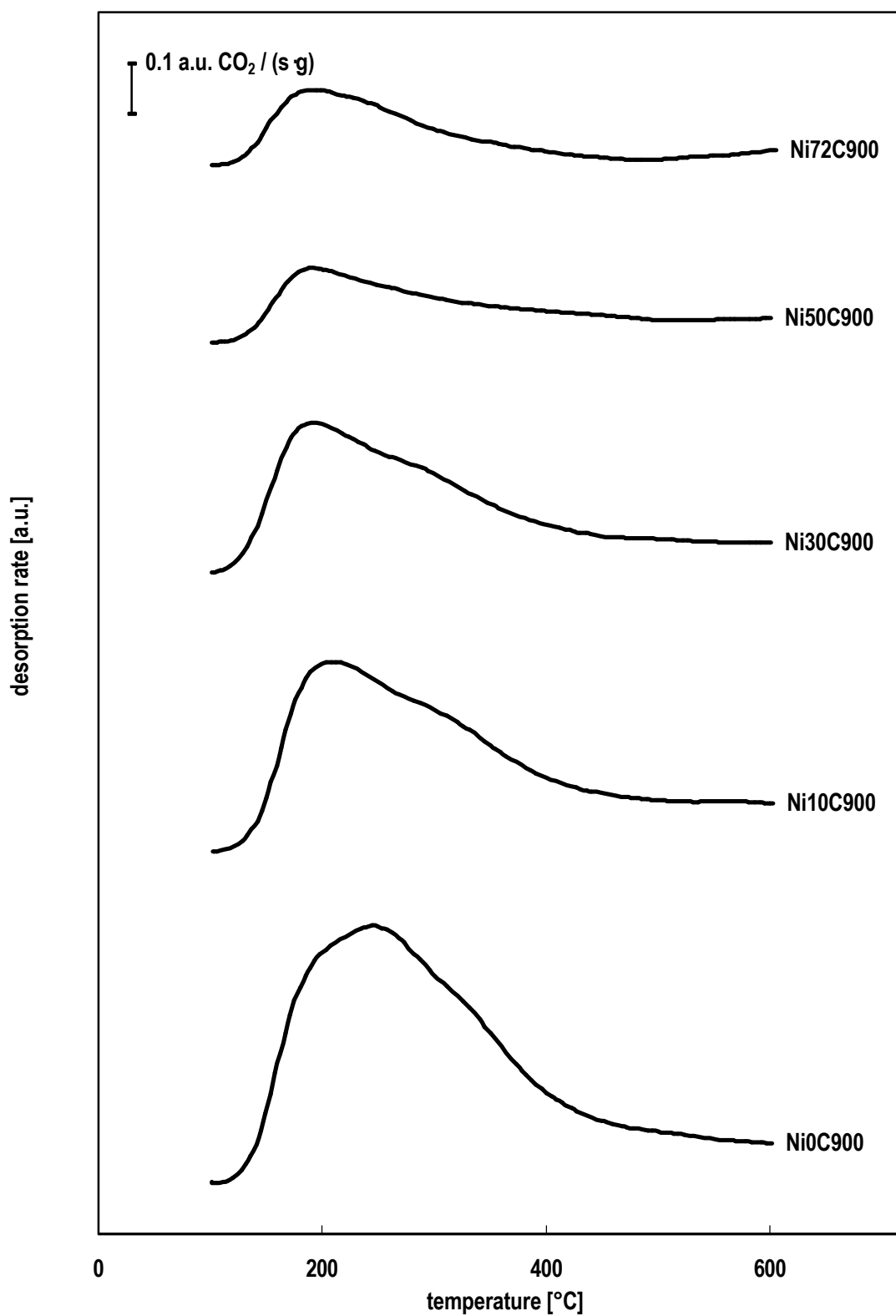


Fig. 27  
Profiles of the TPD of CO<sub>2</sub> of the catalysts calcined at 900°C after 1h adsorption at 100°C. Values are expressed in arbitrary units (a.u.) because no valid calibration data were available for this series of experiments

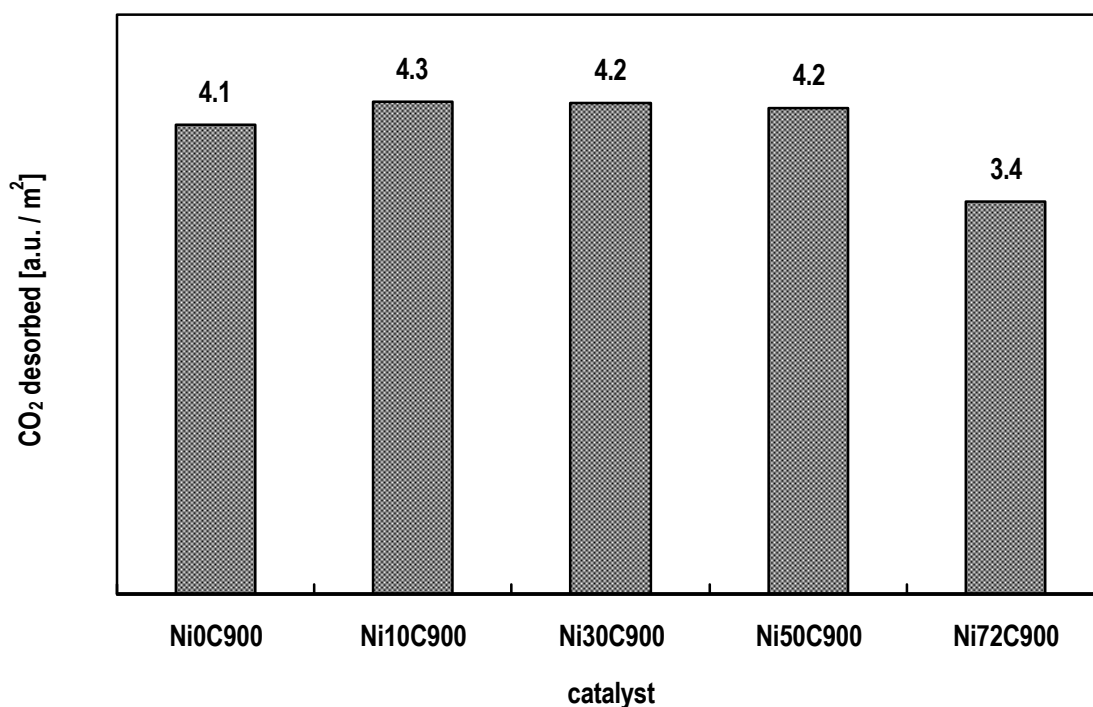


Fig. 28  
specific desorption amount of CO<sub>2</sub> of the catalysts calcined at 900°C determined by TPD of CO<sub>2</sub> after 1h adsorption at 100°C. Values are expressed in arbitrary units (a.u.) because no valid calibration data were available for this series of experiments

In order to improve the TPD conditions detailed studies of the adsorption time and temperature were performed for the catalyst Ni0C900 that was expected to show maximum basicity due to the highest Mg content. These studies revealed that the amount of adsorbed CO<sub>2</sub> increased with the time of adsorption and decreased with increasing adsorption temperature (Fig. 29). Basing on these results TPD of CO<sub>2</sub> after 15 hours adsorption at 100, 150 and 200°C was also performed for the samples Ni0C900, Ni30C900 and Ni72C900 chosen as samples with remarkably different basic properties (Ni free catalyst, catalyst with a medium Ni/Mg ratio and Mg free catalyst, respectively). The specific desorption amount for the catalysts determined at different adsorption temperatures are presented in Figure 30. At 100°C the order was Ni72C900 >> Ni30C900 > Ni0C900, whereas at 150 and 200°C the order was Ni0C900 > Ni30C900 >> Ni72C900.

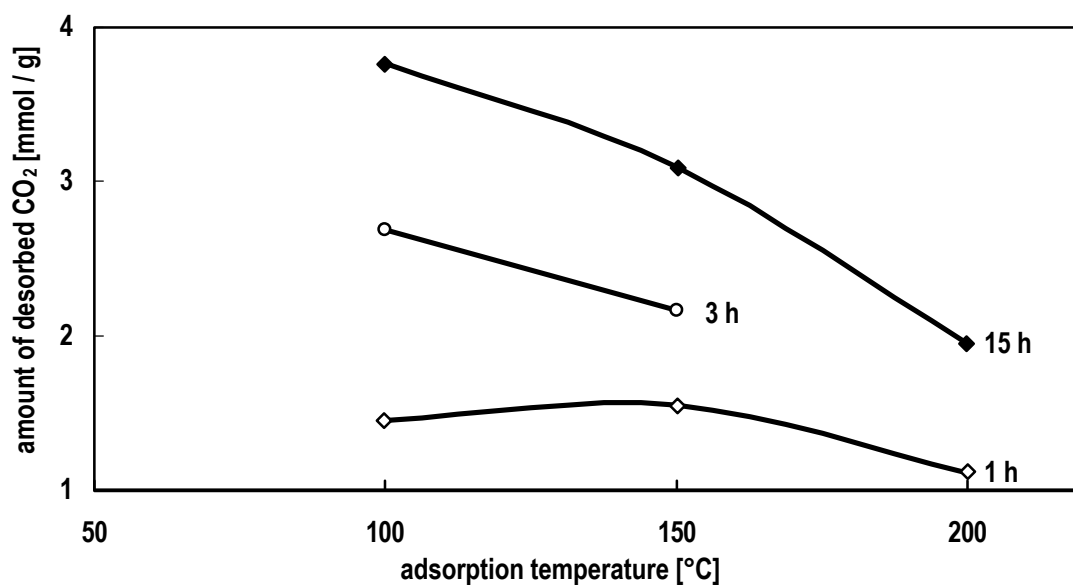


Fig. 29

Amount of desorbed CO<sub>2</sub> after adsorption at different adsorption times (1, 3 and 15 hours) and temperatures (100, 150 and 200°C) for the catalyst Ni0C900

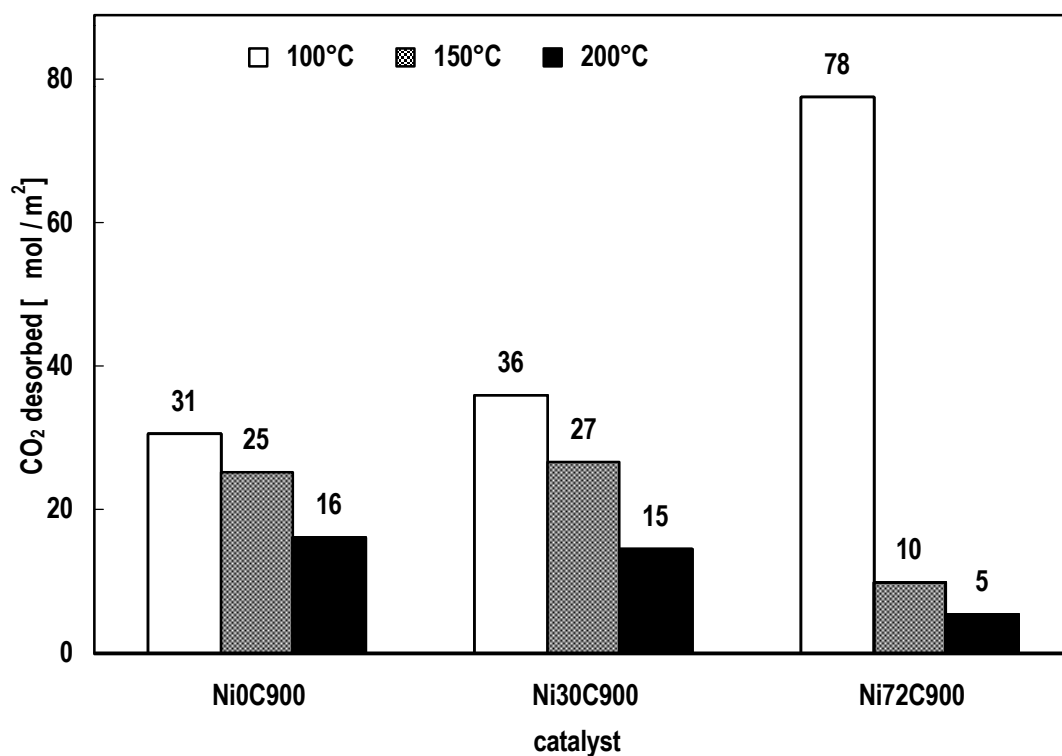


Fig. 30

Specific desorption amount of CO<sub>2</sub> of the catalysts calcined at 900°C determined by TPD of CO<sub>2</sub> after 15 hours of adsorption at 100, 150 and 200°C

The results show that for the temperature programmed desorption of CO<sub>2</sub> after adsorption for 1 hour at 100°C did not allow to differentiate between the catalysts. The experiments performed at different adsorption conditions show that CO<sub>2</sub> desorption is influenced by adsorption time and temperature. Basicity expressed as specific adsorption amount after adsorption at longer time and higher temperature correlates well with the Mg content, but its values are too high compared to those reported in the literature for chemisorption of CO<sub>2</sub> on MgO (1.45 – 4.4 μmol/m<sup>2</sup>) [116]. This may be due to the formation of a superficial carbonate layer or metal hydroxide groups resulting from incomplete removal of water from the CO<sub>2</sub> feed stream. The reverse in the order specific desorption amount at 100°C compared to 150 and 200°C may result from the lower stability of the superficial species formed in the case of Ni72C900.

#### **3.2.8.2. Determination of basicity by catalytic test reactions**

As a research method complementary to TPD of CO<sub>2</sub> two catalytic test reactions were employed for the characterisation of the catalysts' basicity.

As the first test reaction the transformation of isopropanol was performed over selected catalysts (Ni0C900, Ni30C900 and Ni72C900) in the temperature range 200 - 280°C. In this reaction formation of propylene by dehydration of the alcohol over acid sites is observed, whereas on basic sites dehydrogenation of the isopropanol to acetone takes place. The results show a large increase of the catalysts' activity in the conversion of isopropanol with increasing Ni content and also high selectivity towards acetone for all the catalysts (Fig. 31). This indicates that apart from the basic sites also Ni<sup>2+</sup> ions possess considerable activity in the dehydrogenation of isopropanol to acetone [116]. The contribution of the basic magnesium sites in the overall activity is small therefore it

was not possible to compare the catalysts with respect to their basicity basing on the results of these catalytic tests.

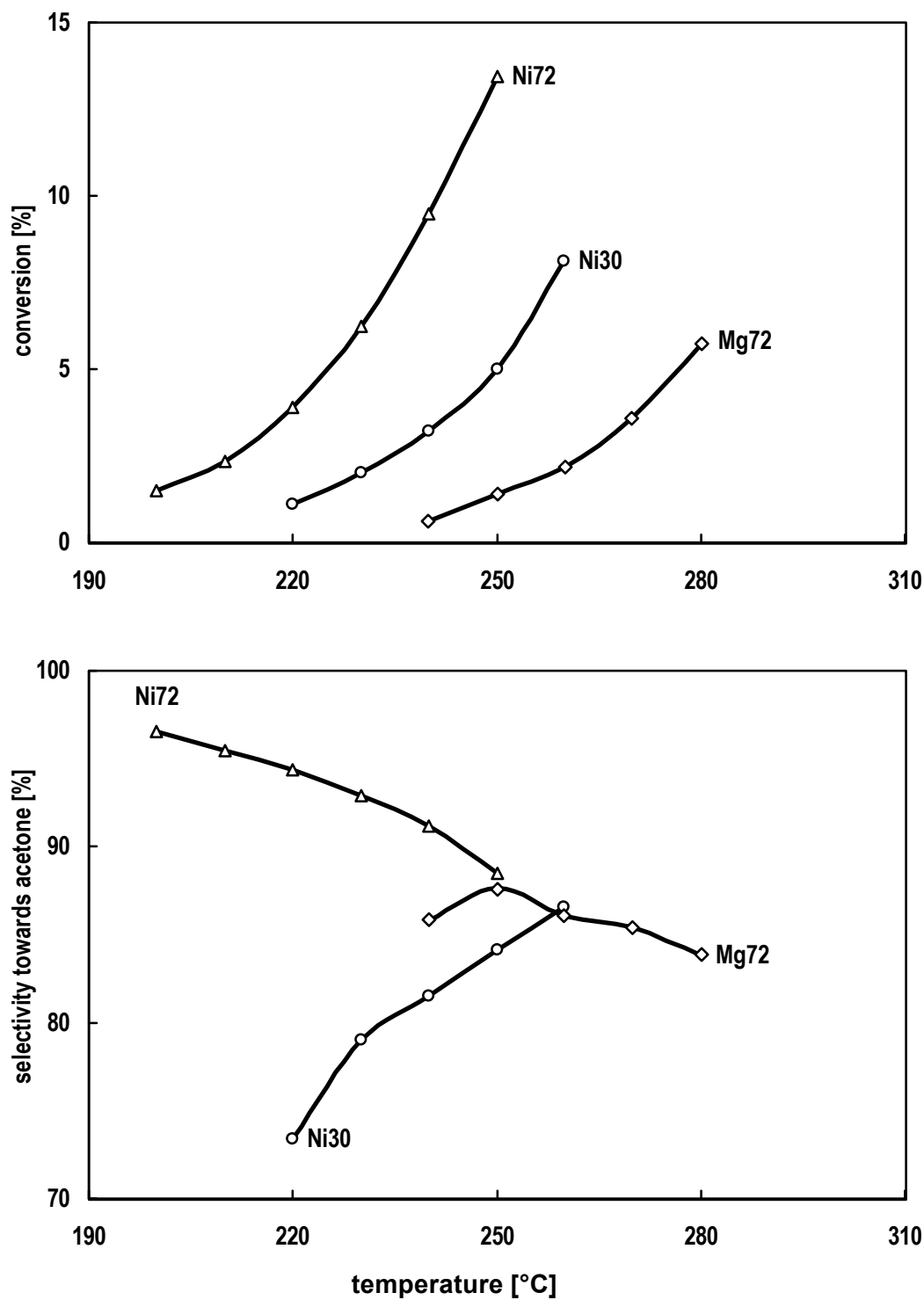


Fig. 31  
Conversion of isopropanol and selectivity towards acetone over the catalysts calcined at 900°C

As another test reaction, the aldol condensation was studied over the catalysts Ni0C900, Ni30C900 and Ni72C900 in the temperature range 270 – 310°C. Formation of  $\alpha,\beta$ -unsaturated carbonyl compounds catalysed by basic sites, was observed. Due to the low specific activity of the catalysts relatively high temperatures had to be applied and under such reaction conditions it was found that primary reaction products were not stable and reacted further to higher condensation products [116, 117, 119]. Therefore the reaction was also regarded as not suitable for the determination of the basicity of the catalysts.

Neither TPD of CO<sub>2</sub> nor the test reactions succeeded in an experimental description of the surface basicity of the catalysts that would be better than simply describing it by the Mg content in the catalysts.



---

## 4. Results and discussion - catalytic partial oxidation of propane

### 4.1. Catalyst screening

All synthesised catalysts were supposed to the standard catalytic tests that were performed for 240 minutes at 700 or 800°C at high space velocity (gas hourly space velocity (GHSV)  $900 \cdot \text{dm}^3 \cdot \text{h}^{-1} \cdot \text{g}(\text{catalyst})^{-1}$ ). 25%  $\text{O}_2$  surplus compared to the stoichiometric reaction was used to suppress excessive coke formation. The same tests were performed employing a conventional steam reforming catalyst  $\text{Ni}/\text{Al}_2\text{O}_3$  (20 wt%  $\text{NiO}$ , 2 wt%  $\text{K}_2\text{O}$ ). The obtained results allowed comparing the catalysts in terms of activity, selectivity, deactivation rate and coking.

The results of the catalytic screening at 700°C are shown in Figure 32. The conversion of  $\text{O}_2$  was found to be almost complete over all catalysts. Although the  $\text{C}_3\text{H}_8$  conversion was never complete, it was always high ( $\geq 74\%$ ). It was found to be highest over the catalysts with a low to medium Ni/Mg ratio. Over all catalysts  $\text{CO}$  and  $\text{H}_2$  were always the main products with yields equal to or above 65 and 47% respectively. The trend in the yield of  $\text{CO}$  reflected the trend in the  $\text{C}_3\text{H}_8$  conversion and was highest over Ni30C900 (85%). For each individual catalyst the yield of  $\text{H}_2$  was lower than the yield of  $\text{CO}$ , here the highest yield was achieved over Ni10C900 (68%). The yield of water exhibited the opposite trend to the yield of  $\text{H}_2$ , with exception of Ni10C900. Other side products were  $\text{CO}_2$  and  $\text{CH}_4$ . Traces of  $\text{C}_2\text{H}_4$  and  $\text{C}_3\text{H}_6$ , were observed over several catalysts ( $Y < 0.5\%$ ). Over the reference catalyst results were obtained very similar to the catalyst Ni72C900.

The results of the catalyst screening at 800°C are compared in Figure 33. Here again the conversion of  $\text{O}_2$  was found to be almost complete in all experiments. The  $\text{C}_3\text{H}_8$



conversion and the yields of CO and H<sub>2</sub> were for each catalyst generally higher than at 700°C and differences between the catalysts less pronounced. Again the catalysts with a low to medium Ni/Mg ratio showed superior performance. As at 700°C the trend in the yield of CO reflected the trend in the C<sub>3</sub>H<sub>8</sub> conversion and the yield of H<sub>2</sub> was lower than the yield of CO and proved dependent on the catalyst. The most CO and H<sub>2</sub> was yielded over the catalysts Ni10C900 (90 and 73%, respectively). As in the catalytic screening at 700°C H<sub>2</sub>O was found to be the main side product followed by CO<sub>2</sub> and CH<sub>4</sub>. Their yield was generally lower at 800°C than at 700°C. Also traces of C<sub>2</sub>H<sub>4</sub> and C<sub>3</sub>H<sub>6</sub> were observed over the catalysts with a high Ni/Mg ratio, but again their yield was very low (Y < 0.5%). The performance of the reference catalyst was similar to that of Ni50C900.

The catalysts exhibited higher stability with time on stream (TOS) and a lower tendency towards coke formation at 800 than at 700°C (Fig. 34). The stability with time-on-stream (TOS) exhibited no clear tendency. Of the HT derived catalysts Ni10C900 showed the best stability. The apparent improvement of several catalysts with TOS, especially for the reference catalyst is mainly due to the fact that here the catalysts needed a longer time to reach steady state conditions at which they were stable as shown in Figure 35. Figure 35 also shows the good reproducibility of the catalytic tests. Except for the reference catalyst the tendency towards coke formation was higher at 700 than at 800°C. At 700°C it was lowest for the reference catalysts and then for Ni10C900. At 800°C it was lowest over Ni10C900. For the Mg containing catalysts it generally increased with increasing Ni/Mg ratio of the catalysts. The pure HT-derived Ni/Al, Ni72C900 exhibited lower tendency towards coking than Ni50C900.

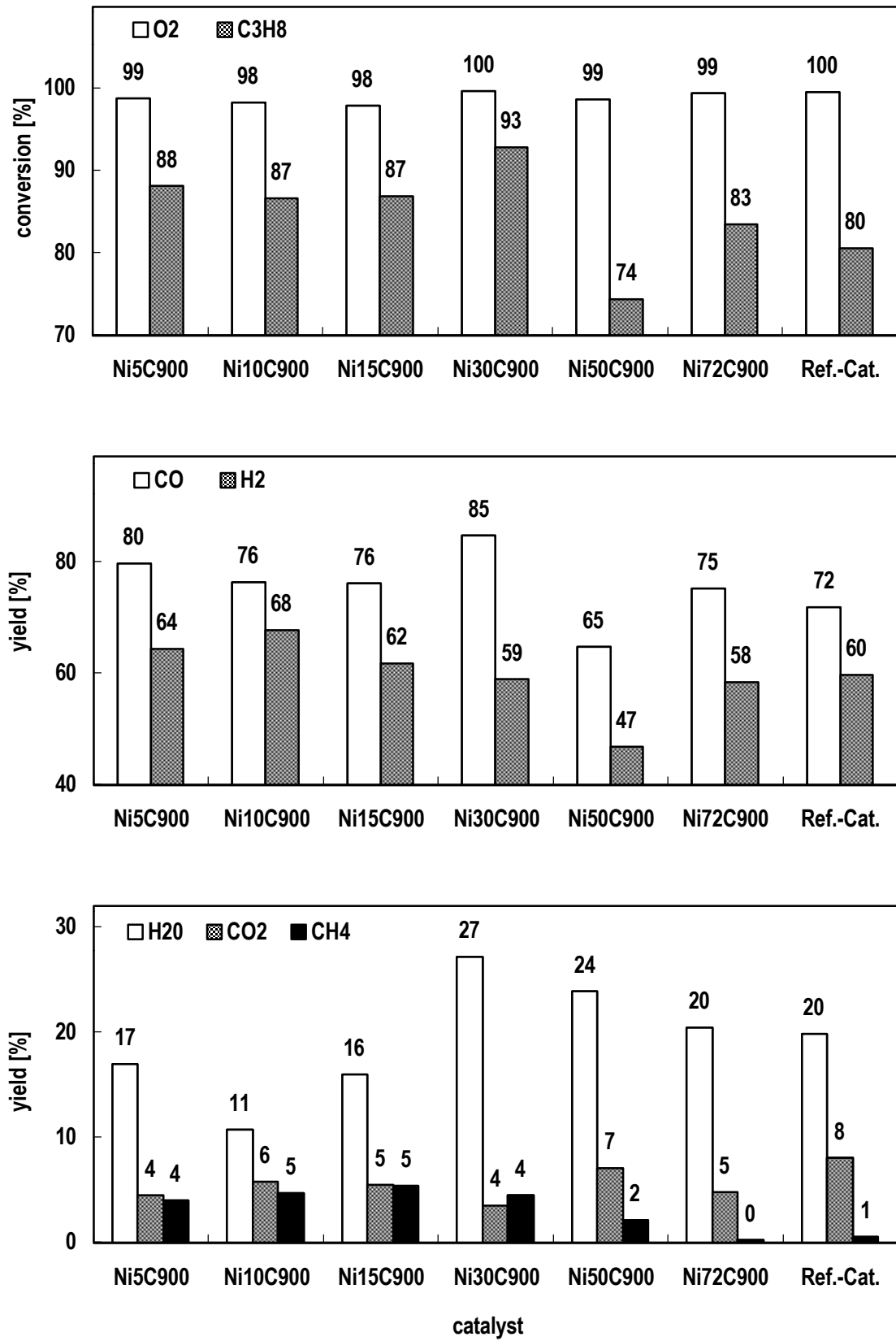


Fig. 32

Catalytic screening at 700°C, 25% O<sub>2</sub> surplus, GHSV 900dm<sup>3</sup>·h<sup>-1</sup>·g<sup>-1</sup>, TOS 240min

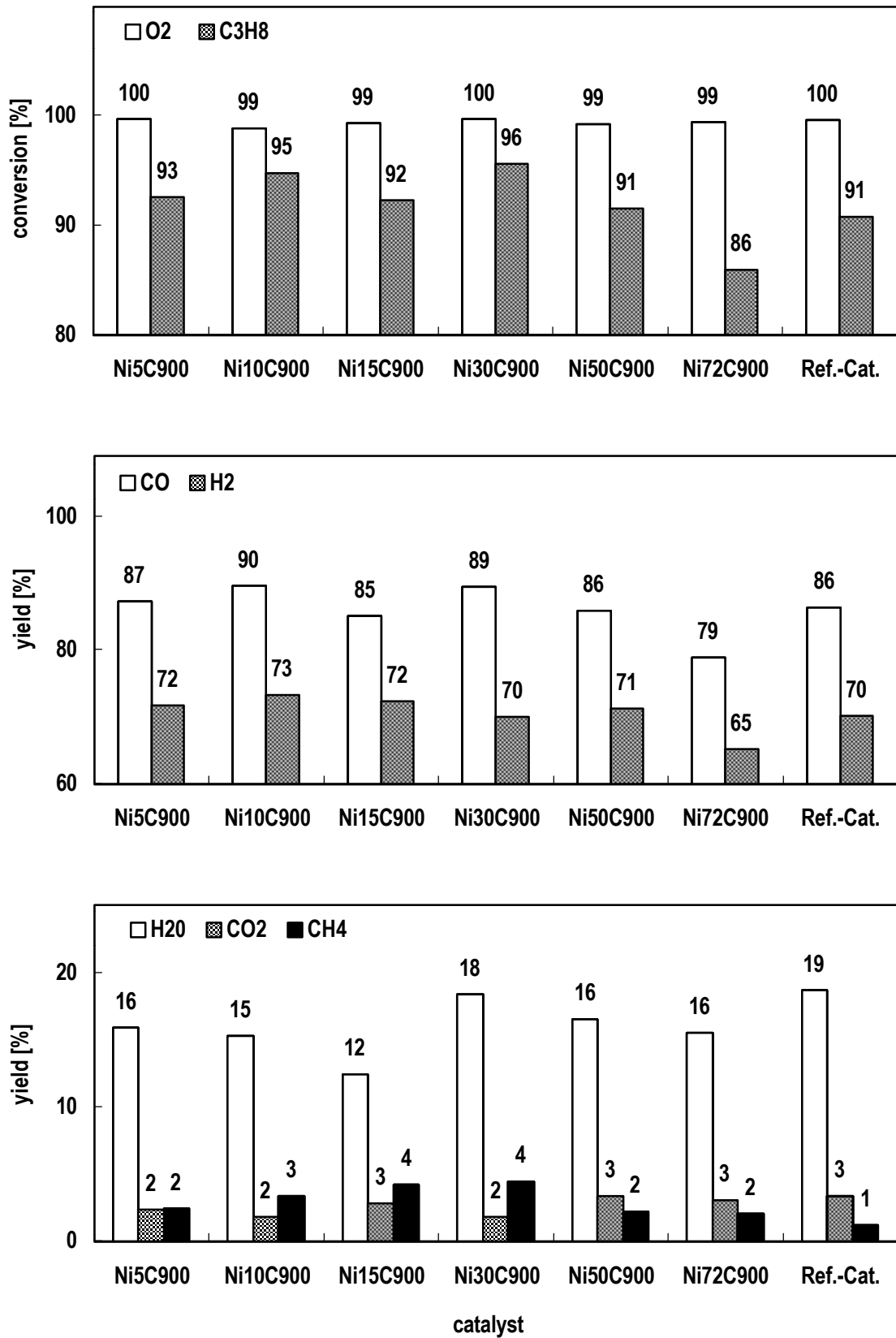


Fig. 33

Catalytic screening at 800°C, 25% O<sub>2</sub> surplus, GHSV 900 dm<sup>3</sup>·h<sup>-1</sup>·g<sup>-1</sup>, TOS 240 min

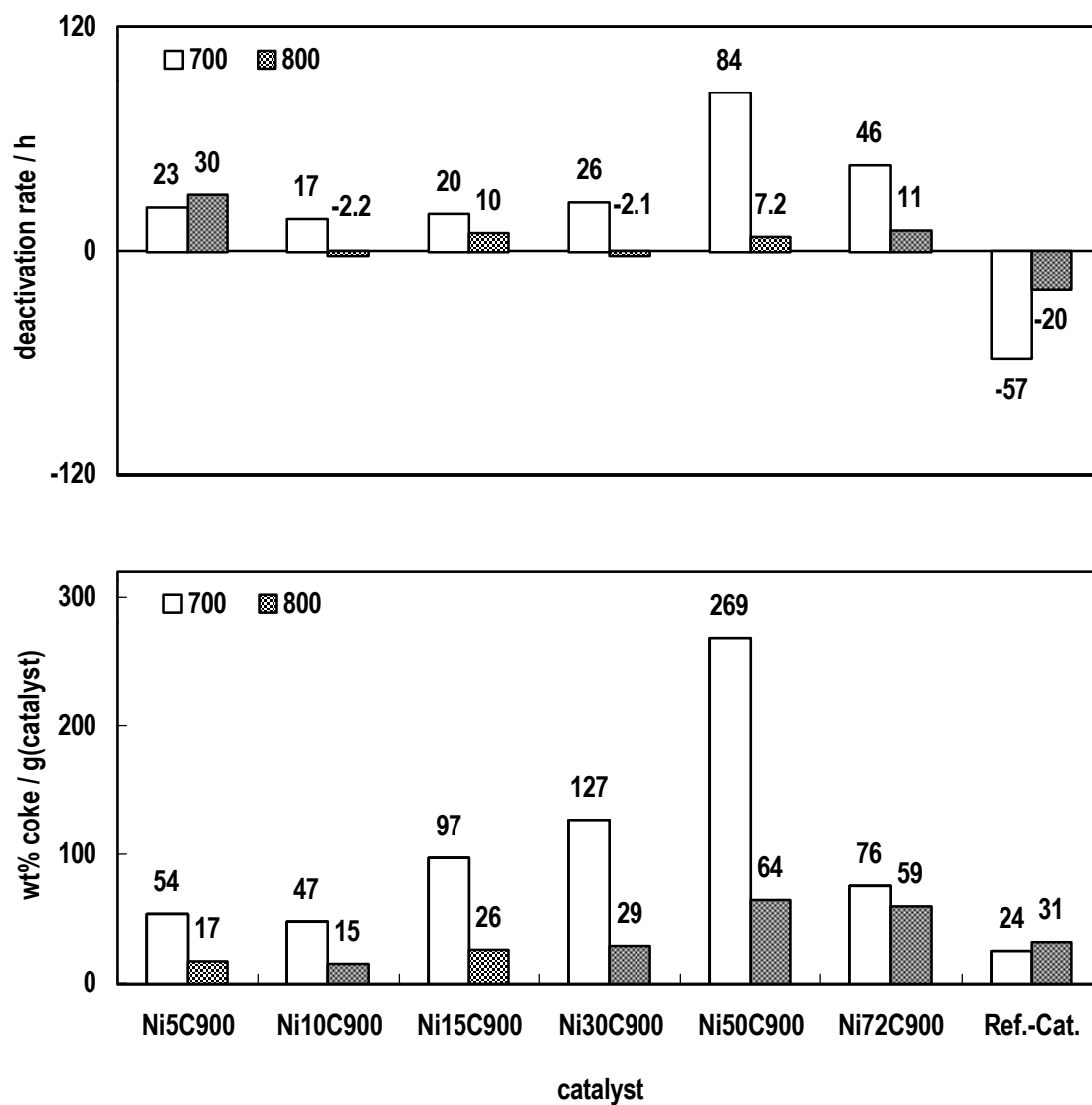


Fig. 34

Coking and catalyst deactivation at 700 and 800°C, 25% O<sub>2</sub> surplus, GHSV 900dm<sup>3</sup>·h<sup>-1</sup>·g<sup>-1</sup>, TOS 240min

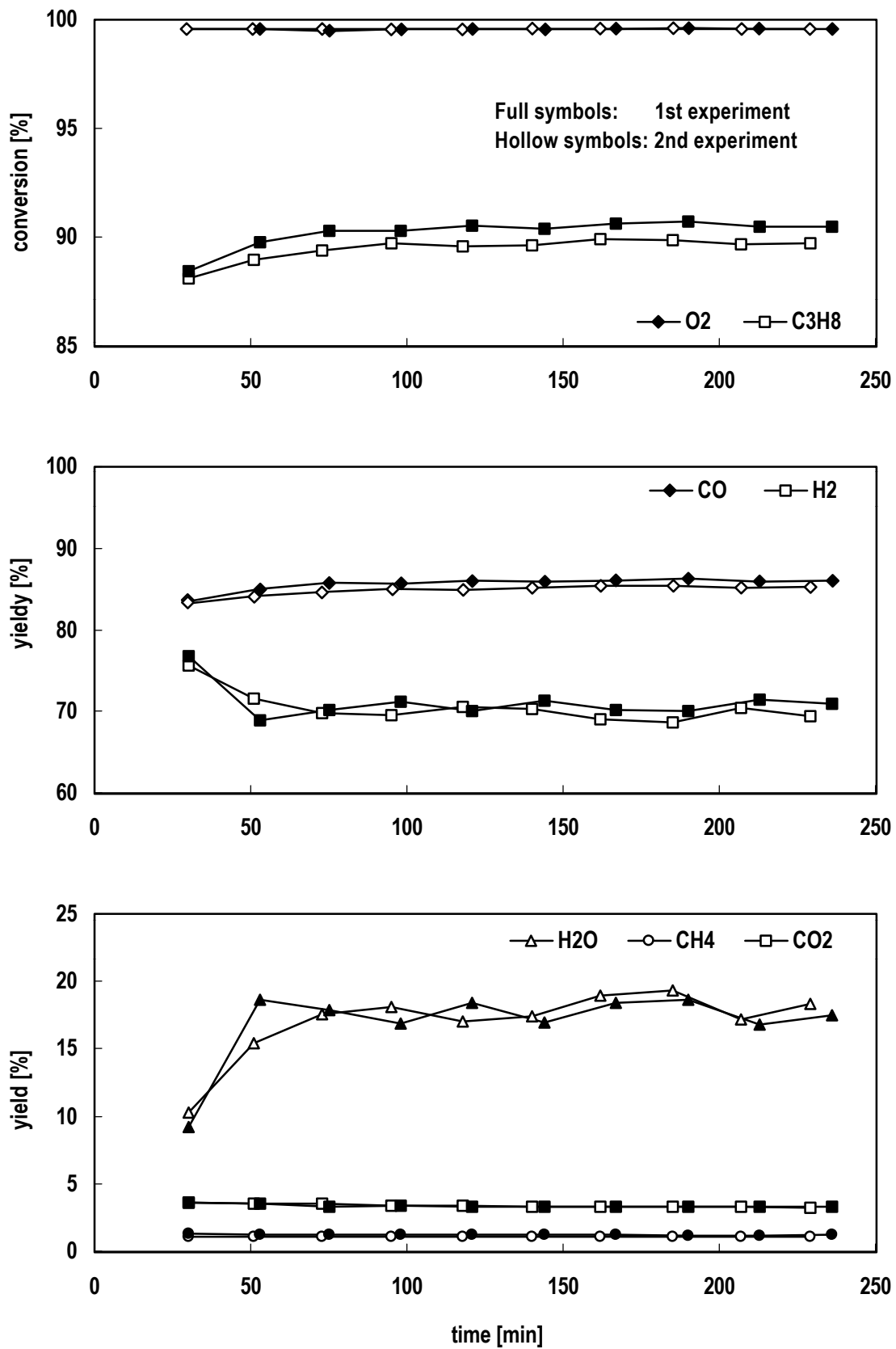


Fig. 35

Catalytic performance and reproducibility with time-on-stream of the reference catalyst at 800°C, 25% O<sub>2</sub> surplus, GHSV 900dm<sup>3</sup>·h<sup>-1</sup>·g<sup>-1</sup>, TOS 240min

All the investigated catalysts were found successful in the partial oxidation of  $C_3H_8$  at 700 and 800°C. Over all catalysts CO and  $H_2$  were at both temperatures the main products and  $H_2O$ ,  $CH_4$  and  $CO_2$  the only considerable side products. This is in contrast to the partial oxidation of propane performed over Pt or Pd containing catalysts [22]. Over Pt the olefins  $C_3H_6$  and  $C_2H_4$  were main products and Pd was not suitable due to rapid deactivation by coking. For a higher yield of syngas over the Ni catalysts it is favourable to perform the reaction at 800 instead of 700°C. The catalysts with a low and medium Ni/Mg ratio are superior in the syngas formation compared to the catalysts with a higher ratio or the reference catalyst. At 800°C the highest yield of CO and  $H_2$  were achieved over the catalyst Ni10C900, at 700°C the highest yield of CO was observed over Ni30C900 and the highest yield of  $H_2$  again over Ni10C900. However, considering both the yields of CO and  $H_2$  also at 700°C Ni10C900 should be regarded as the best of the studied catalyst.

No clear connection between the tendency towards coking and the catalyst deactivation with TOS can be found, which is attributed to the fact that different forms of coke can be formed under the reaction conditions, e.g. deactivating pyrolytic coke and non deactivating filamental coke. The observation that the tendency towards coking found for the HT derived Mg containing catalysts does not extend to the pure Ni/Al catalyst is attributed to the fact that the catalysts consist of a different structure. As shown in the investigation of the reduction process consist the Mg containing catalysts of metallic Ni particles in a MgO matrix and of spinel phases. The catalyst Ni72C900 in contrast consists only of metallic Ni and  $Al_2O_3$  particles. Therefore any correlation of the catalysts' properties in terms of basicity, surface area, Ni dispersion (and linked to it the total Ni surface) should be done only for the Ni and Mg containing catalysts as they have the same structural patterns. The catalyst Ni5C900 should be

excluded as here partial reconstruction of the former HT structure was observed after calcination.

The catalysts' surface area, basicity and both decrease with increasing Ni/Mg ratio of the catalyst, the dispersion of the catalysts Ni10C900, Ni15C900 and Ni30C900 is similar, hence their amount of surface Ni increases with increasing Ni/Mg ratio of the catalyst. As these properties show the same or the reverse trend is impossible to determine the influence of the single properties on the stability, the coke resistance or the catalytic performance.

## **4.2. Catalytic tests of different configurations**

### **4.2.1. Blank experiments**

In order to study the influence of the reduced Ni on the performance of the studied catalysts blank experiments were performed using the empty reactor (homogeneous reaction), quartz wool bed only, the Ni free catalyst and Ni10C900 without previous reduction. The same conditions as in the catalytic screening were applied. Ni10C900 was not only chosen because it was the most successful one, but also because it is the catalyst from the first set of catalysts that is most difficult to reduce and therefore least likely to be reduced by the reaction mixture. In the experiments carried out with an empty reactor or SiO<sub>2</sub> wool 1000°C was set as the upper temperature limit to avoid damaging the furnace and 600°C as the lower temperature limit as here the conversions were almost zero. Over the catalysts again 800°C was set as the maximum temperature as in the catalytic tests.

Using the empty reactor as well the reactor containing only the quartz wool. Almost complete conversions were observed at temperatures  $\geq 700^\circ\text{C}$  for the empty reactor and  $\geq 800^\circ\text{C}$  over the quartz wool bed. At lower temperatures the conversions decreased drastically and were almost zero at  $600^\circ\text{C}$  (Fig. 36). CO ( $Y \leq 51\%$ ),  $\text{H}_2\text{O}$  ( $Y \leq 46\%$ ),  $\text{C}_2\text{H}_4$  ( $Y \leq 32\%$ ) and  $\text{CH}_4$  ( $Y \leq 20\%$ ) were the main products. The trend of their yields versus temperature reflected more or less the conversion. The yield of  $\text{H}_2$  decreased with decreasing temperature ( $Y \leq 20\%$ ) and fell to zero at temperatures  $\geq 900^\circ\text{C}$  over the  $\text{SiO}_2$  wool and  $\geq 700^\circ\text{C}$  in the empty reactor. The yield of  $\text{C}_2\text{H}_2$  exhibited the same trend as that of  $\text{H}_2$ , but was always only a minor product ( $Y \leq 6\%$ ). The yield of  $\text{C}_3\text{H}_6$  exhibited the opposite trend ( $Y \leq 16\%$ ).  $\text{CO}_2$  was only observed at high conversion in low amounts ( $Y \leq 2\%$ ).

Over the catalyst that did not contain the metallic Ni (Ni0C900 and Ni10C900 without prior reduction) similar results were obtained with regard to each other. Over both catalysts higher  $\text{C}_3\text{H}_8$  than  $\text{O}_2$  conversions were observed regardless the reaction temperature. They were highest at  $800^\circ\text{C}$  ( $\geq 79\%$ ) and decreased sharply at lower reaction temperatures ( $\leq 20\%$ ) (Fig. 37). The main products were CO ( $Y \leq 27\%$ ),  $\text{H}_2\text{O}$  ( $Y \leq 31\%$ ),  $\text{C}_2\text{H}_4$  ( $Y \leq 31\%$ ),  $\text{C}_3\text{H}_6$  ( $Y \leq 21\%$ ) and  $\text{CH}_4$  ( $Y \leq 16\%$ ). They followed the same trend observed for the blank reactor and  $\text{SiO}_2$  wool. Again the temperature dependence of the yield reflected more or less the conversion.  $\text{H}_2$  was only observed at temperatures  $> 700^\circ\text{C}$  and only in small amounts ( $Y \leq 7\%$ ).  $\text{CO}_2$  was always present and its yield increased with decreasing reaction temperature ( $Y \leq 6\%$ ).  $\text{C}_2\text{H}_2$  was only found in very small quantities ( $< 1\%$ ). To investigate if the catalyst Ni10C900 without previous reduction would be reduced by the reaction mixture at higher temperatures the reaction was first started at the lower temperature and then increased. This procedure was chosen to avoid possible early reduction of the catalyst by the reaction.



After the maximum reaction temperature was reached, the temperature was decreased to see if any indications of such a reduction process at higher reaction temperatures were visible. No signs of reduction of the unreduced Ni containing catalyst were observed in its temperature cycle, as the catalyst performance was almost unchanged.

#### 4.2.2. The active catalyst (reduced Ni10C900)

Over the reduced catalyst Ni10C900 very different results were observed compared to the other cases. Here regardless the reaction temperature the O<sub>2</sub> conversion was always complete ( $\geq 99\%$ ), whereas the C<sub>3</sub>H<sub>8</sub> conversion decreased with decreasing temperature, but was always high ( $> 60\%$ ) (Fig. 38). Only CO and H<sub>2</sub> were at all temperatures main products. Their yields decreased with decreasing reaction temperature from 84% to 44% and from 72% to 31%, respectively. The opposite trend was observed for H<sub>2</sub>O and CO<sub>2</sub>, their yields increased with decreasing reaction temperature from 14% to 28% for H<sub>2</sub>O and from 3% to 15% for CO<sub>2</sub>. CH<sub>4</sub> was the only considerable hydrocarbon product its yield was between 2-3% independently of the temperature. At 800°C also traces of alkenes (C<sub>2</sub>H<sub>4</sub> and C<sub>3</sub>H<sub>6</sub>) were observed ( $Y < 1\%$ ). To see if Ni10C900 after previous reduction was oxidised or deactivated at lower reaction temperatures the reaction temperature was first decreased after starting at the highest temperature and increased again after the lowest reaction temperature was reached. Upon the increase of the reaction temperature the catalyst's performance was worse with regard to the C<sub>3</sub>H<sub>8</sub> conversion and yields of CO and H<sub>2</sub> but fully recovered at 800°C.

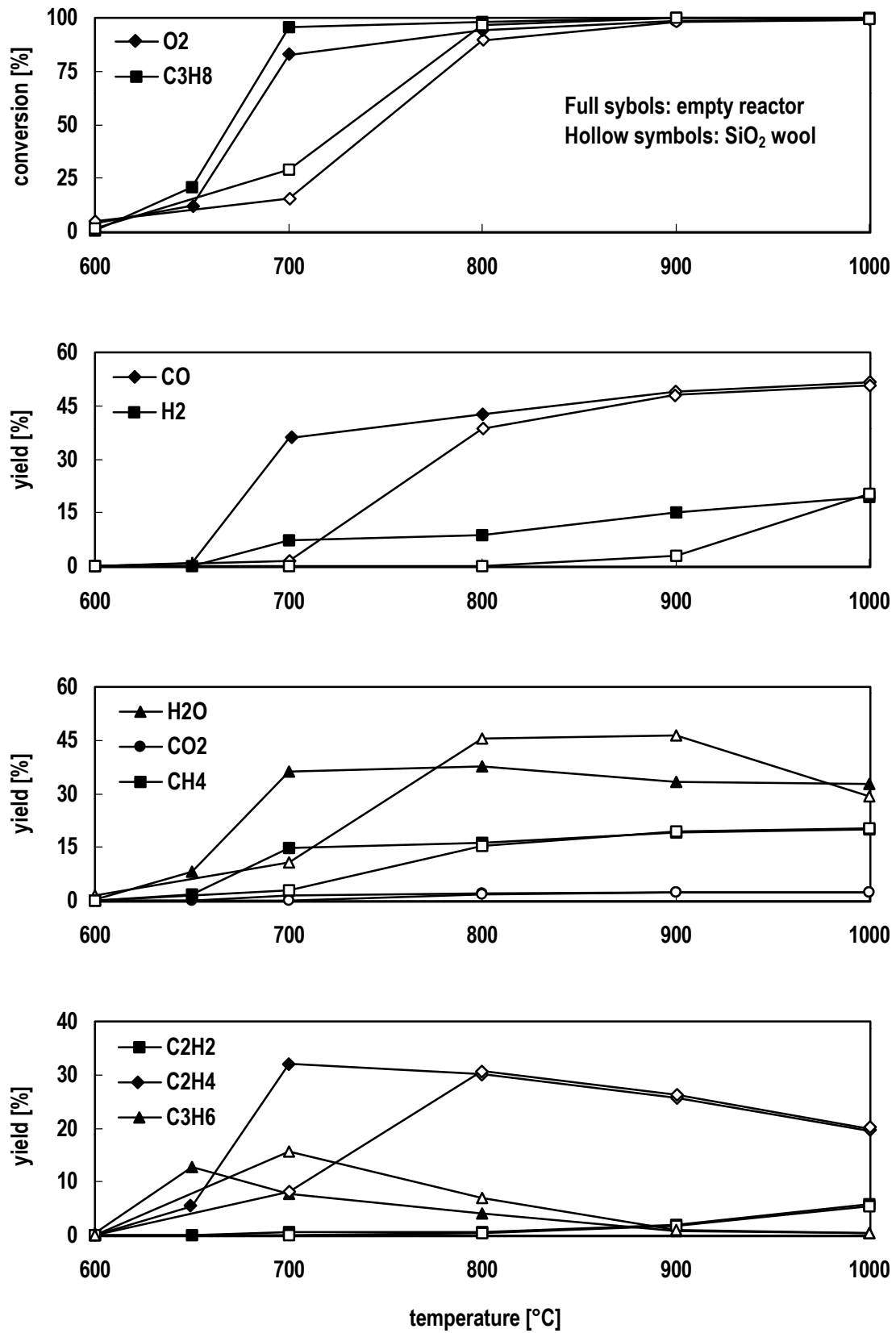


Fig. 36

Catalytic partial oxidation of C<sub>3</sub>H<sub>8</sub> of the homogeneous reaction (empty reactor) and over quartz wool, 25% O<sub>2</sub> surplus

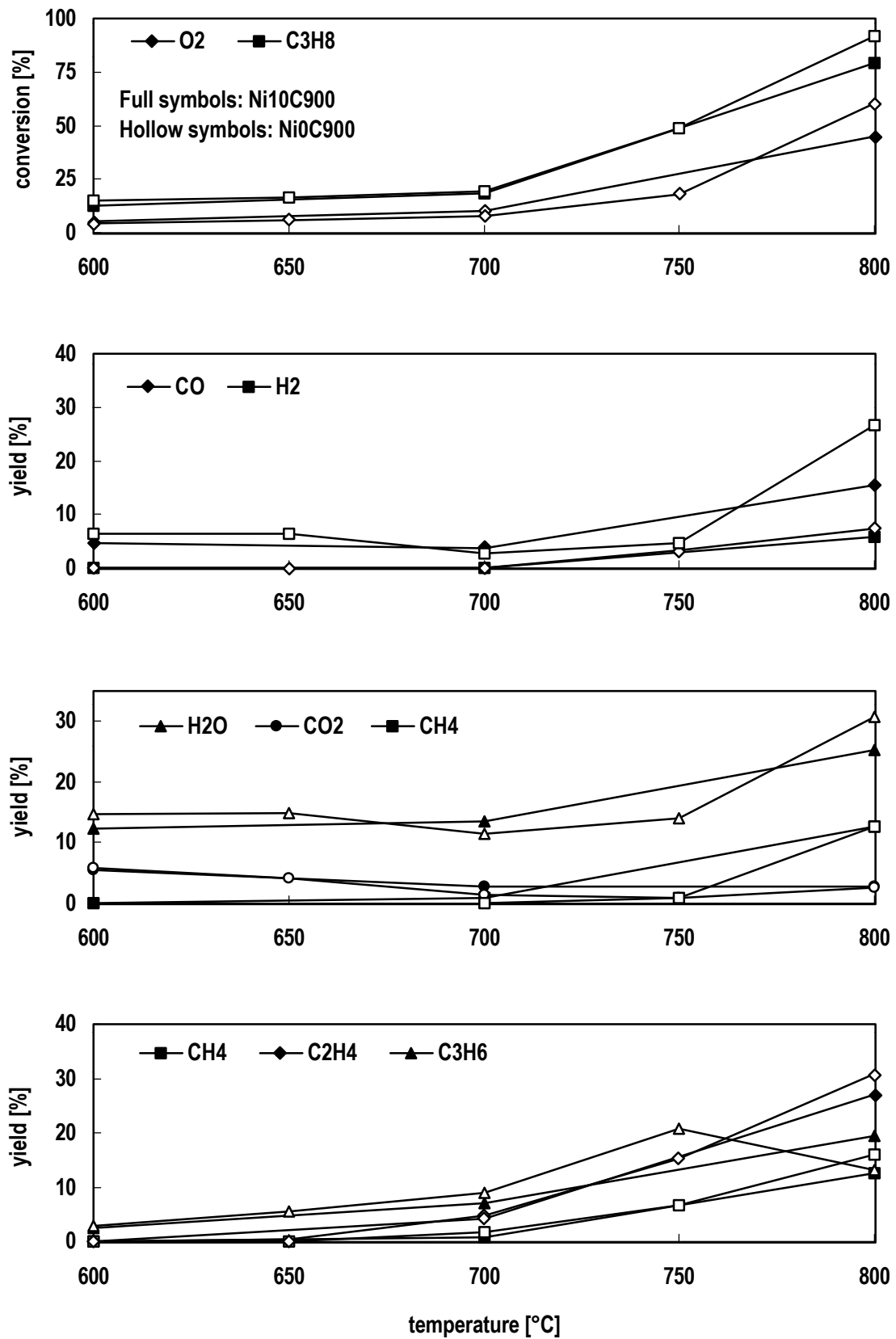


Fig. 37

Catalytic partial oxidation of C<sub>3</sub>H<sub>8</sub> over Ni0C900 and Ni10C900 (not reduced), 25% O<sub>2</sub> surplus, GHSV 900dm<sup>3</sup>·h<sup>-1</sup>·g<sup>-1</sup>

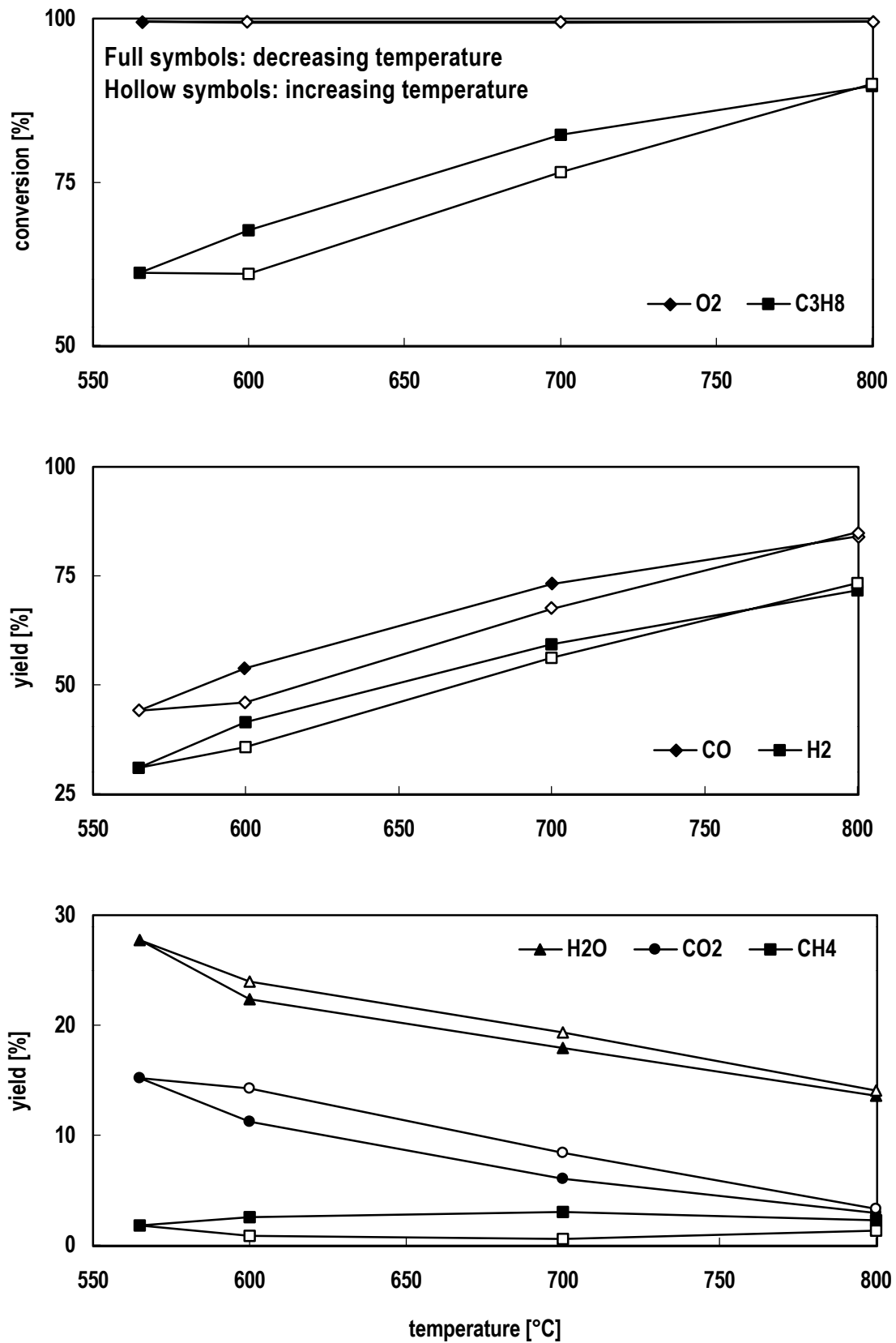


Fig. 38  
Temperature cycle of the catalytic partial oxidation of C<sub>3</sub>H<sub>8</sub> over Ni10C900, 25% O<sub>2</sub> surplus, GHSV 900dm<sup>3</sup>·h<sup>-1</sup>·g<sup>-1</sup>, starting temperature 800°C

All these results show that the partial oxidation of  $C_3H_8$  can be very effectively catalysed by the reduced Ni containing catalyst. Only CO and  $H_2$  were the main products. The not reduced Ni containing catalyst was not effective as it was also reported in the literature for the partial oxidation of  $CH_4$ . Since unreduced Ni/Mg/Al catalyst has no specific catalytic activity compared to the pure Mg/Al oxide catalyst it is clear that  $Ni^{2+}$  ions have no specific activity in the catalytic partial oxidation of  $C_3H_8$ .

The decrease in the conversion at a slightly higher temperature region for the reactor containing the quartz wool bed compared with conversion in the empty reactor (700°C instead of 650°C) results from a slight pressure drop and/or the suppression of homogeneous reactions due to the presence of the solid phase. The further decrease upon adding the Ni free or the not reduced catalyst, both placed on a  $SiO_2$  wool bed, could have the same nature. The results also show that the  $SiO_2$  wool bed has no significant catalytic influence and is therefore suitable to hold the catalyst.

Despite these effects the yields of CO and  $H_2$  over the active catalyst shall be compared to the yields observed for the empty reactor, the most effective set-up among all studied blank experiments (already presented in Figure 36 and 38). In the temperature range common to both configurations the yield could be increased by a minimum of factor 2 for CO and factor 8 for  $H_2$  by the use of the catalyst. At 650°C the non-catalysed reaction ceased, no more  $H_2$  and only very little amounts of CO were produced ( $Y < 1\%$ ), whereas in the presence of the active catalyst even at 600°C higher yields of CO and  $H_2$  were observed than at 1000°C in the empty reactor. In addition, the catalysed reaction yielded fewer undesirable side products. Over the catalyst the only observed side products were  $H_2O$ ,  $CH_4$  and  $CO_2$  as well as traces of  $C_2H_4$  and  $C_3H_6$  at 800°C. Without the catalyst considerable amounts of  $C_2H_4$  and  $C_3H_6$  and also traces of  $C_2H_2$  and  $C_3H_4$  were additionally produced. These unsaturated

products, especially the alkynes can cause severe problems in any downstream processes, e.g. by the formation of so-called green oil [126].

A more detailed further discussion of these different experiments is worthwhile as it can give valuable information and possibly a deeper insight into the reaction. In the blank experiments  $C_3H_8$  and  $O_2$  are only effectively activated at high temperatures ( $\geq 700^\circ C$ ), whereas over the reduced Ni catalyst complete  $O_2$  conversions are achieved regardless the temperature and even at reaction temperatures as low as  $565^\circ C$  the  $C_3H_8$  conversion is still above 60%. With exception of the reduced Ni catalyst considerable amounts of  $CH_4$  and unsaturated hydrocarbons, especially  $C_2H_4$ , were observed. This indicates the occurrence of cracking, according to Equation 9 [22].



This point is not undermined by the fact that at high temperatures the yield of  $CH_4$  is too high for pure cracking.  $CH_4$  is more stable and therefore less likely to react further.  $CH_4$  can also be produced by the hydrogenation of reactive carbon deposits [127]. The considerable amounts of  $C_3H_6$  may be attributed to either oxidative or thermal dehydrogenation of  $C_3H_8$  (Eq. 10 and 11) [22].



The absence of considerable yields of alkyne products may result from their greater reactivity compared to alkenes, e.g. towards coking. The low yield of  $CH_4$  ( $\leq 3\%$ ) and the absence of unsaturated hydrocarbon over the reduced catalyst do not necessarily

exclude the possibility of considerable dehydrogenation or cracking. As unsaturated hydrocarbons are more reactive than  $C_3H_8$ , which is converted to more than 60% even at  $565^\circ C$  over the reduced Ni catalyst, they are expected to react completely over the active catalyst. Furthermore the reduced Ni containing catalysts are active in the partial oxidation of  $CH_4$ .

$H_2O$  and  $CO_2$  were next to  $CO$  the only detected oxygen containing products in all experiments.  $H_2O$  was the main oxygen side product in all experiments, whereas  $CO_2$  was only a minor product. However, different trends were observed in the yields of  $H_2O$  and  $CO_2$ . In the absence of any of the catalysts the yield of  $H_2O$  reflected the conversion, whereas over the different catalysts,  $H_2O$  was still observed in considerable amounts even at low  $C_3H_8$  conversions ( $Y \geq 12\%$ ). The differences are even more obvious for  $CO_2$ . In the absence of the catalysts the yield of  $CO_2$  was always below 2% and decreased to zero at low conversion. In the presence of a catalyst, however, the yield was above 3% even at  $600^\circ C$ , where rather low conversions were achieved. This points out that in all cases the total combustion is promoted by the catalysts, Ni containing or not, reduced or not reduced. Therefore some limited total combustion activity can be attributed to the metal oxide matrix.

#### 4.3. Influence of the $O_2/C_3H_8$ ratio

The influence of the  $O_2/C_3H_8$  ratio was investigated at  $800^\circ C$  in the range from 0.75 – 1.50, where 1.00 corresponds to the stoichiometric value and 1.25 to the generally applied feed composition (25%  $O_2$  surplus). The GHSV was kept at the same value as in the other catalytic tests by adjusting the He flow ( $900 \text{ dm}^3 \cdot \text{h}^{-1} \cdot \text{g}(\text{catalyst})^{-1}$ ). The exact composition of the feed mixture for the different  $O_2/C_3H_8$  ratios is stated in Table 12.

Tab. 12: Feed composition at different  $O_2/C_3H_8$  ratios

$O_2/C_3H_8$ ratio (1.00 = stoichiometric ratio)	Feed composition [%]		
	$O_2$	$C_3H_8$	He
0.75	18.30	16.07	65.63
1.00	24.40	16.07	59.53
1.25	30.50	16.07	53.43
1.50	36.60	16.07	47.33

Over the whole range the  $O_2$  conversion was complete, the  $C_3H_8$  conversion increased with increasing  $O_2/C_3H_8$  ratios to 95% at ratio 1.25 and was complete at  $O_2/C_3H_8$  ratio 1.50 (Fig. 39). The yields of CO followed the same trend as the  $C_3H_8$  conversion. As in the catalytic screening the yield of  $H_2$  was always lower than the yield of CO. It increased steadily from  $O_2/C_3H_8$  ratio 0.75 to 1.25 but decreased at 1.50. The yield of  $H_2O$  increased steadily with increasing  $O_2/C_3H_8$  ratio from 1% to 37%. The yield of  $CO_2$  was low up to  $O_2/C_3H_8$  ratio 1.25, but increased at 1.50.  $CH_4$  was always the main hydrocarbon product, its yield decreased to 1% at  $O_2/C_3H_8$  ratio 1.50. Other hydrocarbon products,  $C_2H_4$  ( $Y \leq 1\%$ ) and  $C_3H_6$  ( $Y \leq 2\%$ ), as well as  $C_2H_6$  ( $Y < 1\%$ ) were observed only up to the stoichiometric  $O_2$  content in the feed. Their yield was higher at  $O_2/C_3H_8$  ratio 0.75 than at 1.00. Under all  $O_2/C_3H_8$  ratios the catalyst exhibited very good stability (Fig. 40). The apparent activation at  $O_2/C_3H_8$  ratio 0.75 and 1.00 results again from the fact that under these conditions the catalyst needed longer time to reach a stable steady state. The tendency for coke formation was in all cases low.



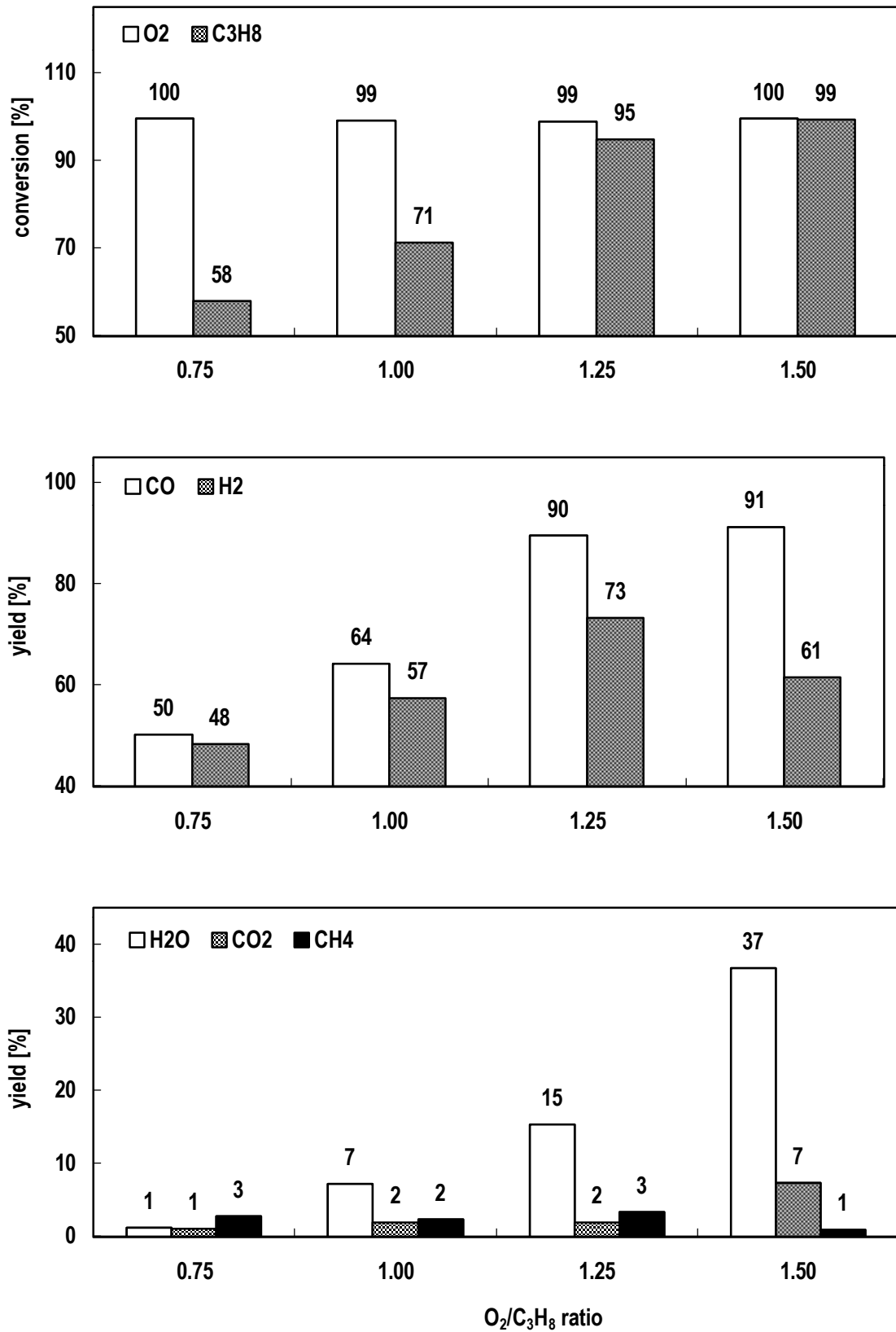


Fig. 39  
Catalytic performance of Ni10C900 for different  $O_2/C_3H_8$  ratios (1.00 = stoichiometric ratio),  
800°C, 25%  $O_2$  surplus, GHSV  $900\text{dm}^3\cdot\text{h}^{-1}\cdot\text{g}^{-1}$ , TOS 240 min

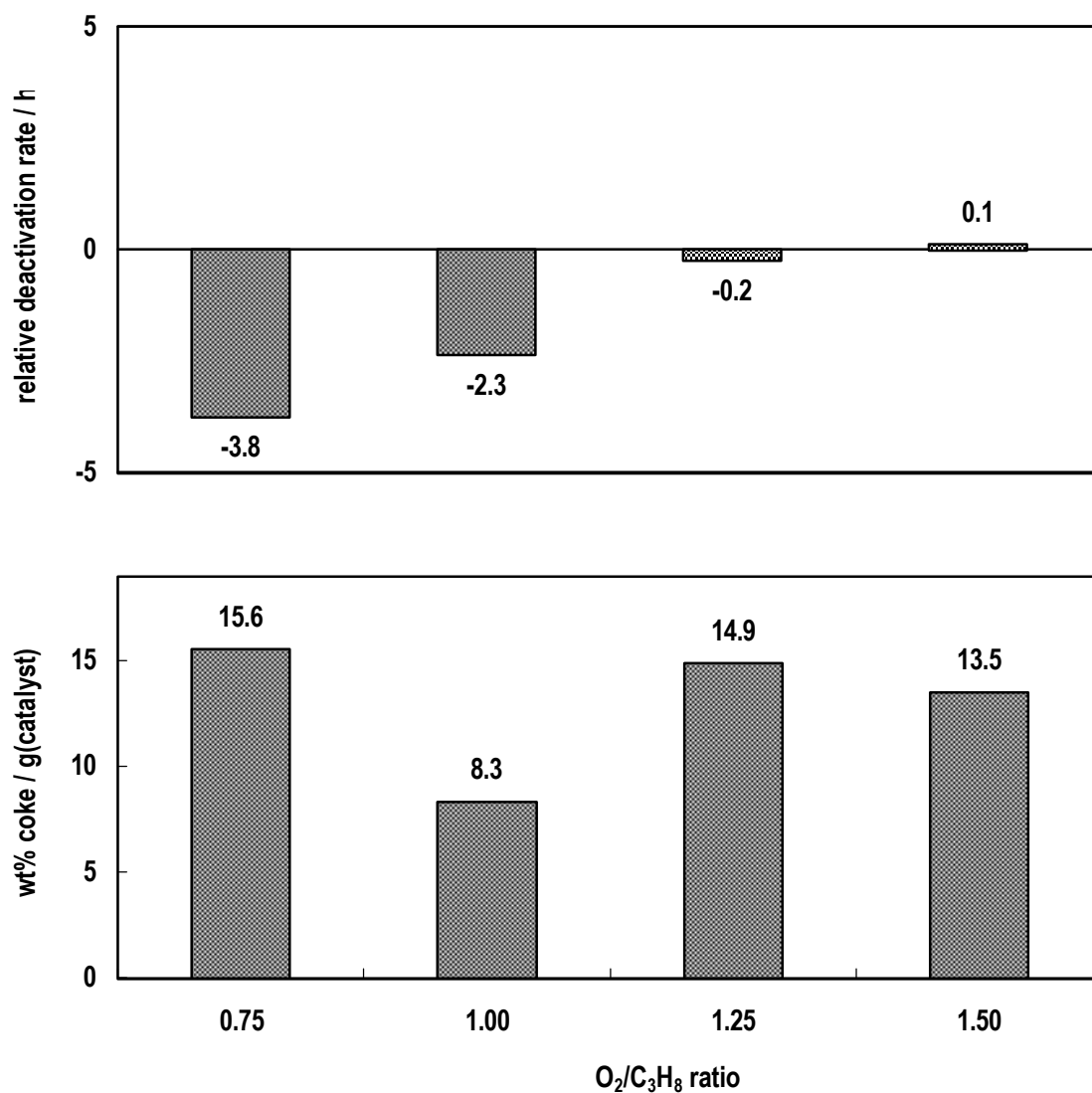


Fig. 40  
Coking and deactivation of Ni10C900 for different  $O_2/C_3H_8$  ratios (1.00 = stoichiometric ratio), 800°C, GHSV  $900\text{dm}^3\cdot\text{h}^{-1}\cdot\text{g}^{-1}$ , TOS 240min

---

These results show that under the chosen reaction condition high  $C_3H_8$  conversion is only possible under  $O_2$  excess in the feed stream because part of the  $O_2$  leads always to total combustion products,  $CO_2$  and especially  $H_2O$ . Their amount increases with increasing  $O_2$  content of the feed. After total  $C_3H_8$  conversion is achieved excess  $O_2$  leads to a sharp increase in total combustion products, but also almost to the disappearance of  $CH_4$  in the product mixture. The observed decrease of the amount of alkenes in the product mixture with increasing  $O_2/C_3H_8$  ratio may be attributed to the higher overall  $C_3H_8$  conversion or the complete conversion of the formed alkenes at higher  $O_2/C_3H_8$  ratio. The fact that the yield of  $CH_4$  only significantly decreases after total  $C_3H_8$  conversion is reached does not necessarily mean that cracking is significantly influenced by the  $O_2$  content of the feed, because excess  $O_2$  should lead to an increase in the conversion of formed  $CH_4$ . Judging from the yields of  $CO$  and  $H_2$  the catalytic partial oxidation is best performed at an  $O_2/C_3H_8$  ratio of 1.25 (25%  $O_2$  surplus). The results show that not reacted  $C_3H_8$  does not lead to higher coke formation under the applied reaction conditions or to the deactivation of the catalyst. Slight excess of  $O_2$  does not result in a decrease of the coke formation nor to the oxidation of the catalyst, which would result in its deactivation.

#### 4.4. Influence of space velocity

To investigate the influence of space velocity on the catalytic performance tests were carried out at 800°C at gas hourly space velocity (GHSV) of 600, 900 and 1200  $\text{dm}^3 \cdot \text{h}^{-1} \cdot \text{g}(\text{catalyst})^{-1}$  using the same feed composition as in the catalytic screening.

Here again almost complete  $\text{O}_2$  conversion was observed as in all experiments. The conversion of  $\text{C}_3\text{H}_8$  were always high ( $\geq 88\%$ ), but highest at GHSV 900  $\text{dm}^3 \cdot \text{h}^{-1} \cdot \text{g}^{-1}(\text{catalyst})$  (Fig. 41). CO and  $\text{H}_2$  were the main products, their yields changed only slightly with GHSV. The yield of CO reflected the trend of the conversion of  $\text{C}_3\text{H}_8$ , whereas the yield of  $\text{H}_2$  increased steadily with increasing GHSV. Again the yields of  $\text{H}_2$  were lower than that of CO. Changes in the GHSV had hardly any influence on the yield of  $\text{CO}_2$ , but at GHSV 600 and 900 higher yields of  $\text{H}_2\text{O}$  and  $\text{CH}_4$  were observed than at GHSV of 1200  $\text{dm}^3 \cdot \text{h}^{-1} \cdot \text{g}(\text{catalyst})^{-1}$ . Small amounts of alkenes  $\text{C}_2\text{H}_4$  and  $\text{C}_3\text{H}_6$  were observed only in case of the lowest GHSV with yields below 1% for each. Considerable catalyst deactivation was observed only at the lowest GHSV (Fig. 42). The amount of coke formed was always low and decreased with increasing GHSV.

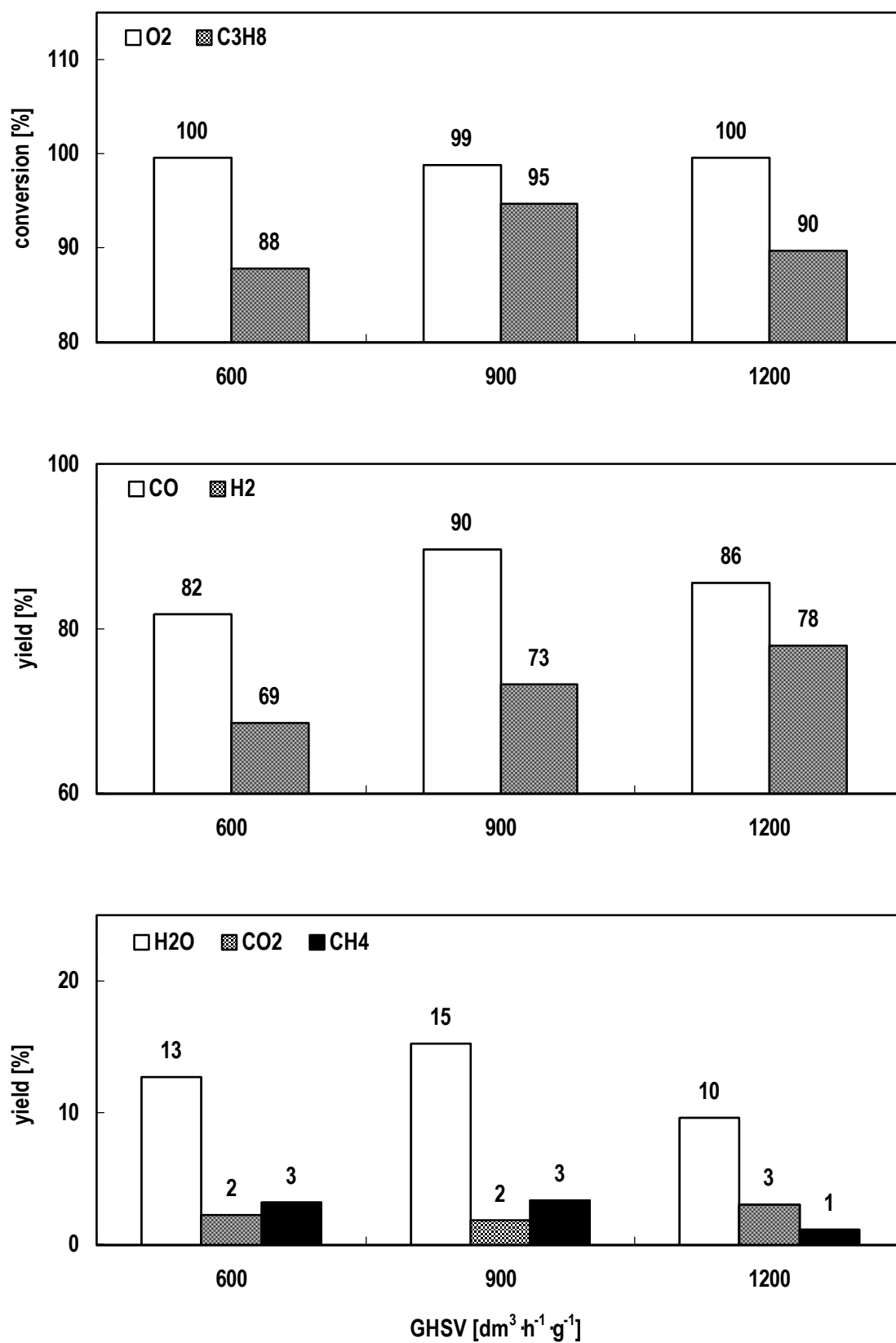


Fig. 41  
Catalytic performance of Ni10C900 for different GHSVs, 800°C, 25% O<sub>2</sub> surplus, TOS 240min

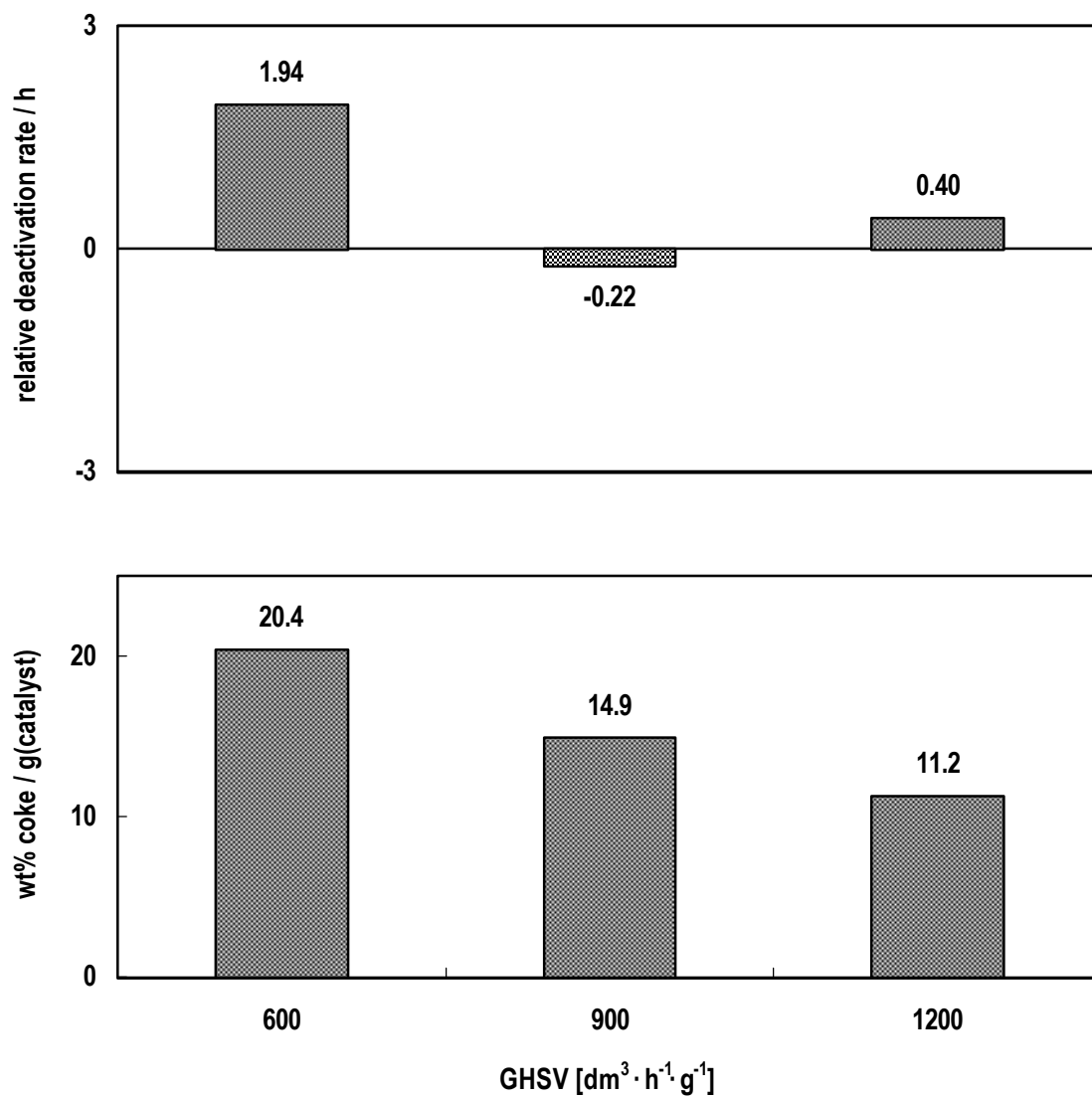


Fig. 42  
Coking and deactivation of Ni10C900 for different GHSVs, 800°C, 25% O<sub>2</sub> surplus, TOS  
240 min

---

The results show that the reaction is only slightly sensitive to changes in the GHSV in the investigated range. However, formation of unsaturated hydrocarbons in the product mixture observed only at the lowest GHSV might be somewhat unexpected. The formed alkenes are supposed to be more reactive than  $C_3H_8$ . Therefore they might be expected to be rather found at higher GHSV (shorter contact time), as it may be more likely that they pass the catalyst unreacted. However, as the yield of  $CH_4$  also decreases, this could be a sign of a decrease in cracking with increasing GHSV. Especially  $CH_4$  and  $C_2H_4$  are typical products of the thermal cracking of  $C_3H_8$  and  $C_3H_6$  is a typical product of the oxidative or thermal cracking. A decrease in cracking may be due to the shorter residence time of the substrate in the reactor, which could suppress homogeneous gas phase reaction such as cracking. Another possibility for this finding may be that with increasing GHSV a higher amount of hot spots is created due to the increase in the turnover rate. As the oxidation reactions, partial as well as total, are exothermic this might lead to a higher local catalyst temperature than measured, although the temperature rise due to the reaction was compensated by decreased heating power of the furnace. This would also explain the increase in the yield of  $H_2$  at the highest GHSV and the increase in the  $C_3H_8$  conversion at medium GHSV. The decrease in the  $C_3H_8$  conversion at the highest GHSV may be explained here by the shortening of the contact time. The differences in the catalyst deactivation and the tendency towards coking can be explained by both concepts. Due to the possible increase of the catalyst temperature with increasing GHSV less coke is formed. At temperatures below  $800^\circ C$  also before slight deactivation was observed. It could also be that by the decrease in homogeneous reactions at increasing GHSV less unsaturated hydrocarbons are formed, which are more likely to form coke, which can depending on its form lead to catalyst deactivation.

#### 4.5. Influence of the calcination temperature

In order to investigate the influence of the calcination temperature on the catalytic behaviour the precursor Ni10 was calcined at 700, 800, 900 and 1000°C. The step from 900 to 1000°C was chosen to investigate how a higher degree of crystallinity influences the catalytic behaviour. Another reason was to perform the reaction at 900°C while fulfilling the set criteria that the maximal reaction temperature should be 100°C lower than the calcination temperature. Calcination at 700 and 800°C was performed especially to investigate the difference in the catalyst behaviour due to the change of the structure. As discussed earlier the catalysts calcined at 700 and 800°C consist of a poorly crystallised divalent metal oxide phases with periclase structure, an amorphous  $\text{Al}_2\text{O}_3$  and a spinel phase at their interfaces, whereas after calcination at 900°C well crystallised divalent metal oxide phases with periclase structure and spinel phases are present. Furthermore, it is also possible for the catalyst calcined at 800°C to reconstruct the HT structure, it is but far less likely for the catalysts calcined at higher temperatures.

It must be pointed out that only over the catalyst calcined at 800°C no reproducible results could be obtained. It can only be speculated about the reason, but it might be due to the (partial) reconstruction of the former HT structure as the reaction was carried out at high temperatures and considerable amounts of water were formed. The catalysts at temperature  $\leq 800^\circ\text{C}$  exhibited partial reconstruction already after calcination. Even though the results for the catalyst Ni10C800 were not reproducible, for a comparison the best results are presented. Due to this problem no catalytic tests were performed for the catalyst Ni10C700. However, as it was originally planned to compare all catalysts including Ni10C700 at one common reaction temperature while fulfilling the reaction temperature criteria, maximal reaction temperature was by 100°C



---

lower than the calcination temperature and catalytic tests were performed at temperatures as low as 600°C.

The catalytic tests were performed under the same conditions as the catalytic screening. The reduction temperature was normally 100°C lower than the calcination temperature. The catalyst Ni10C800 used for the catalytic tests at 800°C was reduced at 800°C, in order to avoid possible ongoing reduction during the reaction performed at 800°C. However, due to the exothermal reactions the temperature increased at the start of the reaction by 70°C, a typical value for the reaction at 800°C. Although the temperature rise was immediately counteracted by reducing the heating power of the furnace, it needed some time to cool down to 800°C, therefore one cannot exclude structural changes in the catalyst. Starting the reaction at lower reaction temperature was not attempted as it could influence the coking of the catalyst and therefore its catalytic behaviour. Therefore this particular experiment was not repeated. It is also noteworthy that only when the reaction was performed at 900°C a temperature decrease of about 20°C was observed at the beginning of the reaction.

Over the catalysts Ni10C900 and Ni10C1000 very similar results were obtained in their common reaction temperature region (600-800°C), at 700°C almost identical conversions and yields were observed, the difference was  $\leq 2\%$ . At all temperatures over these two catalysts the O<sub>2</sub> conversion was always almost complete. The C<sub>3</sub>H<sub>8</sub> conversion increased with increasing reaction. At 900°C over Ni10C1000 even complete C<sub>3</sub>H<sub>8</sub> conversion was observed. Somewhat different results were observed over the catalyst Ni10C800. Here complete O<sub>2</sub> conversion was only observed at 800°C and it decreased with decreasing reaction temperature. The C<sub>3</sub>H<sub>8</sub> conversion was always lower than those observed for the other catalysts and decreased also with

decreasing reaction temperature (Fig. 43). Over all catalysts the yield of CO decreased with decreasing reaction temperature (Fig. 44). The lowest yield of CO was always observed for the catalyst calcined at 800°C. Over Ni10C900 as well as Ni10C1000 the yield of H<sub>2</sub> was almost the same at 700°C and 800°C (around 70%), but decreased at 600°C (around 45%). Over Ni10C800 a similar behaviour was observed but at lower H<sub>2</sub> yield. The yield of CO<sub>2</sub> increased over all catalysts with decreasing reaction temperature. No clear trends of the yield of H<sub>2</sub>O could be noticed, its value was relatively high for the catalyst Ni10C1000 at 800°C (22%). The yield of CO, H<sub>2</sub>, H<sub>2</sub>O, CH<sub>4</sub> and CO<sub>2</sub> over Ni10C1000 at 900°C (not depicted), were 90, 72, 13, 8% and 2%, respectively. C<sub>2</sub>H<sub>4</sub>, C<sub>2</sub>H<sub>6</sub> and C<sub>3</sub>H<sub>6</sub> were only observed at 800 and 900°C over the catalysts Ni10C800 and Ni10C1000 with yields ≤ 1% of each compound.

For the catalysts Ni10C900 and Ni10C1000 catalyst deactivation and coking generally decreased with the increasing reaction temperature and was higher for Ni10C1000 than for Ni10C900 (Fig. 45). No deactivation and lower coking (15%) was observed for Ni10C1000 at 900°C. Ni10C800 showed an increasing catalyst deactivation with increasing reaction temperature and higher coking than the other catalysts. The apparent catalyst activation at 600°C should have the same reason as discussed in more detail above.

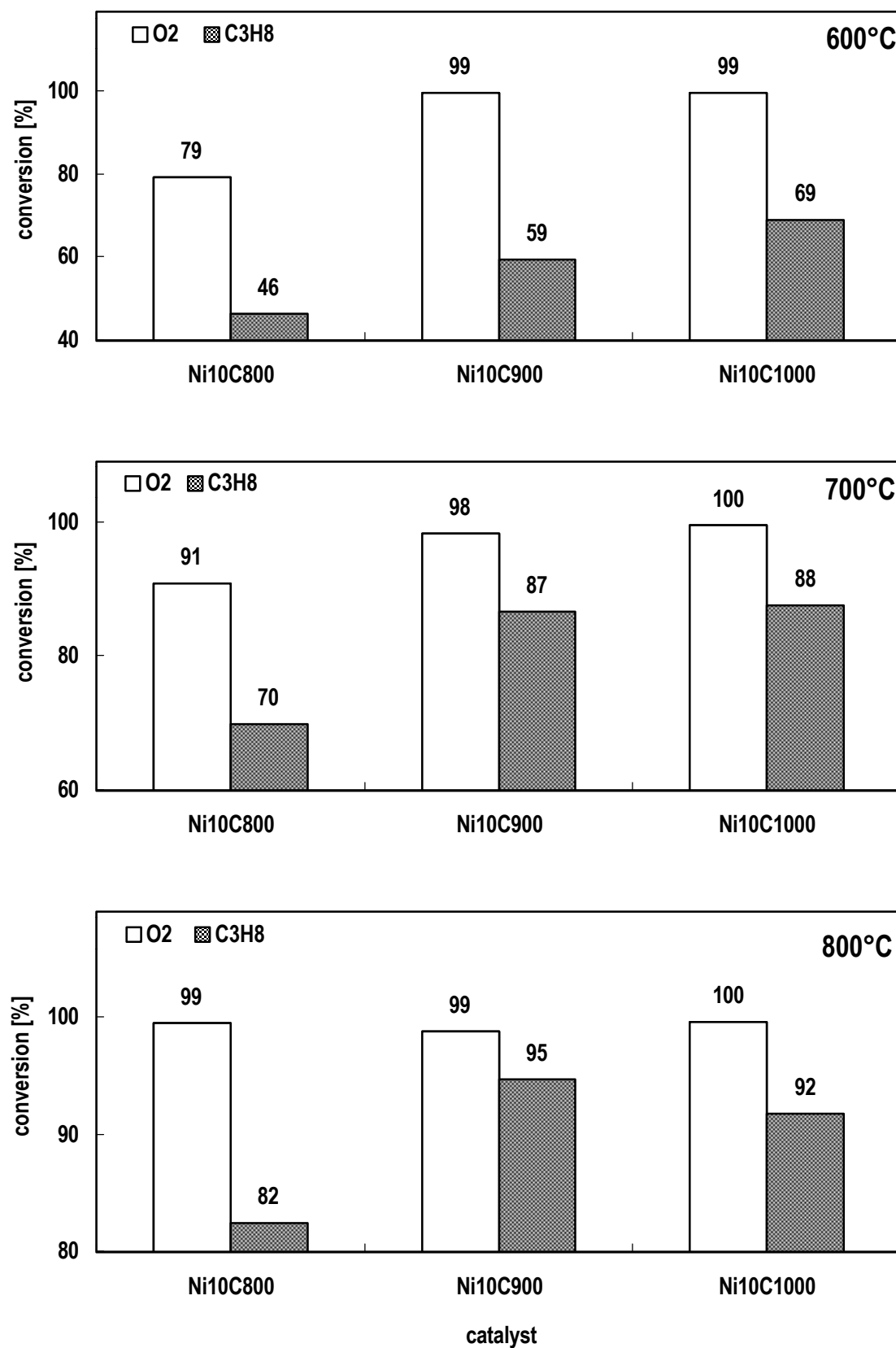


Fig. 43  
Conversion at 600, 700 and 800°C over Ni10 calcined at 800, 900 and 1000°C,  
25% O<sub>2</sub> surplus, GHSV 900dm<sup>3</sup>·h<sup>-1</sup>·g<sup>-1</sup>, TOS 240min

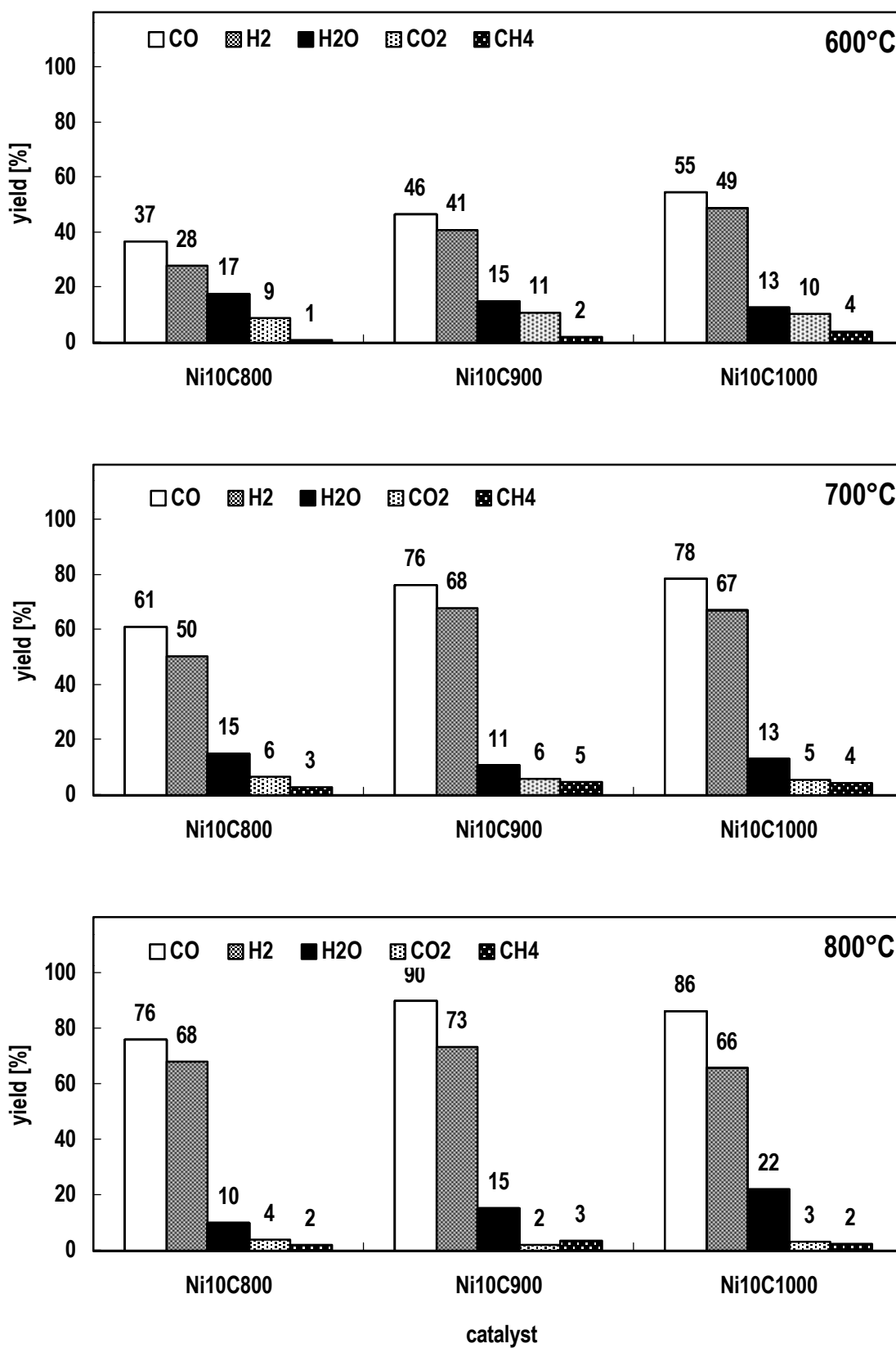


Fig. 44  
Yield at 600, 700 and 800°C over Ni10 calcined at 800, 900 and 1000°C,  
25% O<sub>2</sub> surplus, GHSV 900dm<sup>3</sup>·h<sup>-1</sup>·g<sup>-1</sup>, TOS 240min

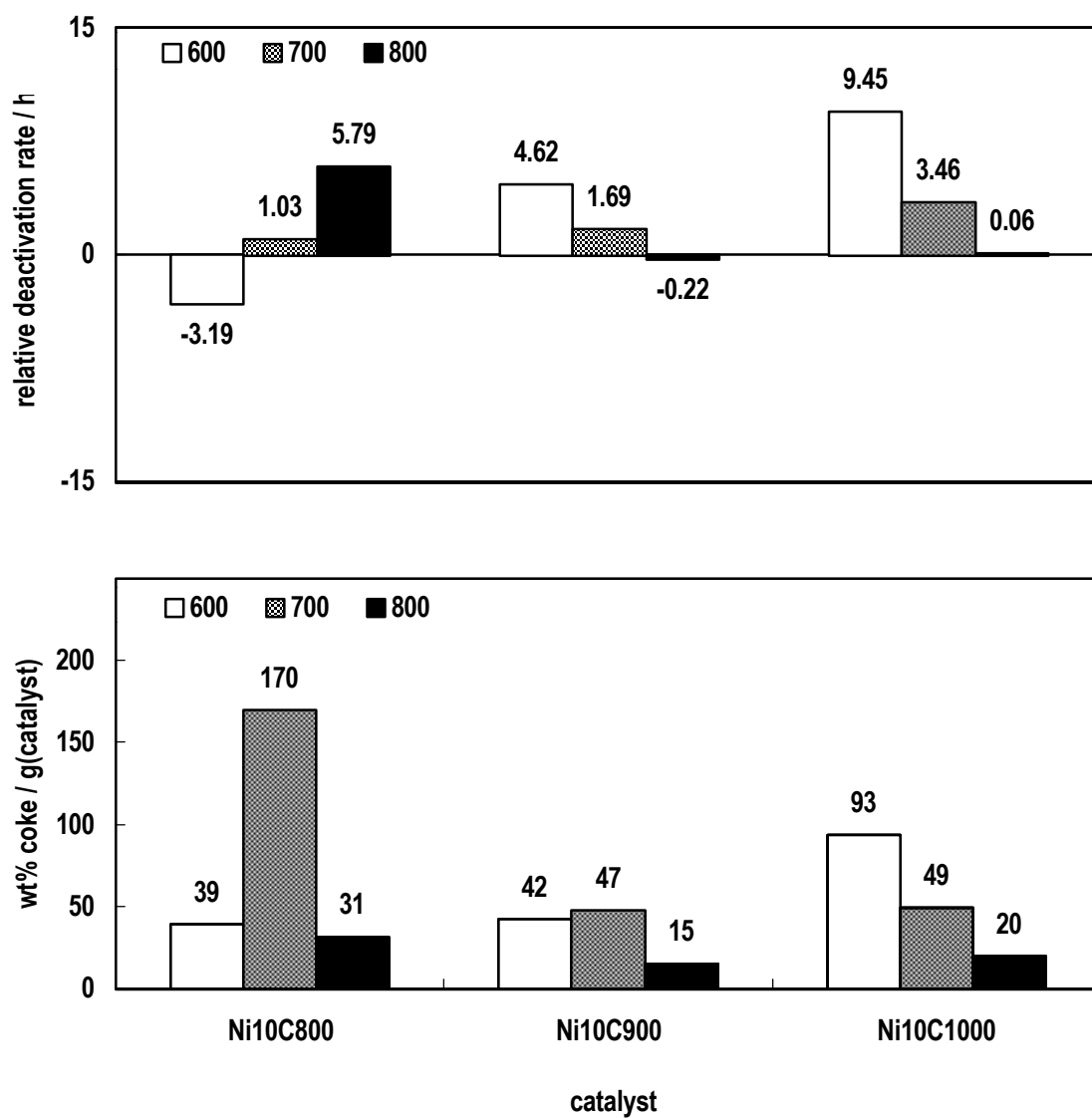


Fig. 45  
Coking and deactivation at 600, 700 and 800°C over Ni10 calcined at 800, 900 and 1000°C,  
25% O<sub>2</sub> surplus, GHSV 900dm<sup>3</sup>·h<sup>-1</sup>·g<sup>-1</sup>, TOS 240 min

The results show that under the reaction conditions the catalysts with a well crystallised structure have a superior catalytic behaviour compared to the catalyst with a poorly crystallised structure, regardless the reaction temperature. They further show that the increase in the calcination temperature from 900 to 1000°C has no significant effect on the catalytic behaviour although the catalyst calcined at 900°C is slightly more effective at 800°C and less effective at 600°C compared to the one calcined at 1000°C. Furthermore the increase in the reaction temperature from 800 to 900°C over Ni10C1000 did not result in an higher yield of CO or H<sub>2</sub>, or a better stability or coke resistance as compared to Ni10C900 at 800°C. At 900°C typical cracking products were observed, which could mean that cracking took place, possibly by homogeneous reactions. This suggestion is supported by the fact that only at 900°C a decrease of the reaction temperature was observed. This may be due to homogeneous reactions leading to total oxidation products (H<sub>2</sub>O, CO<sub>2</sub>), e.g. oxidative cracking or total oxidation of C<sub>3</sub>H<sub>8</sub> taking place before the feed stream gets into contact with the catalyst. Over the catalyst H<sub>2</sub>O and CO<sub>2</sub> are reformed by not reacted C<sub>3</sub>H<sub>8</sub> and this reaction is highly endothermic.

The different trend of Ni10C800 compared to Ni10C900 and Ni10C1000 with regard to catalyst deactivation and coking cannot be explained easily because for this catalyst structural changes like reconstruction must be taken into account. Comparing Ni10C900 and Ni10C1000 shows that Ni10C900 is more stable and has a higher resistance against coking, which is attributed to its lower crystallinity. Ni10C900 and Ni10C1000 are more stable and coke resistant at higher reaction temperatures, which was also found for the other catalysts in the catalyst screening.



## 5. Conclusions

Coprecipitation at low supersaturation at pH  $8 \pm 0.2$  and 60-70°C resulted in the formation of Ni, Mg and Al containing hydrotalcite-type materials of the approximate formula  $[\text{Ni}_x\text{Mg}_{72-x}\text{Al}_{28}(\text{OH})_{200}][(\text{NO}_3)_y(\text{CO}_3)_{(28-y)/2}] \cdot 50\text{H}_2\text{O}$  ( $x = 0, 5, 1, 15, 3, 5, 72$  and  $11 \leq y \leq 16$ ). Their thermal stability was found to decrease with increasing substitution of  $\text{Mg}^{2+}$  by  $\text{Ni}^{2+}$ .

By calcination at temperature  $\geq 900^\circ\text{C}$  in a flow of air these solids were transformed into their corresponding mixed metal oxides consisting of divalent metal oxide phases with periclase structure and spinel phases. At lower temperatures poorly crystallised divalent metal oxides and amorphous  $\text{Al}_2\text{O}_3$  phases with poorly crystallised spinel at their interfaces were formed. The degree of crystallinity increased with increasing calcination temperature. Catalysts with a lower nickel content exhibited remarkably high surface areas suggesting that the removal of the gases formed during the calcination process and slow heating rate had a beneficial influence on the catalysts' preparation.

The studies of the activation process by the reduction in hydrogen of the catalysts calcined at  $900^\circ\text{C}$  showed that the reduction takes place in two distinct steps. First the  $\text{Ni}^{2+}$  ions in the divalent metal oxide phase with periclase structure are reduced and then at higher temperatures also the  $\text{Ni}^{2+}$  ions in the spinel phase. At temperatures up to  $950^\circ\text{C}$  the  $\text{Ni}^{2+}$  ions in the divalent metal oxide phase were reduced in all the catalysts, the  $\text{Ni}^{2+}$  ions in the spinel phase only in the magnesium free one. The catalysts with a lower nickel content were more difficult to reduce but exhibited higher nickel dispersion. These findings are attributed to the substitution of  $\text{Mg}^{2+}$  by  $\text{Ni}^{2+}$  leading to the formation of a NiO-MgO solid solution upon calcination, which stabilises



---

the Ni<sup>2+</sup> ions against reduction and sintering. The formed metallic nickel particles are not stabilised by the MgO matrix against consecutive oxidation.

Investigations of the influence of the calcination temperature on the properties of the catalyst Ni10 revealed that the reduction temperature increases slightly with increasing crystallinity of the catalysts. In the catalysts with a well crystallised structure only the Ni<sup>2+</sup> ions in the divalent metal oxide phase were reducible below 950°C, whereas in the catalysts showing only a poorly crystallised structure almost all Ni<sup>2+</sup> ions could be reduced. For the catalysts with a well crystallised spinel phase the dispersion decreased with increasing calcination temperature of the solid. In the case of the catalyst without a well crystallised spinel phase the total amount of surface Ni is higher, but the dispersion lower, which is attributed to the higher total amount of the reduced Ni atoms.

Investigations of the basicity by temperature programmed desorption of CO<sub>2</sub> after adsorption at 100°C for 1 hour revealed no differences between the Ni/Mg ratio of the catalysts and their specific desorption of CO<sub>2</sub>. In order to see differences in their specific desorption of CO<sub>2</sub> prolonged adsorption times and adsorption temperatures up to 200°C were applied. By adsorption at temperatures of at least 150°C the specific desorption of CO<sub>2</sub> of the catalysts was found to decrease with increasing Ni/Mg ratio. Transformation of isopropanol and aldol condensation were found to be unsuitable test reactions for the determination of the basicity, due to the dehydrogenation activity of Ni<sup>2+</sup> ions in the former and due to the low specific activity of the catalysts at lower temperatures in the latter reaction.

The partial oxidation of propane to syngas could be successfully performed at temperatures between 600°C and 900°C over reduced Ni containing catalysts. CO and

---

H<sub>2</sub> were the main products, H<sub>2</sub>O, CO<sub>2</sub> and CH<sub>4</sub> the only considerable side products. The conversion of C<sub>3</sub>H<sub>8</sub> and the yield of syngas increased with increasing reaction temperature. Unreduced Ni exhibited no specific catalytic activity. Of the hydrotalcite-type derived Ni containing catalyst calcined at 900°C, the ones with a low to medium Ni content exhibited better catalytic performance than those with a higher Ni content or the reference catalyst (20 wt% NiO/Al<sub>2</sub>O<sub>3</sub> + 2 wt% K<sub>2</sub>O). Coking was found to increase with increasing Ni content of the catalysts and to decrease with increasing reaction temperature. As no clear relation was observed between coking and catalyst deactivation it was concluded that different types of coke could be formed over the catalysts of which not all were deactivating. Since several factors characterising the catalysts (BET surface area, Mg content and available Ni surface) follow the same or the opposite trend with the Ni content, so it was impossible to differentiate between these properties and their effect on the catalyst performance or coking.

The hydrotalcite-type derived catalyst with an approximate metal composition Ni<sub>10</sub>Mg<sub>62</sub>Al<sub>28</sub> calcined at 900°C exhibited the best catalytic performance, a good stability with time-on-stream and a high resistance against coking (the highest at 800°C). The partial oxidation of C<sub>3</sub>H<sub>8</sub> performed over this catalyst compared with the results of the non-catalytic reaction showed at least two-fold increase in the yield of CO and eight-fold increase of the H<sub>2</sub> yield. At lower temperatures these differences were even greater.

Calcination of the catalyst Ni10 at 1000°C did not improve the catalytic performance, but resulted in a lower stability and higher coking. Calcination at 800°C lead to a decrease of the catalytic performance and to not reproducible results attributed to the partial reconstruction of the former hydrotalcite-type structure. Therefore Ni10 calcined at 900°C was used for further investigations of the influence of the O<sub>2</sub>/C<sub>3</sub>H<sub>8</sub> ratio and

---

the space velocity on its performance at 800°C. These studies revealed that the total C<sub>3</sub>H<sub>8</sub> conversion was only achieved in excess of O<sub>2</sub> because even under O<sub>2</sub> deficient conditions part of the O<sub>2</sub> lead to the total oxidation products CO<sub>2</sub> and especially H<sub>2</sub>O. When all C<sub>3</sub>H<sub>8</sub> was converted excess O<sub>2</sub> lead not to the catalyst oxidation, but to an increase in the yield of total oxidation products. The highest yields of CO and H<sub>2</sub> are achieved at total C<sub>3</sub>H<sub>8</sub> conversion. Under O<sub>2</sub> deficient conditions only small amounts of unsaturated hydrocarbons were formed. Not reacted C<sub>3</sub>H<sub>8</sub> did not result in a decrease of the stability of the catalysts or an increase of coking. It was also found that the catalytic partial oxidation of C<sub>3</sub>H<sub>8</sub> could be performed at gas hourly space velocities as high as 1200 dm<sup>3</sup> · h<sup>-1</sup> · g(catalyst)<sup>-1</sup>. The observed decrease in coke formation with increasing space velocity may be attributed to an increase in the local catalyst temperature resulting from the higher turnover frequency.

All the findings of this work indicate that Ni catalysts derived from hydrotalcite-type precursors are promising catalyst for the partial oxidation of propane, especially the catalyst with a lower Ni loading (Ni10) calcined at 900°C. It exhibited the best performance compared to the other catalysts including a conventional steam reforming Ni/Al<sub>2</sub>O<sub>3</sub> catalyst doped with K<sub>2</sub>O.

---

**6. Literature**

- [1] F. Cavani, F. Trifirò and A. Vaccari, *Catal. Today* **11** (1991) 173-301
- [2] A. Vaccari, *Catal. Today* **41** (1998) 53-71
- [3] B. Montanari, A. Vaccari, M. Gazzano, P. Käßner, H. Papp, J. Pasel, R. Dziembaj, W. Makowski and T. Łojewski, *Appl. Catal. B* **13** (1997) 205-217
- [4] E.C. Kruissink, L.E. Alzamora, S. Orr, E.B.M. Doesburg, L. van Reijen, J.R.H. Ross and G. van Veen in 'Preparation of Catalysts II', B. Delmon, P. Grange, P.A. Jacobs and G. Poncelet (editors), Elsevier, Amsterdam 1979, pp. 143-157
- [5] K.B. Mok, J.R.H. Ross and R.M. Sambrook in 'Preparation of Catalysts III', G. Poncelet, P. Grange and P.A. Jacobs (editors), Elsevier, Amsterdam, 1983, pp. 291-299
- [6] D.C. Puxley, I.J. Kitchener, C. Komodromas and N.D. Parkyn in 'Preparation of Catalysts III', G. Poncelet, P. Grange and P.A. Jacobs (editors), Elsevier, Amsterdam, 1983, pp. 237-271
- [7] O. Clause, B. Rebours, E. Merlen, F. Trifirò and A. Vaccari, *J. Catal.* **133** (1992) 231-246
- [8] F. Trifirò, A. Vaccari and O. Clause, *Catal. Today* **21** (1994) 185-195
- [9] F. Basile, L. Basini, M. D'Amore, G. Fornasari, A. Guarinoni, D. Matteuzzi, G. Del Pietro, F. Trifirò and A. Vaccari, *J. Catal.* **173** (1998) 247-256
- [10] M.A. Peña, J.P. Gómez and J.L.G. Fierro, *Appl. Catal. A* **144** (1996) 7-57

- 
- [11] J.N. Armor, *Appl. Catal. A* **176** (1999) 159-176
- [12] G. Martino, P. Courty and C. Marcilly in 'Handbook of Heterogeneous Catalysis' G. Ertl, H. Knözinger and J. Weitkamp (editors), VCH, Weinheim, 1997, pp.1804-1818
- [13] J. Scherzer and A.J. Gruia 'Hydrocracking Science and Technology', Marcel Dekker, New York, 1996, pp. 1-8
- [14] Süddeutsche Zeitung, 'Beim Sprit gehören die Briten zu den Vorreitern', 16.11.2000
- [15] N.N. Greenwood and A. Earnshaw 'Chemistry of the Elements', Pergamon Press, 1984, p. 730
- [16] C.E.G. Padró and V. Putsche, 'Survey of the Economics of Hydrogen Technologies', Technical report of the national renewable energy laboratory (U.S. Department of energy laboratory) NREL/TP-570-27079, 1999
- [17] K. Kochloefl in 'Handbook of Heterogeneous Catalysis' G. Ertl, H. Knözinger and J. Weitkamp (editors), VCH, Weinheim, 1997, pp.1819-1831
- [18] D.L. Trimm, *Catal. Today* **49** (1999) 3-10
- [19] A.S. Bodke, S.S. Bharadwaj and L.D. Schmidt, *J. Catal.* **179** (1998) 138-149
- [20] A.G. Dietz III, A.F. Carlsson and L.D. Schmidt, *J. Catal.* **176** (1996) 459-473
- [21] D.A. Goetsch and L.D. Schmidt, *Science* **271** (1996) 1560-1562.
- [22] M. Huff, P.M. Torniainen and L.D. Schmidt, *Catal. Today* **21** (1994) 113-128

- 
- [23] P.M. Witt and L.D. Schmidt, *J. Catal.* **163** (1996) 465-475
- [24] J.M. Parera and N.S. Fígoli in 'Catalytic Naphtha Reforming, Science and Technology', G.J. Antos, A.M. Aitani and J.M. Parera (editors), Marcel Dekker, New York, 1995, pp. 1-17
- [25] F. Trifirò and A. Vaccari in 'Comprehensive Supramolecular Chemistry', J.L. Atwood, J.E.D. Davies, D.D. MacNicol and F. Vögtle (editors), Pergamon Press, Oxford, 1996, pp. 251-291
- [26] R. Allmann, *Chimia* **24** (1970) 99-108
- [27] G. Geismar and J. Lewandowski, *Chemiker-Zeitung* **115** (1991) 297-300
- [28] F. Trifirò, A. Vaccari, G. Del Piero in 'Characterisation of Porous Solids', K.K. Unger, J. Roquerol, K.S.W. Sing and H. Kral (editors), Elsevier, Amsterdam, 1988, pp. 571-580
- [29] A. van der Pol, G.M. Peters, E.J. Reijerse, E. de Boer, J. Lewandowski and G. Geismar, *Appl. Magn. Reson.* **3** (1992) 751-762
- [30] M. Köckerling, G. Geismar, G. Henkel and H.-F. Nolting, *J. Chem. Soc., Faraday Trans.* **93** (1997) 481-484
- [31] R. Trujillano, O. Pietro, P. Malet and R. Rives, *Proceedings Euroclay 1999*, Krakow, Poland, 1999, p.140
- [32] P. Kućrowski, A. Rafalska-Łasocha, D. Majda, D. Tomaszewska and R. Dziembaj, *Solid State Ionics* **141-142** (2001) 241-246

- 
- [33] E.C. Kruissink and L.L. van Reijen, *J. Chem. Soc., Faraday Trans. 1*, **77** (1981) 649-663
- [34] T. Kwon and T.J. Pinnavaia, *J. Mol. Catal.* **74** (1992) 23-33
- [35] J. Evans, M. Pillinger and J. Zhang, *J. Chem. Soc., Dalton Trans.* (1996) 2963-2974
- [36] A. Schutz and P. Biloen, *J. of Solid State Chem.* **68** (1987) 360-368
- [37] G. Charlot 'L' *Analyse Qualitative et les Réactions en Solution*, Masson, Paris, 1963, pp. 114-115
- [38] C.P. Kelkar and A.A. Schutz, *Microporous Materials* **10** (1997) 163-172
- [39] C. Barriga, I. Crespo, M.A. Ulibarri, P. Malet and V. Rives, *Proceedings Euroclay 1999, Krakow, Poland, 1999*, p.59
- [40] M.A. Ulibarri, R. Celis, M.C. Hermosín and M.J. Carrizosa, I. Pavlovic, W.C. Koskinen and J. Cornejo, *Proceedings Euroclay 1999, Krakow, Poland, 1999*, p.141
- [41] M.A. Ulibarri, R. Celis, M.C. Hermosín and J. Cornejo, *Proceedings Euroclay 1999, Krakow, Poland, 1999*, p.141
- [42] O. Lebedeva, D. Tichit and B. Coq, *Appl. Catal. A.* **183** (1999) 61-71
- [43] F.M. Cabello, D. Tichit, B. Coq, A. Vaccari and N.T. Dung, *J. Catal.* **167** (1997) 142-152
- [44] F.M. Vichi and O.L. Alves, *J. Mater. Chem.* **7** (1997) 1631-1634

- 
- [45] G. Geismar, J. Lewandowski and E. de Boer, *Chemiker-Zeitung* **115** (1991) 335-339
- [46] F. Medina, R. Dutartre, D. Tichit, B. Coq, N.T. Dung, P. Salagre and J.E. Sueiras, *J. Mol. Catal. A*, **119** (1997) 201-212
- [47] R. Trujillano, M.A. Vincente and R. Rives, *Proceedings Euroclay 1999*, Krakow, Poland, 1999, p.140
- [48] E. Dumitriu, V. Hulea, C. Chelaru, C. Catrinescu, D. Tichit and R. Durand, *Appl. Catal. A* **178** (1999) 145-157
- [49] A. Béres, I. Pálinkó, I. Kiricsi, J.B. Nagy, Y. Kiyozumi and F. Mizukami, *Appl. Catal. A* **182** (1999) 237-247
- [50] L. Chmielarz, P. Kućetrowski, A. Wê grzyn, P. Gê bala, A. Rafalska-£asocha and R. Dziembaj, submitted to *Polish Journal of Environmental Studies*
- [51] A. Wê grzyn, P. Kućetrowski, L. Chmielarz, P. Gê bala, A. Rafalska-£asocha and R. Dziembaj, submitted to *Polish Journal of Environmental Studies*
- [52] P. Kućetrowski, A. Wê grzyn, L. Chmielarz, A. Rafalska-£asocha, B. Dudek and R. Dziembaj, *Proceedings of 20<sup>th</sup> European Crystallographic Meeting*, Krakow, Poland, August 2001, in press
- [53] B. Rebours, J.-B. d'Espinose de la Caillerie and O. Clause, *J. Am. Chem. Soc.* **116** (1994) 1707-1717
- [54] F.M. Labajos, V. Rives and M.A. Ulibarri in 'Multifunctional Mesoporous Inorganic Solids', C.A.C. Sequeira and M.J. Hudson (editors), Kluwer, Dordrecht, 1993, pp. 207-215



- 
- [55] T. Hibino, and A. Tsunashima, Proceedings Euroclay 1999, Krakow, Poland, 1999, p.92
- [56] R. Prihod'ko, M. Sychev, K. Erdmann, A. Kodentsov and R.A. van Santen, Proceedings Euroclay 1999, Krakow, Poland, 1999, p.123
- [57] E. Kanezaki, Solid State Ionics **106** (1998) 279-284
- [58] W.T. Reichle, S.Y. Kang and D.S. Everhardt, J. Catal. **101** (1986) 352-259
- [59] L.E. Alzamano and J.R.H. Ross, J. Chem. Soc. Faraday Trans. 1, **77** (1981) 665-681
- [60] O. Clause, M. Gazzano, F. Trifirò, A. Vaccari and L. Zatorski, Appl. Catal. **73** (1991) 217-236
- [61] L. Chmielarz, P. Kucetrowski, A. Rafalska-Łasocha, D. Majda and R. Dziembaj, submitted to Appl. Catal. B
- [62] L. Chmielarz, P. Kucetrowski, A. Rafalska-Łasocha and R. Dziembaj, Proceedings of 20<sup>th</sup> European Crystallographic Meeting, Krakow, Poland, August 2001, in press
- [63] P. Kucetrowski, L. Chmielarz, A. Rafalska-Łasocha, Rafa<sup>3</sup> Chyży and R. Dziembaj, Proceedings of EuropaCat-5, Limerick, Ireland, September 2001, in press
- [64] S. Dick and H. Schießling, Proceedings Euroclay 1999, Krakow, Poland, 1999, p.74

- 
- [65] F. Basile, L. Basini, M. D' Amore, G. Fornasari, E. Poluzzi, L. Sartoni, F. Trifirò and A. Vaccari, Proceedings of EuropaCat-3, Kraków, Poland, September 1997, p. 79
- [66] H. Scharper, E.B.M. Doesburg, J.M.C. Quartel and L.L. Van Reijen in 'Preparation of Catalysts III', G. Poncelet, P. Grange and P.A. Jacobs (editors), Elsevier, Amsterdam, 1983, pp. 301-309
- [67] Second Periodic Report of the EU Contract 'DeNOx' (ERB CIPA-CT 93-0266 DG 12 HSMU), 1995
- [68] A. Saus, Vorlesungsmanuskript 'Angewandte/Technische Organische Chemie', Gerhard-Mercator-University Duisburg
- [69] Y. Boucouvalas, Z. Zhang and X.E. Verykios, *Catal. Lett.* **40** (1996) 189-195
- [70] A. York, Chemistry in Britain, August 1999, pp. 25-27
- [71] P. Forzatti and L. Lietti, *Catal. Today* **52** (1999) 165-181
- [72] D.L. Trimm in 'Handbook of Heterogeneous Catalysis' G. Ertl, H. Knözinger and J. Weitkamp (editors), VCH, Weinheim, 1997, pp. 1263-1282
- [73] T. Borowiecki, A. Go³owski, K. Sto³ecki and B. Stasiñska, *Polish Journal of Chemical Technology* **1** (1999) 2-6
- [74] E. Tracz, R. Scholz and T. Borowiecki, *Appl. Catal.* **66** (1990) 133-148
- [75] T. Borowiecki, *Appl. Catal.* **31** (1987) 207-220
- [76] H.M. Swaan, V.C.H. Kroll, G.A. Martin and C. Mirodatos, *Catal. Today* **21** (1994) 571-578

- 
- [77] E. Ruckenstein and Y.H. Hu, *Appl. Catal. A* **97** (1997) 185-205
- [78] C.F. Ng, H. Ye, L. She, H. Chen and S.Y. Lai, *Appl. Catal. A* **171** (1998) 293-299
- [79] L. Kê piński, B.K. Sto<sup>3</sup>eckki and T. Borowiecki *Carbon* **38** (2000) 1845-1856
- [80] Å. Slagtern, U. Olsbye, R. Blom, I.M. Dahl, H. Fjellvåg, *Appl. Catal. A* **165** (1997) 379-390
- [81] J.H. Edwards, *Catal Today* **23** (1995) 59-66
- [82] P. Gronchi, P. Centola, and R. Del Rosso, *Appl. Catal. A* **152** (1997) 83-92
- [83] H.Y. Wang and C.T. Au, *Applied Catal. A* **155** (1997) 239-252
- [84] S. Wang and G.Q.M. Lu, *Appl. Catal. B* **16** (1998) 269-277
- [85] P. Ferreira-Aparicio, A. Guerrero-Ruiz and I. Rodríguez-Ramos, *Appl. Catal. A* **170** (1998) 177-187
- [86] Y.H. Hu and E. Ruckenstein, *Catal. Lett.* **36** (1996) 145-149
- [87] A.T. Ashcroft, A.K. Cheetham, M.L.H. Green and P.D.F. Vernon, *Nature* **352** (1991) 225-226
- [88] Y. Chen, K. Tomishige, K. Yokoyama and K. Fujimoto, *Appl. Catal. A* **165** (1997) 335-347
- [89] Y. Chen, C.M. Hwang and C.W. Liaw, *Appl. Catal. A* **169** (1997) 207-214
- [90] G. C. Bond, *Appl. Catal. A* **149** (1997) 3-25

- 
- [91] P. Marécot and J. Barbier in 'Catalytic Naphtha Reforming, Science and Technology', G.J. Antos, A.M. Aitani and J.M. Parera (editors), Marcel Dekker, New York, 1995, pp. 279-311
- [92] J. Łojewska and R. Dziembaj in 'Catalyst Deactivation 1999', B. Delmon and G.F. Froment (editors), Elsevier Science, Amsterdam, 1999, pp. 121-128
- [93] P.M. Torniainen, X. Chu and L.D. Schmidt, *J. Catal.* **146** (1994) 1-10
- [94] D. Qin, J. Lapszewicz and X. Jiang, *J. Catal.* **159** (1996) 140-149
- [95] P.M. Makoá, N.J. Coville, and V.D. Sokolovskii, *Catal. Today* **49** (1999) 11-16
- [96] V.D. Sokolovskii, N.J. Coville, A Parmliana, I. Eskendirov and M. Makoá, *Catal. Today* **42** (1998) 191-195
- [97] K. Heitnes, S. Lindberg, O.A. Rokstad, A. Holmen, *Catal. Today* **21** (1994) 471-480
- [98] D.A. Hickman and L.D. Schmidt, *J. Catal.* **138** (1992), 267-282
- [99] E.P.J. Mallens, J. H. B. J. Hoebink and G. B. Marin, *J. Catal.* **167** (1997) 43-56
- [100] D.A. Hickman and L.D. Schmidt, *Science* **259** (1993) 343-346
- [101] C.T. Au, and H.Y. Wang, *Catal. Lett.* **41** (1996) 159-163
- [102] C.T. Au, H.Y. Wang and H.L. Wan, *J. Catal.* **158** (1996) 343-348
- [103] C.T. Au and H.Y. Wang, *J. Catal.* **167** (1997) 337-345
- [104] V.R. Choudhary, A.M. Rajput and B. Prabhakar, *J. Catal.* **139** (1993) 326-328

- 
- [105] V.R. Choudhary, B.S. Uphade and A.S. Mamman, *Catal. Lett.* **32** (1995) 387-390
- [106] V.R. Choudhary, B.S. Uphade and A.S. Mamman, *J. Catal.* **172** (1997) 281-293
- [107] D. Dissanayake, M.P. Rosynek, K.C.C. Kharas and J.H. Lunsford, *J. Catal.* **132** (1991), 117-127
- [108] N. Nichio, M. Casella, O. Ferretti, M. González, C. Nicot, B. Maroweck and R. Frety, *Catal. Lett.* **42** (1996) 65-72
- [109] F. Van Looij, J.C. Van Giezen, E.R. Stobbe and J.W. Geus, *Catal. Today* **21** (1994) 495-503
- [110] F. Van Looij and J.W. Geus, *J. Catal.* **168** (1997) 154-163
- [111] A. Santos, M. Menéndez and J. Santamariá, *Catal. Today* **21** (1994) 281-488
- [112] M. Soick, O. Buyevskaya, M. Höhenberger and D. Wolf, *Catal. Today* **32** (1996) 163-169
- [113] R. Burch, D.J. Crittle and M.J. Hayes, *Catal. Today* **47** (1999) 229-234
- [114] B.H. Davis and G.J. Antos in 'Catalytic Naphtha Reforming, Science and Technology', G.J. Antos, A.M. Aitani and J.M. Parera (editors), Marcel Dekker, New York, 1995, pp.113-180
- [115] A. Zecchina, C. Lamberti and S. Bordiga, *Catal. Today* **41** (1998) 169-177
- [116] J.I. Di Cosimo, V.K. Díez and C.R. Apesteguía, *Appl. Catal. A* **137** (1996) 149-166

- 
- [117] M.A. Aramunedía, V. Boráu, I.M. García, C. Jiménez, A. Marinas, J.M. Marinas, A. Porras and F.J. Urbano, *Appl. Catal. A* **184** (1999) 115-125
- [118] M. Lewandowski and Z. Sarbak, *Appl. Catal. A* **168** (1998) 179-185
- [119] A. Corma, V. Fornés and A. Rey, *J. Catal.* **148** (1994) 205-212
- [120] F. Kooli, C. Martín and V. Rives, *Langmuir* **13** (1997) 2303-2306
- [121] F. Kapteijn and J.A. Moulijn in 'Handbook of Heterogeneous Catalysis' G. Ertl, H. Knözinger and J. Weitkamp (editors), VCH, Weinheim, 1997, pp. 1359-1376
- [122] 'Handbook of Chemistry and Physics', R.C. Weast, M.J. Astle and W.H. Beyer (editors), CRC Press, Boca Raton, 1985 (66<sup>th</sup> edition), p. E-2
- [123] F. Basile, G. Fornasari, M. Gazzano and A. Vaccari, *Appl. Clay. Sci.* **16** (2000) 185-200
- [124] R. Dziembaj, J. Łojewska and T. Łojewski, *Solid State Ionics* **117** (1999) 87-93
- [125] D. Tichit, F. Medina, B. Coq and R. Dutarte, *Appl. Catal. A* **159** (1997) 241-258
- [126] M. Haake, T. Hill, G. Kons, E. Schwab and H. Wörz, *Proceedings XXXIII. Jahrestreffen Deutscher Katalytiker, Weimar, Germany, 2000*, pp.9-10
- [127] L. Chmielarz, R. Dziembaj, J. Jamrozik, I. Kargulewicz and W. Makowski, *J. Therm. Anal. Cal.* **55** (1999) 867-875

## Curriculum Vitae

Name	Kai Schulze
Date of birth	09.12.1969
Place of birth	Duisburg (Germany)
Personal status	single

### School education

1976-1980	Grundschule Musfeldstraße in Duisburg
1980-1989	Landfermann-Gymnasium in Duisburg
June 1989	Permission to study any subject (Allgemeine Hochschulreife)

### Military service

1989-1990	Flakregiment 7 in Borken/Westphalia
-----------	-------------------------------------

### University education

1990	Commencement of M.Sc. studies in Chemistry at the Gerhard-Mercator-University Duisburg
1993	Finishing of the pre-master examinations (Diplomvorprüfung)
1993-1994	On leave from the Gerhard-Mercator-University Duisburg for one year of studies abroad. Final year of B.Sc. studies in Chemistry at the University of Durham (England)
1994-1996	Continuation of the M.Sc. studies in Chemistry at the Gerhard-Mercator-University Duisburg
February 1997	Receiving M.Sc. in Chemistry

### Ph.D. studies

February 1997	Entrance examination to the Jagiellonian University in Krakow (Poland)
March 1997	Commencement of Ph.D. studies at the Gerhard-Mercator-University Duisburg, Supervisor Prof. Dr. Günter Geismar
August 1997- June 2001	Continuation of Ph.D. studies at the Jagiellonian University in Krakow, Supervisor Prof. Dr. Roman Dziembaj